X-RAY ABSORPTION FINE STRUCTURE OF ADSORBATES ON METAL SURFACES

Michael Derek Crapper

Submitted for the degree of Doctor of Philosophy
to the University of Warwick

Department of Physics June 1986

TABLE OF CONTENTS

LIST OF FIGURES AND TABLES

ACKOWLEDGEMENTS

I would like to take this opportunity to thank all the people who have given me invaluable assistance throughout the research presented here.

Firstly, I must give thanks to Phil Woodruff, my supervisor, who has been a constant source of ideas and has given me excellent guidance throughout. Thanks are also due to Rob Johnston, Peter Lander and Donna Phillips for their competent technical support. Synchrotron research requires teamwork, and I am indebted to Rob Jones, Chris Riley, Paul Sweeney, Jochen Haase, Alfred Puschmann and Martin Bader for their collaboration on experimental work. I am also grateful to Chris and Jochen for discussions on data analysis and general scientific matters. Thanks are also due to the late Professor McMillan and Professor Forty for the provision of research facilities within the Departmant of Physics. I would also like to thank the staff of the SRS at Daresbury and at BESSY for the help they have given me.

I would like to thank my parents for their support and encouragement throughout my university career. Finally I would like to thank my wife, Patricia, for her patience, encouragement and understanding and for typing this thesis.

DECLARATION

The work presented in this thesis is my own except where stated otherwise and was performed in the Physics Department, University of Warwick, the SERC Daresbury Laboratory and at BESSY in West Berlin during the period October 1982 to September 1985. No part of this material has been previously submitted to this or any other University.

The analysis of the surface iodide phase introduced in Chapter 1 has been published in Surface Science 152/153 443-452 (1985) and in EXAFS and Near Edge Structure III pp258-260 ed. by K.O.Hodgson, B.Hedman, and J.E.Penner-Hahn. Springer-Verlag (1984).The analysis of the Cu(110)/HCOO system using NEXAFS and single shell SEXAFS analysis presented in Chapter 5 has been published in Physical Review Letters 54 2250-2252 (1985) and Surface Science 171 1-12 (1986). It is also intended to publish the analysis of the chemisorbed overlayers of I on Ni(100) from Chapter 1, the SEXAFS and photoelectron diffraction analysis of the Cu(111) [$\sqrt{3}\times\sqrt{3}$]R30°-Cl overlayer from Chapter 4 and the multi-shell analysis of HCOO adsorption from Chapter 5 in the near future.

M. Crapper

M.D.CRAPPER

ABSTRACT

The structural techniques of SEXAFS, NEXAFS and photoelectron diffraction have been applied to several adsorption systems. In combination they have allowed detailed surface structural studies to be achieved and the usefulness of these complementary techniques (which employ the same experimental geometry) has been demonstrated.

SEXAFS studies have been carried out for atomic and molecular adsorption systems. It has been found that for several systems the (usual) Fourier filtering analysis method is not applicable due to the superposition of EXAFS from different shells. Some systems have been successfully analysed by the Fourier method, however. In particular, EXAFS from the Cu(111)[$\sqrt{3}$x$\sqrt{3}$]R30°-Cl adsorption system yield the same result when analysed by both the Fourier filtering method and a multiple shell simulation routine. Adsorption occurs in the three-fold hollow with a Cl-Cu bond length of 2.39±0.02Å. This is in contrast with earlier analysis of I chemisorbed on Ni(100) where it was found that only the multi-shell method was applicable. Photoelectron diffraction measurements for both normal and off-normal geometries confirmed the site found by SEXAFS and further revealed that adsorption was in the fcc-like three-fold hollow (as opposed to the hcp-like one).

A study of the formate intermediate on Cu(110) using NEXAFS revealed that the molecule is adsorbed with it's plane parallel to the [1$\bar{1}$0] azimuth. Single shell SEXAFS analysis determined the adsorption site to be atop a Cu atom on the 'ridges' with the O atoms in the pseudo bridge sites. The average O-Cu distance being 1.98±0.07Å.

Reanalysis of the SEXAFS data of formate adsorbed on Cu(110) and Cu(100) using the multi-shell method revealed that the 'anomalous chemisorption bond' proposed for the latter was erroneous. A misleading result had been obtained with the Fourier filtering method because of the superposition of EXAFS from two similar bond lengths.

NEXAF studies of the reaction of ethanol and oxygen on Cu(110) revealed that ethanol and an ethoxy intermediate were coadsorbed with the O-C bond effectively parallel to the surface in the ethanol and perpendicular in the ethoxy.

CHAPTER 1: INTRODUCTION

During the past twenty years, there has been a massive increase in the amount of work that has gone into studying the properties of surfaces. This has occured because there is an increased need for an understanding of surface processes which are important in many fields of technology, including materials science, device physics and catalysis. This expansion in surface science has been greatly facilitated by the development of ultra-high vacuum (UHV) technology. UHV is required for surface science because in order to keep the surface free from contamination by impinging gas molecules for long enough to be studied, residual vacua of less than 10^{-9}Torr are required.

The drive to understand the physics of surfaces is spurred by their novel properties. Whilst bulk crystalline materials are fairly well understood, the reduced (two dimensional) periodicity of surfaces creates differences in the electronic structure. These differences can be important in semiconductor devices where some sort of interface is usually involved. Another branch of science where surfaces have an important function is catalysis. Atoms at surfaces have, due to the nature of their position, unsatisfied bonds. These 'dangling' bonds can participate in chemical reactions involving molecules adsorbed on the surface.

Surface studies have progressed along two distinct lines; the study of 'real' surfaces, that is those which may be involved in real technological situations,

and of low index faces of single crystal materials known as 'ideal' surfaces. It is these so called 'ideal' surfaces that are investigated here; in particular, the adsorption of gases upon these surfaces. Whilst the study of simple adsorption systems is not directly applicable to real chemical processes such as catalysis it is hoped that information extracted from these will increase the understanding of more complex systems.

In studying surfaces, there are three main questions to be answered; what is the chemical composition of the surface, what is its structure and what is its electronic structure? The work presented in this thesis concerns itself mainly with the structure of adsorbate systems. By far the most commonly used technique for surface structure determination is Low Energy Electron Diffraction (LEED)[1]. This has been successfully used on many systems and its theory is well understood. It is limited, however, to the study of systems with long range order (as are all diffraction techniques) and it requires the use of complex multiple scattering calculations because of the high scattering cross-section of electrons of low energy. Recently, the bulk technique Extended X-ray Absorption Fine Structure (EXAFS)[2] has been applied to surface studies. EXAFS is sensitive to local order, so it can be used on systems with no long range order, and its analysis is simplified by the dominance of single scattering events.

EXAFS is an 'internal electron diffraction' technique; the scattering of electrons photoemitted from a core level of one atom off surrounding atoms is monitored by

measuring the X-ray absorption coefficient as a function of energy. This scattering and the resulting interference effects produce oscillations in the X-ray absorption coefficient as a function of k, the electron wavevector, at a frequency of 2r (where r is the separation of the central atom and the scattering atom) plus a factor due to the phase shifts introduced by both atoms involved. The standard method of analysing EXAFS is to perform a Fourier transform of the modulation function to obtain a frequency spectrum in which there should be a large peak corresponding to 2r. The phase shifts are extracted by performing an EXAFS experiment on a compound containing the same two atomic species at a known separation. The physics and analysis of EXAFS is discussed in more detail in Chapter 2.

Initial studies of adsorbates on surfaces using surface EXAFS have been carried out on iodine on Ni(100). This work is discussed extensively elsewhere[3-5] but is only presented briefly here. This data was analysed mainly by S. Ainsworth. The adsorption of iodine has been studied extensively by several techniques[6-9]. Work using LEED and Auger electron spectroscopy (a technique sensitive to the chemical constituents of the surface) has revealed that there are several phases of I on Ni(100) depending on the conditions of adsorption and the temperature to which the crystal has been heated following adsorption. If the Ni(100) surface is exposed to iodine vapour (at a pressure of 10^{-6} mbar) whilst cooling from its annealing temperature, a single layer of NiI_2 is formed. If the crystal is dosed at room

temperature a c(2x2) structure is formed (this is an ordered overlayer of iodine which has the same four-fold symmetry of the substrate but the side of the unit mesh is $\sqrt{2}$ times longer and the axes of symmetry are rotated by 45° with respect to the substrate). If either of these phases are heated to above 490K, a variable mesh of chemisorbed iodine is formed. This has a unit mesh which has one side which is twice the Ni-Ni spacing whilst the other side is continuously variable as a function of temperature. This gives rise to two other coincidence structures, the c(2x8) and the (2x3) at successively lower coverages. These structures are summarised in Fig. 1.1.

These structures have been studied using surface EXAFS, and the data has been analysed using both the standard Fourier filtering method and by a multi-shell simulation process. The comparison of the results obtained by these two methods have revealed a problem which has not previously investigated with regard to surface EXAFS; the effect of two superimposed bond lengths on the EXAFS modulations. The EXAFS spectra for the different systems are shown in Fig. 1.2. The wiggles in the X-ray absorption coefficient is the structure known as EXAFS. Analysis of the bulk iodide data using the multi-shell modelling method revealed that only the two wiggles at highest energy are due to the nickel nearest neighbour only. The lower energy structure is considerably influenced by the more distant iodine neighbour (see Table 1.1) because the iodine back-scattering magnitude is quite strong in this region whereas the back-scattering

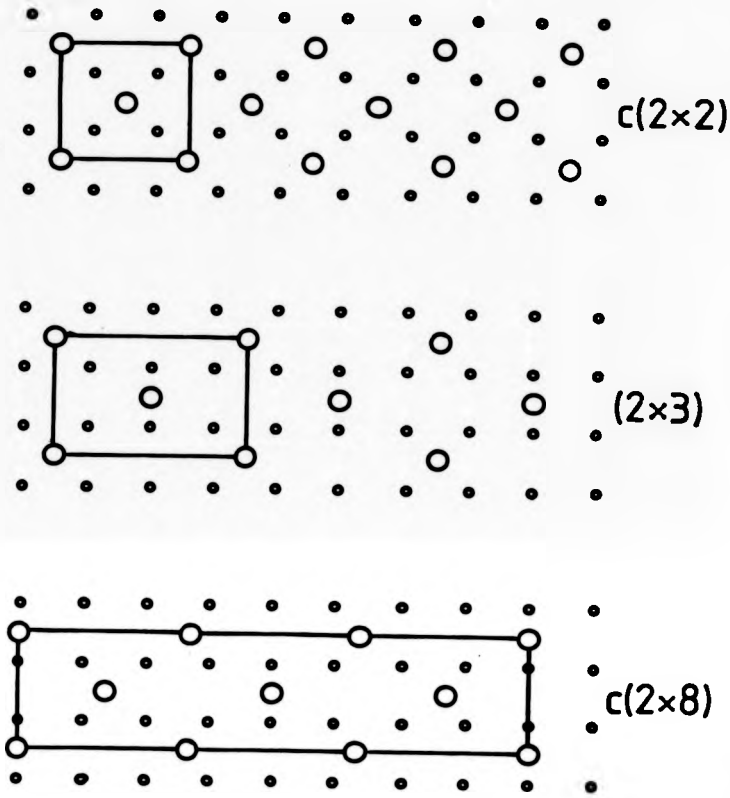

Figure 1.1 Schematic representation of the three commensurate overlayers of iodine chemisorbed on Ni(100).

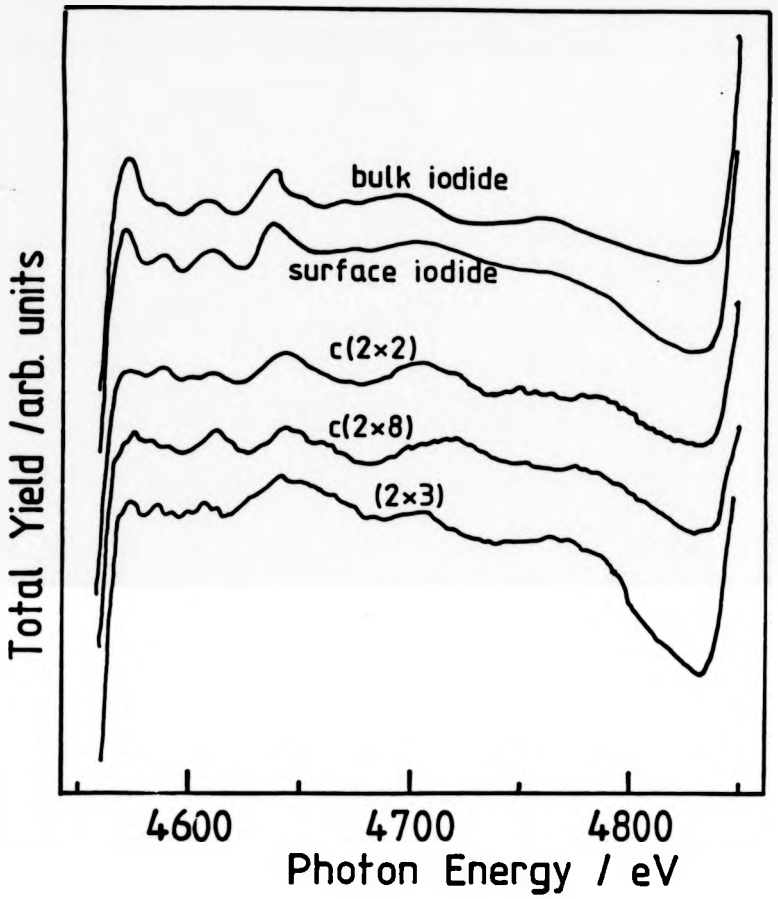

Figure 1.2 EXAFS spectra for bulk NiI_2, the surface iodide and the chemisorbed phases.

TABLE 1.1

THE FIRST THREE SHELLS AROUND AN IODINE ATOM IN NiI_2.

ATOM TYPE	R/Å	COORDINATION NO.
Ni	2.78	3
I	3.89	6
Ni	4.78	3

from the nickel is fairly weak. This means that the phase shifts extracted from bulk NiI_2 using the Fourier filtering analysis method, which assumes that the sole contributor to the main peak in the transform is the nearest (Ni) neighbour, will be wrong. Since the phase shifts are stongly linked to the bond length, any interatomic separations extracted for I on Ni(100) using the Fourier filtering method would be incorrect.

Analysis of the surface data showed that a multi-shell simulation approach was capable of resolving the contributions due to the Ni and the I. The surface iodide phase was shown, as was suspected, to be a single layer of bulk iodide with essentially no difference in structure between the bulk and surface phases. Analysis of data taken from the c(2x2) phase revealed both the adsorption site, and the I-Ni separation. The site was revealed by comparing simulations based on all three possible high symmetry sites (the atop site, the bridge site and the 4-fold hollow) with the experimental spectrum. The atop and bridge sites showed extra structure which was not present in the data, and so the site was revealed to be the 4-fold hollow.

The analysis of the two lower coverage structures was not as straight forward as this, however, because each must involve more than one kind of site. Attempts were made to fit the (2x3) data using coordination numbers based on models with a 50:50 split between hollow and bridge sites, with all iodine atoms sitting halfway between the hollow and bridge sites, and with I displaced 0.3Å from the hollows and (in equal numbers) 0.3Å

from the bridges. Of these models, the latter achieved the best fit, and revealed an I-Ni distance of 2.79±0.10Å (essentially the same as in bulk nickel iodide). Similar problems were found in the c(2x8) system, but it was concluded that the number of iodine atoms in hollow sites involved must be greater than one third of the total. These simulations also indicated that the bridge site must be an energy saddle point for the iodine atoms.

These studies of iodine adsorption revealed some interesting features of SEXAFS. This was the first SEXAFS study to take advantage of multi-shell analysis. This multi-shell analysis revealed that the Fourier filtering method, previously used for all SEXAFS work, was inappropriate for this system. This revealed the need for further studies, in which the analysis methods could be compared, to see whether the I/Ni(100) system was a special case, or if such problems will play an important part in surface EXAFS.

The work presented in this thesis involves the study of widely different adsorption systems (both atomic and molecular) using surface EXAFS, and a comparison of the two analysis methods in each case. The surface EXAFS results are also supplemented by information from the related techniques of photoelectron diffraction and near-edge X-ray absorption fine structure. The lay-out of the thesis[10] is as follows. In Chapter 2 the physical principles of the three techniques are discussed, with particular reference to their applications to surfaces, and in Chapter 3 the experimental techniques are outlined.

Chapters 4 and 5 include the results for atomic and molecular adsorption systems respectively. For convenience. the discussion of results is presented along side the results in the relevant chapter. Chapter 6 presents some final discussion and conclusions. The references used in each chapter are given at the end of that chapter.

CHAPTER 1: REFERENCES

1) J.B. Pendry, "Low Energy Electron Diffraction", Academic Press, (1974).

2) P.A. Lee, P.H. Citrin, P. Eisenberger and B.M. Kincaid, Rev. Mod. Phys. 53, 769-806 (1981).

3) R.G. Jones, S. Ainsworth, M.D. Crapper, C. Somerton, D.P. Woodruff, R.S. Brooks, J.C. Campuzano, D.A. King, G.M. Lamble and M. Prutton, Surf. Sci. 152/153, 443 (1985).

4) R.G. Jones, S. Ainsworth, M.D. Crapper, C. Somerton, D.P. Woodruff, R.S. Brooks, J.C. Campuzano, D.A. King, G.M. Lamble and M. Prutton, Proc. Third. Int. EXAFS Conf., p.258, Springer Verlag (1984).

5) R.G. Jones, S. Ainsworth, M.D. Crapper, C. Somerton and D.P. Woodruff, submitted to Surface Science.

6) R.G. Jones and D.P. Woodruff, Vacuum 31, 411 (1981).

7) R.G. Jones, C.F. McConville and D.P. Woodruff, Surf. Sci. 127, 424 (1983).

8) C.F. McConville and D.P. Woodruff, Surf. Sci. 152/153, 434 (1985).

9) C. Somerton, C.F. McConville, D.P. Woodruff and R.G. Jones, Surf. Sci. 136, 23 (1984).

10) This thesis was written according to the guidelines given in the University of Warwick, Department of Physics document PHYS/PG/2.

CHAPTER 2 : THE BASIC PRINCIPLES OF THE EXPERIMENTAL TECHNIQUES

2.1 INTRODUCTION

In this chapter, the ideas behind the experimental techniques which have been used are discussed. The two 'standard' surface science techniques, Low Energy Electron Diffraction and Auger Electron Spectroscopy are briefly introduced as these were used for preliminary sample characterisation. The technique of EXAFS is discussed in more detail, as is its application to surfaces. The near edge structure of small molecules is discussed and the uses of this technique for surface studies are introduced. Finally, the technique of photoelectron diffraction is briefly discussed.

2.2 LOW ENERGY ELECTRON DIFFRACTION

Low Energy Electron Diffraction (LEED) is the most commonly used method of surface structure determination of single crystal samples[1]. It involves an electron beam impinging normal to a surface and measurement of the diffraction of elastically scattered electrons. Electrons of energy 50-150eV have an escape depth of only about 5Å, so using such electrons makes LEED very surface sensitive. The typical experimental layout for collecting LEED data is shown in figure (2.1). The grid G1 is earthed to ensure a field free region between the sample and the detector, and the grids G2 and G3 allow only elastically scattered electrons through to the fluorescent screen.

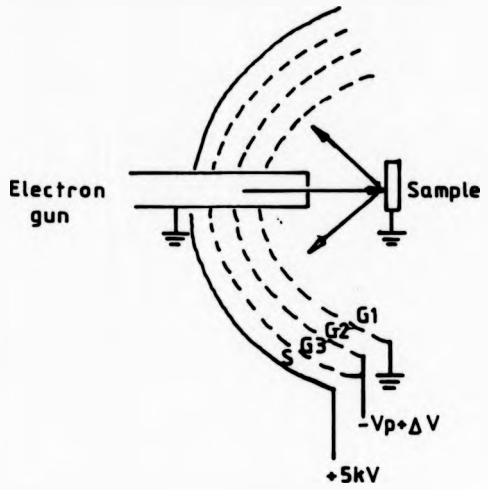

FIGURE 2.1 Three grid LEED system.

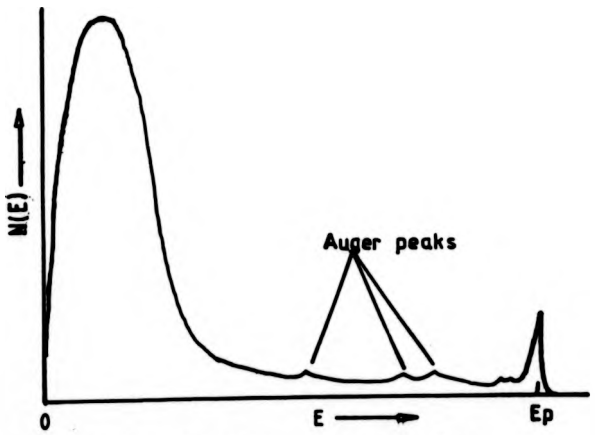

FIGURE 2.2 Secondary electron spectrum.

The periodicity of the surface is immediately obtainable from the LEED pattern, but there are complications in obtaining the number and positions of atoms within the unit mesh. This can only be obtained by measuring the intensities of the scattered beams as a function of energy. The analysis of these intensities is not as simple as the equivalent process for the interpretation of X-ray diffraction intensities. The high cross-section for the interaction of electrons with atoms (which makes them ideal for studying surfaces where the number of scatterers is very small) leads to strong multiple scattering effects which are not significant in X-ray diffraction. The analysis of LEED intensities requires the use of time-consuming and expensive computational modelling of the surface[2]. Another limitation of LEED is that it can only be used to study overlayers which have long range order. For this reason, it is of limited use for the structure determination of molecular adsorption systems which often do not exhibit long range order. Electron beams are also known to dissociate some molcules, and so great care must be taken when studying such systems.

In the work reported here, LEED was only used in a qualitative fashion to check the order of the substrate, and to ascertain the periodicity of some overlayer systems (this can be obtained directly from the the LEED pattern).

2.3 AUGER ELECTRON SPECTROSCOPY

When a core hole is created in an atom by either X-ray or electron excitation, it can decay by one of two processes: fluorescence or Auger electron emission. The latter is a two electron process, in which an electron from a higher shell or conduction band drops into the core hole. The energy released by this is taken up by another electron in a higher level which is ejected from the atom. These emitted or Auger electrons have characteristic energies which can be used to identify different elements (see Figure 2.2).

The main attraction of Auger Electron Spectroscopy (AES)[3] for chemical analyis in surface science is that both the probe and detected particle are electrons, which can be handled fairly easily in a vacuum chamber using standard equipment. The use of low energy electrons (typically a primary energy of about 2keV and Auger energies of a few hundred eV) will make AES surface sensitive because of their short mean free paths.

AES is an important chemical analysis tool for surface science. The typical experimental set up is to use an electron beam to excite the transitions and an electron energy analyser to detect Auger transitions. The most common energy analysers are the Retarding Field Analyser (RFA), the Cylindrical Mirror Analyser (CMA) and the Concentric Hemispheres Analyser (CHA). The RFA is essentially the same apparatus as used in LEED: the two retarding grids are ramped in energy and the current arriving at the screen is the integral

of N(E) from the ramp energy to the primary energy. This can be differentiated using modulation techniques[3]. The CHA and CMA are energy dispersive analysers which selectively allow electrons of one particular energy through to the detector using electric fields. These measure the spectrum ExN(E) (with the CHA in fixed retard ratio mode). Auger electron spectra are usually collected in derivative (dN(E)/dE) mode as this increases the contrast of the small, sharp Auger peaks on the large slowly changing background.

2.4 QUALITATIVE DESCRIPTION OF EXAFS

Extended X-ray Absorption Fine Structure (EXAFS) is the term given to modulations in the X-ray absorption cross-section found above core-level absorption edges of most condensed materials (Figure 2.3a). As these modulations are not found in absorption spectra taken from monatomic gases[4], it is clear that they are due to the presence of other atoms in the neighbourhood of the absorbing atom. The phenomenon of EXAFS has been known for over fifty years and it was generally agreed that the effect was due to modifications of the final state of the photoelectron. It was not clear, however, whether these modifications were due to long or short range order[5]. The controversy was resolved in 1971 when a point scattering theory was developed which relied on short range order only[6].

A qualitative description of EXAFS can be given as follows. An incoming photon ejects an electron from

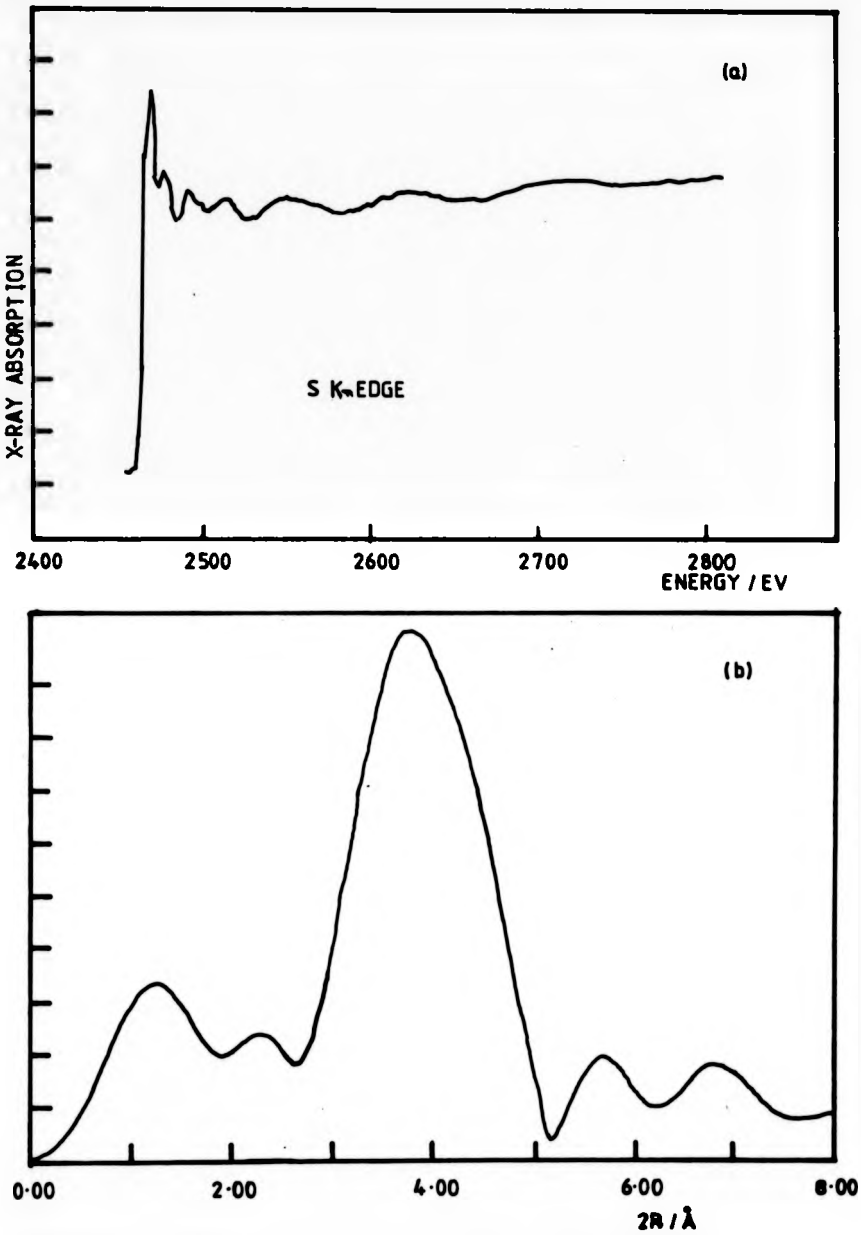

FIGURE 23 EXAFS of Cu_4S (a) and its Fourier transform (b).

a core level. This outgoing electron wave then scatters off neighbouring atoms. The returning electron wave will then interfere with the outgoing electron wave in the region of the (highly localised) core state. This interference will be constructive or destructive, depending on the phase of the scattered wave. This phase depends on two things: the optical path length and the phase shift due to the central and scattering atoms. As the photon energy is increased, the kinetic energy (and so the wavelength) of the photoelectron will increase, so changing the phase of the returning electron wavefunction. The absorption process is governed by the golden rule:

$$\sigma \sim |\langle f|\underline{H}'|i\rangle|^2 \qquad (2.4.1)$$

where f is the final electron state, i is the initial state and $\underline{H}'$ is the dipole operator. Thus, modifications of the final state caused by interference from the scattered wave will influence the absorption cross section, σ. These changes in σ will be oscillatory in the electron wavevector and the frequency of these oscillations will depend on the seperation of the central atom and the scattering atom.

2.5 EXAFS FORMALISM

In order to describe the EXAFS effect, it is convenient to define the X-ray absorption modulation as

$$\chi(k) = \frac{\mu(k) - \mu_0(k)}{\mu_0(k)} \qquad (2.5.1)$$

where $\mu(k)$ is the total X-ray absorption of the species being studied, and $\mu_0(k)$ is the smooth, atomic-like absorption (k is the wave vector of the photoelectron).

Assuming only single scattering occurs, and approximating the electron wave at the scattering atom as a plane wave, the generally accepted form[7,8] of EXAFS for a K absorption-edge is

$$\chi(k) = -\sum_j \frac{N_j^* F_j(k)}{k\, r_j^2} \sin(2kr_j + \phi_j(k)) \exp(-2\langle u_j^2 \rangle k^2) \exp(-2r_j/\lambda(k)) \qquad (2.5.2)$$

where N_j^* is the effective number of neighbours at a distance r_j, $F_j(k)$ is the backscattering amplitude, $\langle u_j^2 \rangle$ is the mean squared amplitude of vibration in a Debye-Waller type term, and $\lambda(k)$ is the electron mean free path.

The total phase shift ϕ_j includes the phase shifts for the photoelectron passing through the atomic potentials of the central atom (twice) and the scattering atom. This is given in the following equation,

$$\phi_j(k) = 2\delta_e(k) + \delta_s(k) \qquad (2.5.3)$$

where the subscripts refer to the electron-emitting atom and the scattering atom.

The effective coordination number N_j^* takes into account the fact that electron emission is more probable

in the direction of the electric vector, and so atoms in this direction contribute more to the EXAFS. For an initial s-state the effective coordination number is

$$N_j^* = 3 \sum_i^{N_j} \cos^2\theta_{ij} \qquad (2.5.4)$$

where θ_{ij} is the angle between the electric vector and the vector joining the central atom and the i^{th} scattering atom in the j^{th} shell. It should be noted that for polycrystalline or amorphous samples, $\cos^2\theta_{ij}$ averages to 1/3 and so the effective coordination number, N_j^*, becomes equal to the actual coordination number, N_j.

The two exponential factors in the EXAFS equation introduce amplitude damping into the oscillations. The first accounts for disorder effects (both thermal and static) which lead to a 'smearing out' of the radial distribution function. This Debye-Waller factor differs from that used in X-ray diffraction experiments because it is in terms of the mean-square difference in displacements, rather than the mean-square displacement. The second exponential term takes into account the loss of electrons due to inelastic scattering, which stops them taking part in the EXAFS effect.

Implicit in the EXAFS equations are several assumptions, the most important being the plane wave approximation and the lack of multiple scattering. The plane wave approximation is a good one as long as the electron energies involved are not to small. The importance of multiple scattering in EXAFS has been the subject of much discussion[8] because the electron energies in

EXAFS are similar to those in Low Energy Electron Diffraction (LEED), and it is known that multiple scattering is very important in LEED[2]. Multiple scattering events in EXAFS would involve long path lengths for the electron, and so should be separable from the nearest neighbour distance. A multiple scattering path that would bring the photoelectron back to the absorbing atom would, in general, involve a series of large scattering angles. These large scattering angles are improbable, especially at the higher electron energies, because the scattering probability is sharply peaked about the forward direction, with a smaller backscattering lobe. The one situation where multiple scattering is important, is when two neighbours are co-linear with the central atom. This will result in strong multiple scattering because of the high probability of forward scattering from the first neighbour on to the second one. This first neighbour will 'focus' the photoelectron onto the second one, so effectively enhancing its coordination number. This 'shadowing' effect will also change the apparent separation of the central and scattering atoms due to the phase shift caused by the atom in between. Generally speaking, however, except in special geometric circumstances, the single scattering, plane wave EXAFS equation is a good approximation, as long as the photoelectron energy is not too low ($\lesssim$50eV).

2.6 ANALYSIS - SINGLE SHELL METHOD

Inspection of the EXAFS equation shows that it is

basically a sum of sine waves of frequencies $2kr_j+\phi_j(k)$. Thus if the phase shifts, $\phi_j(k)$, are known it is possible to extract bondlengths from the EXAFS modulations. The first step, however, must be to obtain $\chi(k)$, i.e. to express the modulations of a function of electron wave vector instead of photon energy. This is not a trivial exercise because, in general, the kinetic energy of the photoelectrons at the absorption threshhold will not be known. It is usual to define a photon energy, E_0, for which the kinetic energy of the photoelectrons is zero. As this is unknown, the first stage in the analysis is to set this at some fixed point on the spectrum (halfway up the edge for example). The modulation function can then be extracted as a function of the wave vector, k, using equation (2.6.1).

$$k = [2m\hbar^2(h\nu - E_0)]^{1/2} \qquad (2.6.1)$$

Studies of the EXAFS phase shifts[9] have shown that the phase $\phi_j(k)$ is, to a close approximation, linear in k. So a Fourier transform[10] of the data should show a peak at $2r_j$ displaced by a small amount because of the phase shift. Now all that remains is to correct for the phase shift and the bond length r_j can be extracted.

These phase shifts can be calculated, but the best precision ($\sim\pm0.01$Å) is obtained by using phase shifts extracted from a model compound. That is a compound containing the same absorbing atom coordinating at a known separation to the same scattering atom as in

the unknown system. This process relies on the idea of phase shift transferability: the phase shifts of a pair of atoms are constant despite a change in chemical enviroment. This is found to be the case for photo-electron energies above about 50eV.

Assuming that EXAFS data is available for a model compound and for the unknown system, the single shell analysis proceeds as follows[1,2]. The first stage is to find the atomic-like absorption, μ_0. In all single shell analyses shown here, this was done by fitting a cubic spline[11] to the data above the edge. The next step is to select an E_0 for both systems: at this stage it is sufficient just to set both on the absorption edge. $\chi(k)$ is then extracted, using this E_0, and usually the data is multiplied by k^n(where n=1,2 or 3) to weight the data equally along its full range.

A Fourier transform of $\chi(k)$ is usually dominated by a single peak corresponding to the nearest neighbour bond (Figure 2.3b). In order to filter out all the information except that from this first neighbour, the transform is multiplied by a window function (a flat topped function with Gaussian sides) centred about the peak. The back transform of this has both imaginary and real parts. The arc tangent of the ratio of imaginary to real components gives the phase of the EXAFS ($2kr_j+\phi_j(k)$). If the phase of the model compound EXAFS is subtracted from the 'unknown' EXAFS, the result (remembering the principle of phase shift transferability) should be $2k\Delta r$, where Δr is the difference in bond length. The process is not that straight forward, however, because

of the lack of knowledge about E_0: this was initially set to an arbitrary value. When the E_0 values are correct. the phase difference should be a linear function of k. passing through the origin. If this is not the case. then ΔE_0. the difference in E_0 between model and unknown. must be incorrect. The final stage in the analysis is to adjust ΔE_0 until the phase difference passes through the origin. When this condition is satisfied. then the gradient of the function is $2\Delta r$.

2.7 ANALYSIS - MULTI-SHELL SIMULATION

Although the majority of EXAFS analyses are performed using the single shell analysis. the analysis can also be carried out by simulating the data. Such simulations also require a model compound to provide the best phase shifts. All the EXAFS simulations reported here were carried out using the EXCURVE package written by S.J Gurman N. Binsted and I. Ross[13]. This program calculates EXAFS using the curved wave theory which allows lower photoelectron energies to be used than are appropriate in the plane wave approximation. The EXAFS are calculated from a model defined by a series of parameters which can be stipulated by the user or iterated to a best least mean squares fit. These parameters are:-

r_j the bond length of the atoms in the j^{th}shell.

E_0 the energy of the photoelectrons at the point which was selected as the origin in the background subtraction.

N_j the number of neighbours at the distance r_j (EXCURVE assumes an isotropic sample. so for anisotropic systems such as single crystals. N_j^* must be entered instead).

A_j the Debye-Waller factor ($2\langle u^2 \rangle$) for the j^{th} shell.

VPI an imaginary component of the inner potential of the sample which produces a decaying electron wave amplitude to allow for the finite mean free (usually -1 to -4eV).

APAC an amplitude factor to allow for reduction in EXAFS amplitudes due to factors such as the finite lifetime of the core hole (usually 0.7-0.9).

An analysis of EXAFS data using this package proceeds as follows.

The first step is to extract the phase shifts. This is done by fitting the model compound data (for which the structural parameters are known) with theoretical phase shifts produced by the program MUFPOT[14]. These phase shifts are modified to fit the data by multiplication by a factor $Ca_jk+Cb_jk^2$.

The modified phase shifts produced from the model compound are then used as a starting point for fitting the 'unknown' data. The parameters A_j.VPI and AFAC are initially set to reasonable values based on knowledge of similar systems. but these can be altered to produce a better fit provided they remain physically sensible.

The N_j used depend on the structure to be fitted and. in general. all available structures are investigated. The parameters r_j and E_0 can then be varied to provide

a best fit. It should be pointed out that EXCURVE is a multi-shell analysis routine. That is, several shells (each of a different r_j) can be fitted at once, but all atoms within one shell must be of the same species.

2.8 SURFACE EXAFS

In bulk EXAFS studies, the absorption coefficient is measured by monitoring the X-ray transmision through the sample[12]. The absorption coefficient, μ is

$$\mu \propto \ln(I/I_0) \qquad (2.8.1)$$

where I is the intensity behind the sample and I_0 is the intensity of the incident beam. This measurement technique is not sensitive enough for surface EXAFS (SEXAFS) because of the small number of atoms in the surface compared with those in the bulk. The alternative to measuring the loss in X-ray intensity is to monitor either a direct product of the absorption process or a product of the decay of the core hole. The direct product of the absorption process is the photoelectron and so, in principle, the intensity of the photoemission peak should contain EXAFS information. Most SEXAFS experiments, however, are performed on single crystals which create strong diffraction effects in the photo-electron spectrum[15]. These diffraction effects would dominate the EXAFS effects unless it where possible to collect signals from a full 4π steradians (a maximum of 2π steradians is available in principle, but in

practice most energy dispersive detectors only subtend a small solid angle).

Having ruled out the use of direct products of absorption, there only remain the indirect products. Bulk EXAFS measurements of dilute samples make use of the fluorescent decay of the core hole. This method has rarely been applied to surface studies, however, but some recent measurements of S on Ni(100) have used fluorescence[16]. For atoms of low Z ($\lesssim 20$) it is more probable for the core hole to decay by Auger emission, rather than fluorescence. Detection of Auger electrons is surface sensitive because of the short electron escape depth ($\lesssim 20$Å). This can be made even more surface sensitive by measuring the X-ray absorption of an adsorbate, which would only be found at the surface (in fact almost all SEXAFS experiments to date have been performed on adsorbate systems). One problem with Auger detection is that photoemission peaks may sweep through the energy window, drowning out the signal.

Another SEXAFS detection technique that makes use of electrons is the Total Electron Yield (TEY) method. In TEY, electrons of all energies (which must all be due, originally, to absorption processes) are detected. The total signal detected in this way is clearly much greater than that for Auger detection, so that the signal to noise ratio for TEY may be significantly better even though the signal to background ratio will be much smaller (since TEY monitors all absorption processes and is not specific to the adsorbate). The surface specificity of TEY is vastly inferior to that of Auger

detection because the majority of the electrons detected are from the low energy cascade. These electrons are released by the (multiple) inelastic scattering of absorption related Auger and photo- electrons, which may originate deep in the bulk. Measurements of oxide films grown to various thicknesses on aluminiun foil[17] have shown that TEY samples to a depth of the order of 100Å. So, the only way TEY can be used for Surface EXAFS is if adsorbates are studied. Electron yield measurements can be made more surface sensitive by using a high pass energy filter to eliminate the low energy cascade electrons: this is known as Partial Electron Yield (PEY). The use of PEY, however, is still restricted to the study of adsorbates, although it gives a higher signal to background ratio than TEY. It should be pointed out that the X-ray absorption, $\mu(E)$, measured by electron yield is simply I/I_0 (not the logarithm). This is because the escape depth of electrons is much shorter than the X-ray penetration depth, and so the volume sampled is virtually independent of the absorption probability.

Other SEXAFS detection techniques include ion yield[18] and the measurement of reflected X-ray intensities for total external reflection incidence angles[21]. As these were not made use of in the investigations reported here, they will not be discussed.

2.9 THE ADVANTAGES & DISADVANTAGES OF SEXAFS AS A SURFACE STRUCTURE TECHNIQUE

The most obvious advantage of SEXAFS for surface

structure determination is the high precision with which it is possible to determine bond lengths (±0.01Å is the limit of accuracy which has been found in bulk EXAFS). Differences in bond length between bulk and surface species are typically a few hundredths of an Ångstrom, and the more common diffraction techniques (e.g. LEED) are only capable of a resolution of the order of five hundredths of an Ångstrom. Another apparent advantage of SEXAFS is that it can be analysed in a model-independent manner; that is, the Fourier filtering method can produce a figure for the bond length without the need for any preconceived ideas about the structure. This is in contrast with Low Energy Electron Diffraction (LEED) which is analysed by comparing the intensities of diffracted beams that have been measured with calculated intensities based on a model structure. The model is then varied until a best fit is obtained.

One problem with SEXAFS is that if a system has two bond lengths which are very close together, then it may not be possible to resolve them. In this case, the bond length obtained will be a weighted average of the two, or, in certain circumstances, the bond length obtained may not even be in between the two[20].

A major attraction of SEXAFS is its usefulness in the determination of adsorption sites. This can be found by two methods. The first (and most commonly used) involves the use of the dependence of EXAFS amplitudes on the direction of the polarisation vector. If equation (2.5.4) is applied to the adsorption of an atomic species on a surface, the expression for N* becomes (in the

case of a K-edge).

$$N_j^* = 3N_j (\cos^2\theta\cos^2\beta+\sin^2\theta\sin^2\beta\cos^2\phi) \qquad (2.9.1)$$

where θ is the angle between the surface normal and the polarisation vector, β is the angle between the surface normal and the bond between the adsorbate and scattering atom (of which there are N at this distance and angle) and ϕ is the azimuthal angle between the electric vector and the bond. For surfaces with a symmetry higher than 2, the azimuthal variation disappears and the $\cos^2\phi$ term averages to 0.5.

Making use of this expression, and the very strong horizontal polarisation of synchrotron radiation sources, it is possible to determine the adsorption site by measuring the variation of SEXAFS amplitudes with the angle of incidence (and, in the case of 2-fold symmetric surfaces, with azimuthal angle). For example, consider the situation of an atom adsorbed directly atop a substrate atom. At normal incidence, the amplitude of the SEXAFS, due to nearest neighbour, will be zero, whereas at grazing incidence the amplitudes from this neighbour will be very strong.

This amplitude variation is not as useful for L_3 edges, however. Unlike the situation for an s initial state (where the photoelectron will be a p-wave), a p initial state will give rise to a final state of mixed s and d waves. This modifies the expression for the effective coordination number to,

$$N_j^* = 0.7N_j + 0.9\sum_{i}^{N_j}\cos^2\theta_{ij} \qquad (2.9.2)$$

This constant term in the effective coordination number reduces the dependence of the SEXAFS amplitudes on the direction of the electric vector, and so makes adsorption site determination more difficult.

The second way in which adsorption sites can be determined is by extraction of the second nearest neighbour distance. This recquires data of high quality because of the $1/R^2$ fall off in EXAFS amplitude, and so is rarely used. If the second nearest neighbour distance is found, this can be used to narrow down the number of possible sites.

A combination of these two methods of site determination can be used if a simulation program such as EXCURVE is used. In such a program each possible site can be modelled by setting up a suitable cluster of scatterers. The structural input for such a simulation is the effective coordination number of, and distance to, each shell. By comparing the simulation for each site with data collected at several angles of incidence, and modifying the inter-atomic separations if necessary, the adsorption site can be determined.

One major limitation of SEXAFS is that it can only be used effectively for the study of adsorbates: it is not, in general, possible to separate the surface and bulk signals for clean surfaces. Despite this, there are still a great number of systems to which it can be applied. One area in which it may be possible for SEXAFS to make a useful contribution is to the study

of molecular adsorbates: site identification for these has rarely been achieved. The advantage SEXAFS has over other techniques is that it depends only on local order, unlike diffraction methods such as LEED. This means that SEXAFS can be used to study systems for which no long range ordered structures are found. Another advantage of SEXAFS for the study of molecular adsorbates is that the probe is a photon. Electron beams which are used in other techniques can cause the molecule to dissociate on the surface.

2.10 NEAR EDGE X-RAY ABSORPTION FINE STRUCTURE

The X-ray absorption structure that lies up to about 50eV above the threshold is generally discarded in EXAFS analysis, because it is more strongly influenced by multiple scattering, and the phase shifts will be more chemically dependent. This multiple scattering makes the Near Edge X-ray Absorption Fine Structure (NEXAFS), or X-ray Absorption Near Edge Structure (XANES) as it is sometimes called, difficult to analyse. In spite of this, it has received much attention because it contains a great deal of structural information that cannot be obtained from EXAFS. In general, analysis of near-edge structure[22] has used multiple scattering calculations similar to those used in Low Energy Electron Diffraction[2].

The near-edge structure of many low Z diatomic molecules is dominated by two large resonances[23]. In molecules with multiple bonding, there is a very sharp

resonance (width ~ 2-3eV) situated on the absorption threshold. Centred at between 5 and 20 eV above this, is a very broad resonance (which occurs in all low Z diatomic molecules). These resonances have been assigned to excitation to antibonding molecular orbitals and to multiple scattering between the two atoms of the molecules, respectively. Using these two assignments and a knowledge of the symmetry of the final states it is possible to extract structural information from near-edge structure, without resort to complex and time consuming multiple scattering calculations.

2.11 π RESONANCE

The carbon near-edge absorption spectrum for CO adsorbed on Ni(100) (see Figure 2.4) shows a very sharp resonance on the absorption threshold. This resonance has been shown to correspond[23] to a transition from a carbon 1s electron to an unoccupied antibonding molecular orbital of π symmetry (i.e. an orbital which is antisymmetric with respect to the molecular axis). To be precise, this is an excitation of the 1s electron into, in the case of CO, the empty 2π molecular orbital. For neutral, gas phase CO this orbital lies above the vacuum level, but the coulomb interaction of the electron in this state with the core hole produced by the absorption process, lowers its energy to below the vacuum level: hence the so called π-resonance is a bound state resonance. It should be noted that the π-resonance is only present for species with multiple bonds.

FIGURE 2.4 Carbon K-Edge of CO on Ni(100) taken from ref. 23.

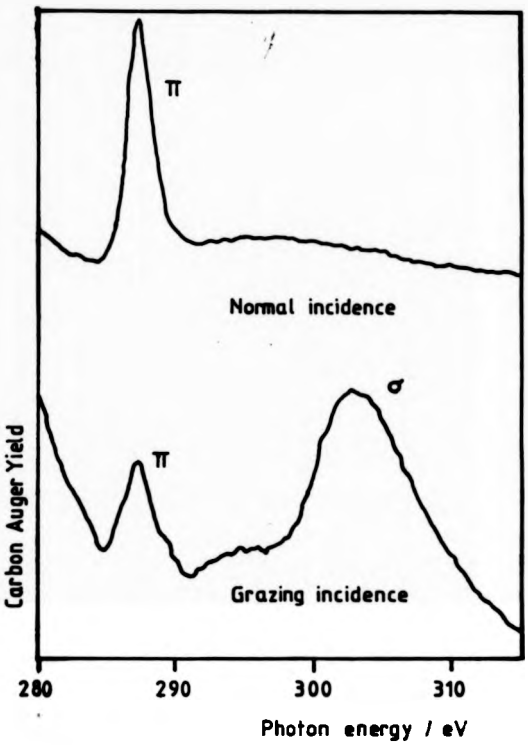

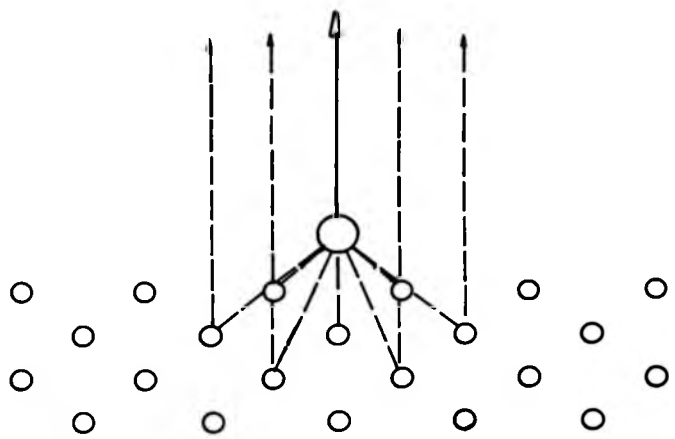

FIGURE 2.5 Schematic diagram of photoelectron diffraction.

2.12 σ-RESONANCE

The broad resonance which lies about 20eV above the π-resonance, is known as a shape resonance[24]. This structure is caused by an enhancement of the photo-absorption cross-section due to resonant multiple scattering between the oxygen and carbon atoms. This quasi-bound state, in which the photoelectron is trapped, is symmetric with respect to the molecular axis, and so is known as the σ-resonance.

This resonance can also be thought of in terms of molecular orbitals. Unfilled orbitals of σ symmetry which lie above the vacuum level enhance the continuum density of states in this energy region and so increase the intensity of the X-ray absorption.

2.13 POLARISATION DEPENDENCE

The two absorption resonances discussed here involve the excitation of an electron from the (spherically symmetric) 1s level to final states which are purely antisymmetric in the one case (π-resonance), and purely symmetric in the other (σ-resonance). Using this knowledge and the dipole selection rules, it is possible to extract from the variation of resonance intensity with the direction of the polarisation vector, the orientation of the molecular axis. This dependence has been derived by Stöhr and Jäger[23] by taking the known expression for angle resolved photoemission[25] and integrating over all possible electron emission angles.

It was found that the σ-resonance intensity is proportional to $\cos^2\theta$ (where θ is the angle between the molecular axis and the electric vector), whereas the π-resonance intensity varies as $\sin^2\theta$.

2.14 INTRA-MOLECULAR BOND LENGTHS FROM THE POSITION OF THE σ-RESONANCE

As the σ-resonance derives from multiple scattering of the photoelectron along the axis of a diatomic molecule, it is a reasonable idea that the wavevector (and so energy) of this resonance should be related to the intra-molecular bond length. A study of CO, HCOO and CH_3O adsorbed on Cu(100)[26] indicated the possibility of such a relationship. The σ-resonance (measured at the O K-edge) was found to peak at the highest energy position for CO, followed by HCOO and CH_3O. This trend is interesting because the O-C bond length is shortest for the triple bonded CO (1.13Å) and longest for the single bonded CH_3O (1.43Å).

The theoretical frame work for this relationship has been studied by several workers[27] using multiple scattering theory, and the position of the resonance has been found to be related to the intra-molecular bond length as follows.

$$(\delta - V_0)R^2 = C_0 \qquad (2.14.1)$$

where δ is the difference in energy between the σ-resonance and the 1s binding energy (referenced to the

vacuum level). V_0 is the mean intra-molecular potential (also relative to the vacuum level), R is the intra-molecular bond length and C_0 is a constant which is dependent upon the atomic phase shifts of the scattering atoms. Subsequent empirical studies of gas phase molecules by Sette et al.[28,29] have found that for a given total Z (e.g. CO. N_2 $Z_{sum}=14$) the relationship between δ and R is linear. This could only be made compatible with equation (2.14.1) if V_0 is a function of R. The variation of δ with Z was also explained by making V_0 a function of Z.

Using these relationships it should be possible to find the intra-molecular bond length of most molecules (containing 1st row periodic table elements) by measuring the position of the σ-resonance and the binding energy of the core electron. It should be noted that these relationships break down for linear tri-atomic molecules where forward scattering (which is much stronger than back-scattering) by the central atom will cause the third atom to have a significant effect on the σ-resonance.

2.15 APPLICATION TO SURFACES

Several factors make NEXAFS a potentially useful tool for surface science. The large size of the near-edge resonances with respect to the absorption edge means that the signal to noise ratio necessary is smaller than that for EXAFS: an important difference considering the small number of atoms involved in an adsorption

system. The behaviour of the resonances is most easily interpreted for small organic molecules and it is these that are of interest to surface scientists for use in model reaction systems. The most useful feature of NEXAFS, however, is the dependence of the intensity on the angle between the electric vector and the molecular axis. This polarisation dependence, which is unimportant for gas phase studies, becomes a very valuable tool for chemisorption systems where the symmetry is reduced by the presence of the surface.

Several chemisorption systems have been studied, mainly by Stöhr and co-workers, on single crystal surfaces. These include C_2H_4[30,32], C_2H_2[32] and C_4H_4S[31] on Pt(111), CO, NO, N_2 on Ni(100)[23,33] and CO, CH_3O and HCOO on Cu(100)[26,34]. In these experiments the use of NEXAFS has enabled the molecular orientation with respect to the surface plane to be found. All these experiments, however, involved surfaces of three or four fold symmetry, so it was not possible to extract an azimuthal orientation (this is a similar problem to that found in SEXAFS).

2.16 PHOTOELECTRON DIFFRACTION

If photoemission from a core state of an atom on a surface is measured using an angle resolved detector, then its intensity will be influenced by scattering of the electron wave by neighbouring atoms (Figure 2.5). This variation of photoemission intensity due to interference of the direct and scattered waves can be used

as a probe of the surface structure. This diffraction effect can be recorded, either as a function of take off angle for constant electron kinetic energy, or as a function of photon (and so electron) energy at a fixed take off angle. Only the latter was used in this work, so only this method will be considered here.

The analysis of photoelectron diffraction (PD) data was generally thought to require sophisticated multiple scattering calculations[35] because the electron energies typically used are similar to those in LEED. It is necessary to use reasonably low electron energies otherwise the back-scattering magnitude becomes so small that sizeable interference effects can only be obtained at grazing take off energies where forward scattering is important. Recently, however, studies have shown that single scattering calculations can provide useful information on the structure of adsorbates on surfaces[36], for data collected in the 100-400eV range.

In justifying the applicability of a single scattering approach to PD, it is useful to compare the technique with EXAFS which is known to be dominated by single scattering. One of the main reasons for the insensitivity of EXAFS to multiple scattering, is that it is an intensely local probe; the electron source is highly localised on the atom under study. This, of course, is also true for PD, but not for LEED where the probe is an incident plane wave. This difference in probe means that LEED is sensitive to the two dimensional periodicity of the surface, whereas EXAFS (and so PD to a lesser extent) is sensitive mainly to the nearest one or two

shells of atoms: the contribution of different atoms falling off as $1/R^2$ for EXAFS and $1/R$ for PD. This localisation in EXAFS is further enhanced by the effects of correlated and uncorrelated thermal vibrations; the mean square difference in displacement is much less for the nearest neighbour than for any others[37]. These arguments in favour of the application of small cluster, single scattering calculations in EXAFS also apply to PD. Using similar approximations as have been used in EXAFS (in particular, the plane wave and single scattering approximations), the intensity of photo-emission from an initial s-state can be given as[36],

$$I(k) \propto \left| \cos\theta_k + \sum_j [\cos\theta_j / r_j] f(\theta_j, k) w(\theta_j, k) \exp[-L_j/\lambda(k)] \exp[ikr_j(1-\cos\theta_j)] \right|^2 \qquad (2.16.1)$$

where the first term gives the directly emitted component at an angle θ_k with respect to the electric vector. The remaining term is the component due to the sum of scattering from neighbouring atoms (at a distance r_j). θ_j is the scattering angle at the j th scatterer and $\cos\theta_r$ gives the amplitude incident on this atom. $f(\theta_j, k)$ is the scattering factor and $w(\theta_j, k)$ is a Debye-Waller factor. $\lambda(k)$ is the mean free path length and L_j is the additional path. The final term introduces the phase shift due to the extra path length.

CHAPTER 2 : REFERENCES

1) L.J. Clarke, "Surface Crystallography: An Introduction to Low Energy Electron Diffraction", John Wiley & Sons Ltd., (1985).

2) J.B. Pendry, "Low Energy Electron Diffraction", Academic Press, (1974).

3) J.T. Grant, Appl. Surf. Sci. 13, 35-62 (1982).

4) B.M. Kincaid and P. Eisenberger, Phys. Rev. Lett. 34, 1361-1364 (1975).

5) L. Azaroff, Rev. Mod. Phys. 35, 1012 (1963).

6) D.E. Sayers, F.W. Lytle and E.A. Stern, "Advances in X-ray Analysis", ed. B.L. Henke, J.B. Newkirk and G.R. Mallet (Plenum, New York, 1970), 13, 248-271.

7) C.A. Ashley and S. Doniach, Phys. Rev. B11, 1279-1288 (1975).

8) P.A. Lee and J.B Pendry, Phys. Rev. B11, 2795-2811 (1975).

9) B.K. Teo and P.A. Lee, J. Am. Chem. Soc. 101, 2815-2832 (1979).

10) D.E. Sayers, E.A. Stern and F.W. Lytle, Phys. Rev. Lett. 27, 1204-1207 (1971).

11) C.H. Reinsch, Numerische Mathematik 10 177-183 (1967).

12) P.A. Lee, P.H. Citrin, P. Eisenberger and B.M. Kincaid, Rev. Mod. Phys. 53, 769-806 (1981).

13) S.J. Gurman, N. Binsted and I. Ross, J. Phys. C17, 143-151 (1984).

14) E. Pantos and G.D. Firth, "The EXAFS Database: Proposed Specification", Daresbury Laboratory technical memorandum, DL/CSE/TM21, October 1982.

15) D.P. Woodruff, D. Norman, B.W. Holland, N.V. Smith, H.H. Farrell and M.M. Traum, Phys. Rev. Lett. 41, 1130-1133 (1978).

16) J. Stöhr, E.B. Kollin, D.A. Fischer, J.B. Hastings, F. Zaera and F. Sette, Phys. Rev. Lett. 55, 1468-1471 (1985).

17) R.G. Jones and D.P. Woodruff, Surf. Sci. 114, 38-46 (1982).

18) R. Jaeger, J. Feldhaus, J. Haase, J. Stöhr, Z. Hussain, D. Menzel and D. Norman, Phys. Rev. Lett. 45, 1870-1873 (1980).

19) J. Stöhr, R. Jaeger and S. Brennan, Surf. Sci. 117, 503-524 (1982).

20) S. Ainsworth and D.P. Woodruff, Sol. St. Comm. 56, 461-463 (1985).

21) G. Martens and P. Rabe, J. Phys. C14 1523-1534 (1981).

22) D. Norman, J. Stöhr, R. Jaeger, P.J. Durham and J.B. Pendry, Phys. Rev. Lett. 51, 2052-2055 (1983).

23) J. Stöhr and R. Jaeger, Phys. Rev. B26, 4111-4131 (1982).

24) S. Wallace, D. Dill and J.L. Dehmer, J. Chem. Phys. 76, 1217-1222 (1982).

25) J.W. Davenport, J. Vac. Sci. Technol. 15, 433-439 (1978).

26) J. Stöhr, J.L. Gland, W. Eberhardt, D. Outka, R.J. Madix, F. Sette, R.J. Koestner and U. Döbler, Phys. Rev. Lett. 57, 2414-2417 (1983).

27) A. Bianconi, M. Dell'Ariccia, A. Gargano and C.R. Natoli, "EXAFS and Near Edge Structure", pp. 57-61, Springer-Verlag (1983).

28) F. Sette, J. Stöhr and A.P. Hitchcock, J. Chem. Phys. 81, 4906-4914 (1984).

29) F. Sette, J. Stöhr and A.P. Hitchcock, Chem. Phys. Lett. 110, 517-520 (1984).

30) R.J. Koestner, J. Stöhr, J.L. Gland and J.A. Horsley, Chem. Phys. Lett. 105, 332-335 (1984).

31) J. Stöhr, J.L. Gland, E.B. Kollin, R.J. Koestner, A.L. Johnson, E.L. Muetterties and F. Sette, Phys. Rev. Lett. 53, 2161-2164 (1984).

32) J. Stöhr, F. Sette and A.L. Johnson, Phys. Rev. Lett. 53, 1684-1687 (1984).

33) J. Stöhr, K. Baberschke, R. Jaeger, R. Treichler, and S. Brennan, Phys. Rev. Lett. 47, 381-384 (1981).

34) J. Stöhr, D. Outka, R.J. Madix and U. Döbler, Phys. Rev. Lett. 54, 1256-1259 (1985).

35) N.V. Smith, H.H. Farrell, M.M. Traum, D.P. Woodruff, D. Norman, M.S. Woolfson and B.W. Holland, Phys. Rev. B21, 3119-3130 (1980).

36) D.P. Woodruff, submitted to Surface Science.

37) E.A. Stern, D.E. Sayers and F.W. Lytle, Phys. Rev. B11, 4836-4846 (1975).

CHAPTER 3 EXPERIMENTAL DETAILS

3.1 INTRODUCTION

In this chapter brief details of the experimental systems are given. The experiments were carried out using synchrotron radiation from the SRS at Daresbury and from BESSY in Berlin. The experimental chamber at each location was of standard stainless steel U.H.V construction and had a typical base pressure of 1×10^{-10} mbar after baking at 180° for about eight hours. The procedures used in forming the adsorbate structures to be studied. are outlined and any specific problems encountered are discussed.

3.2 DARESBURY SYSTEM

The experimental chamber used at Daresbury was a two level system (Figure 3.1) of standard stainless steel construction. The chamber, which was dedicated to SEXAFS measurements, was equipped in the upper level with a V.G. Scientific D.C. discharge argon ion gun and an electrochemical cell for chlorine dosing (a brief description is given in Section 3.5). It was on this upper level that samples were prepared. Crystal manipulation was carried out using a V.G. HPT model which was equipped with two rotational (polar and azimuthal), and three translational, motions. Sample heating was achieved by conduction/radiation from a filament behind the crystal (Figure 3.2) and the crystal temperature

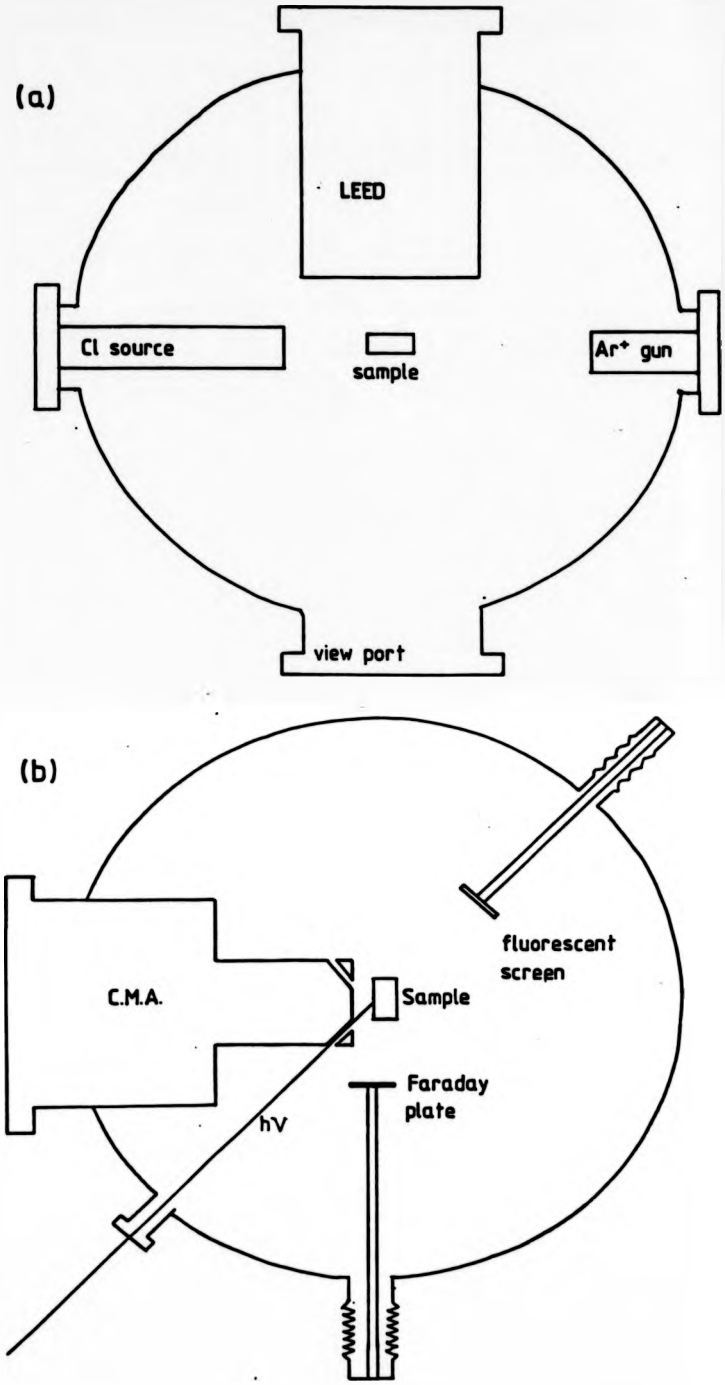

Figure 3.1 The Daresbury experimental chamber; upper level (a) and lower level (b).

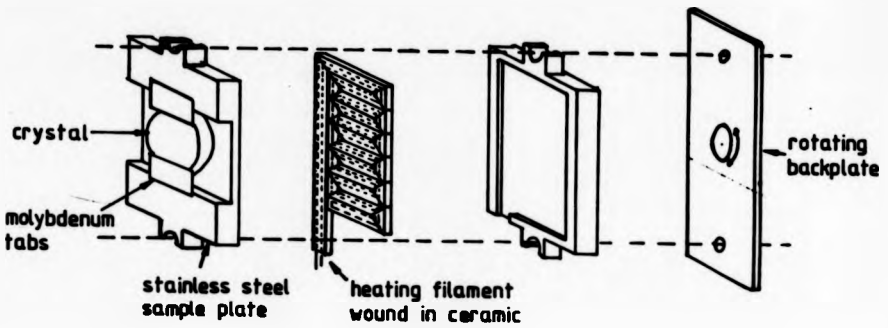

Figure 3.2 The sample holder used at the SRS.

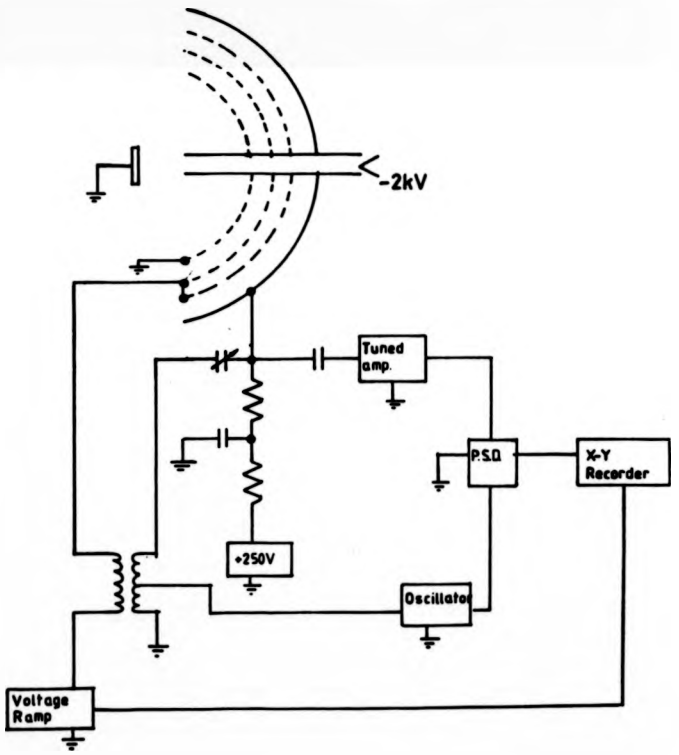

Figure 3.3 Auger electron spectroscopy using the R.F.A.

was monitored using a chromel-alumel thermocouple. Sample cleanliness was checked by A.E.S. using the retarding field analyser of the LEED system (Figure 3.3).

The X-ray absorption measurements were carried out on the lower level of the chamber. This was equipped with a Cambridge Consultants Ltd. Concentric Hemispheres Analyser (CHA) and a Faraday plate for total electron yield detection (each of these was at 45° to the light). This level was also equipped with a fluorescent plate to facilitate sample positioning. The quality of the vacuum could be measured using standard Bayerd-Alpert ionisation gauges and a V.G. Gas Analysis SX700 residual gas analyser.

The SEXAFS chamber is situated on beamline 6.3. This beamline has a toroidal premirror, upon which the synchrotron radiation impinges at a grazing angle (0.5°), with its focal point in the experimental chamber. Single energy X-ray selection is achieved using a double crystal monochromator[1]. A schematic of the monochromator is shown in Figure 3.4. Monochromation was achieved by Bragg reflection from the two crystals. The crystals used here were Ge(111), although Ge(220) and InSb(111) were also available. The two crystals were controlled by three stepper motors, giving independent rotation to each, and translational motion to the second crystal. To select a particular energy, the monochromator worked as follows. The crystals were rotated to the angle which would define the required energy, and the second crystal was moved so that the Bragg reflection from the first crystal fell upon its centre. The first crystal was

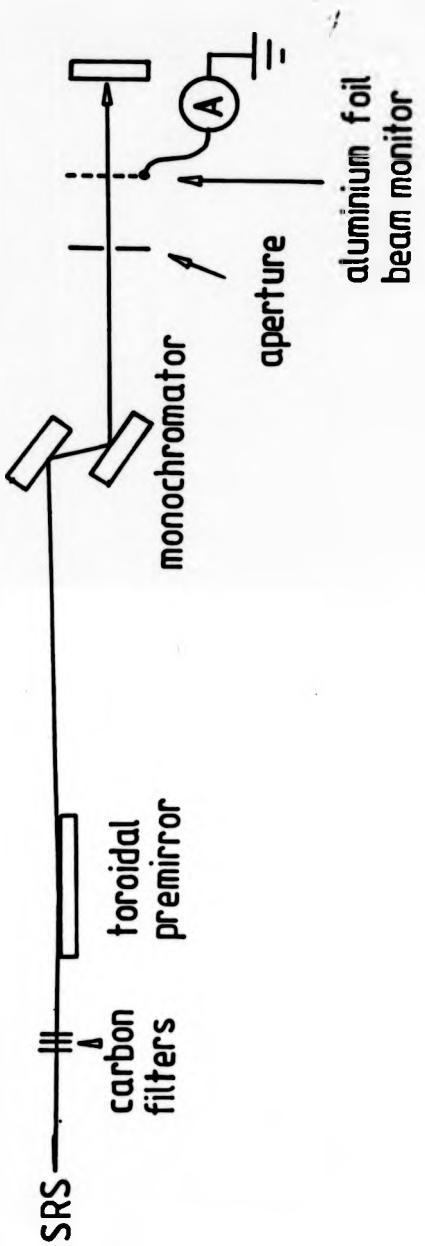

Figure 3.4 Schematic of beamline 6.3 at the SRS.

then rocked to maximise the output intensity (the peak-finding procedure). This peak-finding was complicated by the heating of the first crystal due to the (white) synchrotron radiation. This resulted in a change in the lattice parameter (and so Bragg angle for specific energy) which was dependent on beam intensity. This resulted in the Bragg peak often being far away from the expected position. The peak-finding routine which achieved this, was developed jointly by Drs. R.G. Jones and J.C. Campuzano and staff at Daresbury Laboratory. The monochromator has an energy range of 2-10keV and a resolution of about 1eV at the chlorine K-edge.

Ultra-violet radiation, which could pass through the monochromator by reflection off the crystal surfaces, was filtered out of the beam using carbon films of 1 micron thickness. Situated between the monochromator and the experimental chambers were a set of apertures, which could be used to define the size of the X-ray spot on the sample, and a beam monitor consisting of a 1 micron thick aluminium foil. The beam monitor was necessary to normalise out structure in the beam that was a product of the beamline optics and random fluctuations in the signal from point to point, introduced by the peak-finding routine. This foil could be cleaned by ion bombardment with argon or oxygen.

The analogue current drain from the Faraday plate for Total Electron Yield (TEY) mode was measured using a Keithley Solid State Electrometer. The output of this was converted to a digital signal by a voltage to frequency converter. The photoelectron diffraction

measurements were made using the CHA in pulse counting mode.

The whole experiment (monochromator control, signal counting and CHA) was under the control of a DEC PDP11/34 minicomputer. The software for the SEXAFS experiments was provided by Daresbury Laboratory and the software for the photoelectron diffraction experiments was written by Drs. C.E. Riley and R.G. Jones.

3.3 BESSY SYSTEM

The experimental system used at BESSY (Fig. 3.5) was similar to that used at Daresbury in that it was a two level system. The upper, sample preparation, level was equipped with a Varian LEED system and Physical Electronics argon ion gun. The lower level was equipped with a Physical Electronics double pass Cylindrical Mirror Analyser (CMA) and a Partial Electron Yield (PEY) detector. The PEY detector[2] excluded all electrons of energy below 400eV by means of a set of retarding grids. The electron yield was measured using a channel plate in analogue mode driven off a battery box, with the drain current to earth being measured by a Keithley electrometer (Fig. 3.6). This signal was digitised in a similar way to the Daresbury system.

The measurements reported here were made using the SX700 monochromator[3], although preliminary experiments were carried out on the High Energy TGM[4]. The SX700 monochromator comprises a plane premirror, a plane diffraction grating (600 lines/mm) and an elliptical

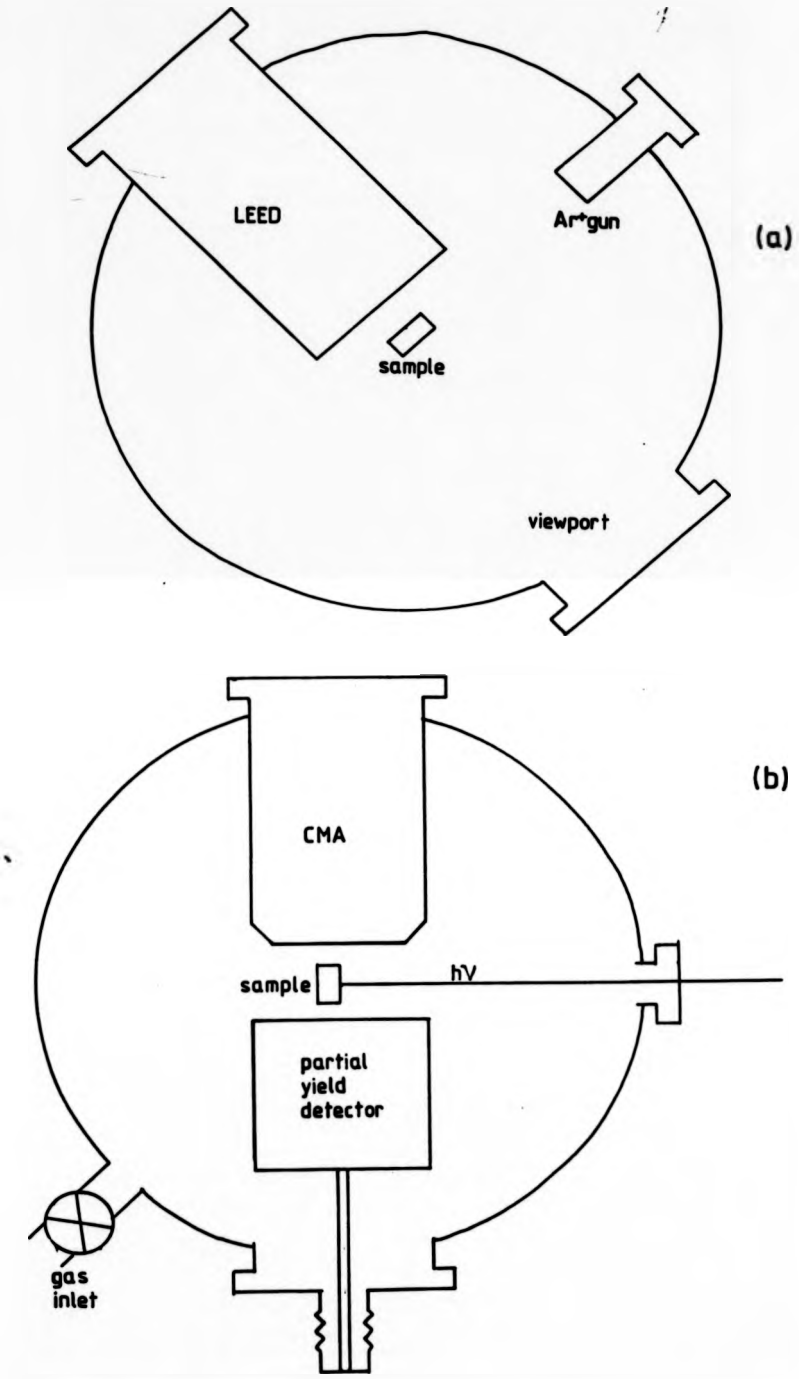

Figure 3.5 The experimental chamber used at BESSY showing the upper (a)- and lower (b) levels.

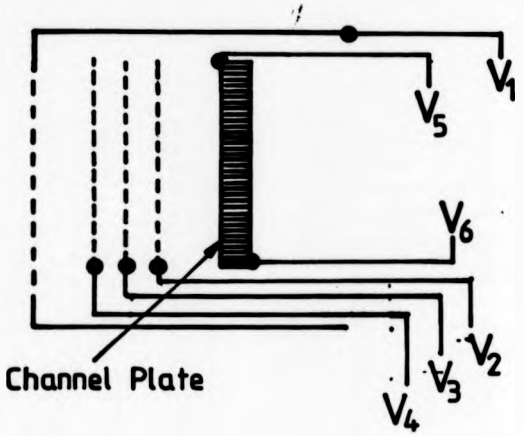

Figure 3.6 The partial electron yield detector.

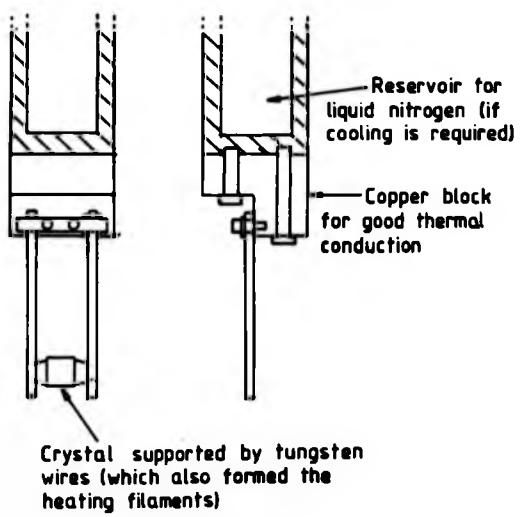

Figure 3.7 The sample holder used at BESSY.

post-focussing mirror. This monochromator and the counting electronics were also under the control of a DEC computer.

The manipulator used here was similar to the one at Daresbury but it did not possess an azimuthal drive. This meant that the system had to be opened up to air to change the azimuth of the crystal. The sample was suspended from two tungsten filaments. which also formed the sample heating system (Fig. 3.7). The sample temperature was monitored using a chromel-constantan thermocouple.

3.4 SAMPLE PREPARATION

The samples consisted of slices spark-machined from a single crystal bar, after orientation to ±1° by Laue diffraction. The dimensions of the crystals were approximately 12mmx12mmx1-2mm thick. Ex-situ sample preparation consisted of polishing with diamond paste down to a grade of 1 micron, followed by electro-polishing.

In-situ sample preparation consisted of cycles of argon ion bombardment at 1-2keV, 20μA at the Daresbury system and at 0.8keV, 15μA at BESSY for 15-20 minutes, followed by annealing to temperatures of between 600K and 800K. Sample cleanliness was checked using AES, and surface order by LEED.

3.5 CHLORINE ON Cu(111)

Sample dosing was accomplished using an electrochemical cell based on a design by Spencer et al.[5] (Fig. 3.8). This consists of a pellet of AgCl doped with 4% $CdCl_2$ to improve its ionic conductivity. The whole cell was heated to approximately 160°C by passing a small current (about 10mA) through a resistive coating of SnO_2 deposited on the outside of the glass tube. An excess of chlorine ions was produced at the anode by passing a current of about 50μA through the pellet. This excess chlorine then evaporated as molecular Cl_2. The glass tube collimated these molecules into a beam which could be directed at the crystal.

The clean crystal was dosed using the cell until a sharp $(\sqrt{3}\times\sqrt{3})R30°$ LEED pattern was seen (Fig.3.9). The TEY SEXAFS measurements were then made using the Faraday plate at the SRS at Daresbury. In collecting the SEXAFS spectra, it was found that the Cu K-edge (8979eV) intruded into the Cl K-edge (2820eV) SEXAFS region at about 3000eV due to the presence of higher energy radiation in the beam originating from third order Bragg reflection from the monochromator. This was remedied by rocking the upper monochromator crystal off the Bragg peak until the radiation intensity had dropped to 80% of its maximum value. This had the effect of eliminating the third order radiation because its rocking curve is much narrower than that for first order reflection. It should be noted that the experiments were carried out during a period of running at 1.8GeV (compared with the

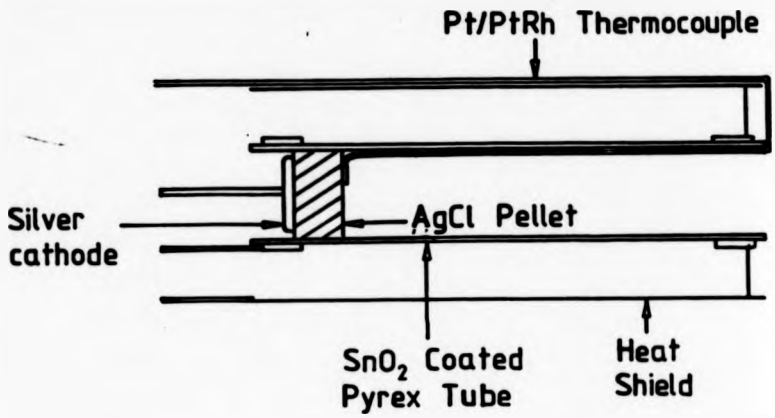

Figure 3.8 The electrochemical cell used for chlorine dosing.

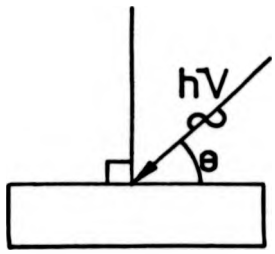

Figure 3.10 Definition of the angle of incidence used throughout.

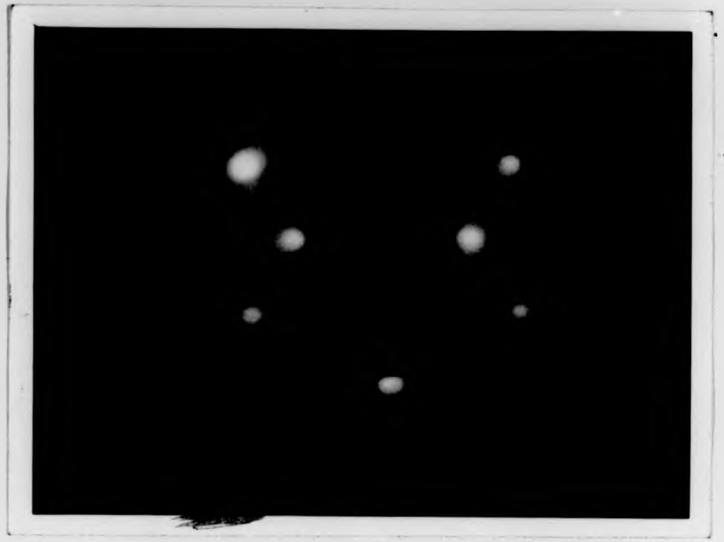

(a)

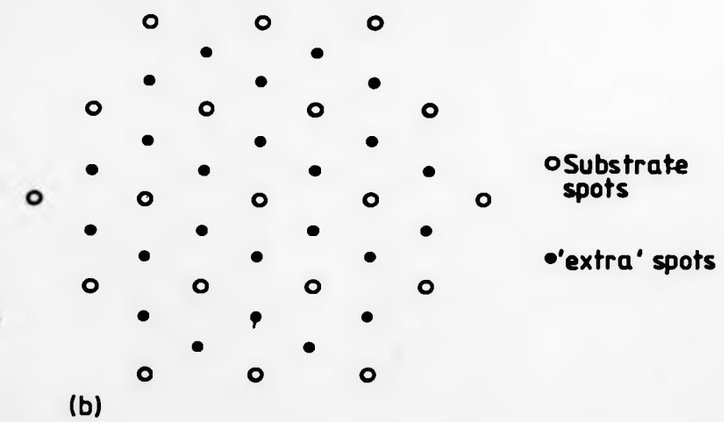

(b)

Figure 3.9 The Cu(111)[√3x√3]R30°-Cl LEED pattern at Ep=100eV (a) and a schematic of the pattern (b).

(a)

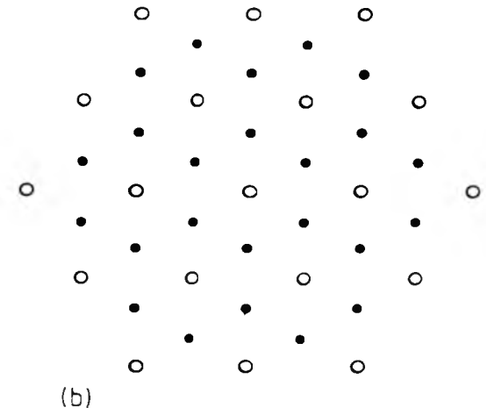

(b)

Figure 3.9 The Cu(111)[√3x√3]R30°-Cl LEED pattern at Ep=100eV (a) and a schematic of the pattern (b).

SX700 monochromator.

Dosing with formic acid was carried out by raising the whole chamber to a pressure of 10^{-7}torr for 100 seconds (10 Langmuirs). It was found necessary to reduce the vapour pressure of formic acid to improve control during dosing. This was achieved by cooling the flask in a slurry of acetone and liquid nitrogen. Dosing was carried out at room temperature.

The measurements of the NEXAFS were made in Auger mode by tuning the pass energy of the CMA to the oxygen KLL Auger peak at 511eV. The SEXAFS measurements were made in PEY mode using the high pass filter which excluded all electrons with energy less than 400eV.

It was not possible to have a beam monitor because of the short focal length of the SX700, but it was found that the light intensity from this monochromator was very stable and repeatable so the effect of this was not significant (especially since all the spectra were produced by multi scanning). This absence of point to point intensity fluctuations, which is in complete contrast to the monochromator at Daresbury, is due to the single dispersing element design of the SX700. Structure in the light intensity as a function of energy due to the characteristics of the monochromator were removed by subtracting clean surface spectra from covered surface spectra, after normalisation to the X-ray absorption before the edge. All spectra reproduced here are such subtraction spectra.

3.7 ETHANOL ON Cu(110)

The ethanol experiments were very similar to those involving formic acid. Dosing was achieved by raising the chamber pressure to 10^{-7} torr of ethanol or oxygen for the requisite amount of time. It was not found to be necessary to cool the ethanol due to its lower vapour pressure. The major difference between this experiment and the previous ones was the need for sample cooling. This was accomplished by filling the tube which supported the sample holder with liquid nitrogen (Figure 3.7).

3.8 CuCl MODEL COMPOUND

The model compound used to obtain the phase shifts for analysing the Cu(111)[$\sqrt{3}$x$\sqrt{3}$]R30°-Cl structure was CuCl. A pellet of this was formed by compressing powder under vacuum. EXAFS were collected from this using the total electron yield method, in the same way as for surface EXAFS.

3.9 INCIDENCE ANGLES

The definition of incidence angles in surface EXAFS literature is different from that which is most commonly used in optics. In surface EXAFS, the grazing incidence angle is usually quoted; that is the angle between the surface plane and the direction of propagation of the X-rays (see Figure 3.10). All angles of

incidence given in this thesis are such grazing incidence angles and not the (more usual) angle between the surface normal and the direction of propagation.

CHAPTER 3: REFERENCES

1) A.A. MacDowell, D. Norman, J.B. West, J.C. Campuzano, and R.G. Jones, Nuc. Inst. Meth. in press.

2) U. Döbler, K. Baberschke, J. Haase and A. Puschmann, Phys. Rev. Lett. 52, 1437 (1984).

3) H. Petersen, Optics Commun. 40, 402-406 (1982).

4) E. Dietz, W. Braun, A.M. Bradshaw and R.L. Johnson, Nuc. Inst. Meth. A239, 349 (1985).

5) N.D. Spencer, P.J. Goddard, P.W. Davies, M. Kitson and R.M. Lambert, J. Vac. Sci. Technol. A1, 1554-1555 (1983).

CHAPTER 4 ADSORPTION OF Cl ON Cu(111)

4.1 INTRODUCTION

The $(\sqrt{3}\times\sqrt{3})R30^\circ$ overlayer of chlorine on copper has been studied by the two related techniques of SEXAFS and photoelectron diffraction. The SEXAFS data has been analysed by both the single shell and multiple shell analysis methods. The single shell analysis was shown to be adequate for this simple, high symmetry overlayer. Both analysis methods indicated that absorption occured in the three-fold hollow, but neither could distinguish between the two possible hollows. This distinction was made using photoelectron diffraction which retains azimuthal information, even on this three-fold symmetric surface.

4.2 STUDIES OF Cl_2 ADSORPTION ON SILVER AND COPPER

The adsorption of chlorine on close packed silver and copper surfaces has been the subject of a certain amount of controversy. LEED studies of chlorine overlayers on the Ag(100)[1] surface led to the conclusion that the chlorine atoms chemisorbed in a simple overlayer, which involved no major reconstruction of the metal surface; this is known as the Simple Overlayer Model (SOM). Subsequent photoemission studies[2], however, were believed to indicate that an epitaxial layer of AgCl was formed on the surface; this is known as the Mixed Layer Model (MLM). Studies of chlorine adsorption on

the Ag(111) suface[3,4] (where a $\sqrt{3}\times\sqrt{3}R30^\circ$ structure is found) also concluded that the MLM geometry was more appropriate.

In an attempt to resolve the discrepancies, Citrin et al.[5] carried out a study of a similar system, Cu(001)-c(2x2)Cl, using the techniques of SEXAFS and angle resolved photoemission. They found that the SOM geometry was the only one which could fit the SEXAFS results. A single shell analysis of the SEXAFS revealed a Cl-Cu bond length of 2.37±0.02Å, and the amplitude ratio for data collected at 90° (normal) incidence and 5° incidence revealed that the adsorption site was the four-fold hollow. This conclusion was supported by a LEED study of the same system[6,7,8]. LEED intensity analysis also revealed that the SOM geometry was correct and that the adsorption site was the four-fold hollow. The d-spacing which gave the best fit was 1.60±0.03Å (this gives a bond length of 2.41±0.02Å). This result is in fair agreement with the SEXAFS measurements and was regarded as the first reliable comparison of the two techniques. A subsequent study of Cl on Ag(111) and Ag(100) using SEXAFS[9] also indicated that SOM was the correct model. Multi-shell analysis revealed that the bond lengths of chlorine on Ag(111) and Ag(100) was 2.69±0.03Å and 2.70±0.01Å, respectively (this involved a small contraction with respect to the value for bulk AgCl of 2.77Å).

The system studied here is the adsorption of Cl_2 on Cu(111). This was first studied by Goddard and Lambert[10], who reported four ordered overlayers; in order of

increasing coverage ($\sqrt{3}\times\sqrt{3}$)R30°, ($12\sqrt{3}\times12\sqrt{3}$)R30°, ($4\sqrt{7}\times4\sqrt{7}$)R19.2° and ($6\sqrt{3}\times6\sqrt{3}$)R30°. Of these four surfaces, it is thought that only the first could correspond to simple adsorption, with every Cl atom in an equivalent site. The three higher coverage structures are thought to be caused by compression of the chlorine overlayer which gives rise to these coincidences at particular coverages. The ($\sqrt{3}\times\sqrt{3}$)R30° structure has also been studied using angle resolved photoemission[7].

The aim of this study was to use SEXAFS, and the related techniques of Normal and Off-normal Photoelectron Diffraction (NPD/OPD), to find the Cl-Cu bond length and to identify the adsorption site.

4.3 RESULTS: SEXAFS

SEXAFS spectra collected above the Cl K-edge from the ($\sqrt{3}\times\sqrt{3}$)R30° Cl overlayer (Fig. 4.1), at angles of 60° and 35° between the surface normal and the polarisation vector, are shown in Fig. 4.2 along with the spectrum for polycrystalline CuCl (zinc blende structure[11]). The surface spectra are the sum of several scans, each taking about one hour. The edge height is about 50% of the total signal for the bulk CuCl, whereas for the surface data it is about 1%. This is a clear indication of the problems in collecting surface, as opposed to bulk, EXAFS. Comparing the spectra, it can be seen that the SEXAFS modulations have a higher frequency for the surface species than for the bulk. This implies that the surface Cl-Cu bond length is expanded compared with

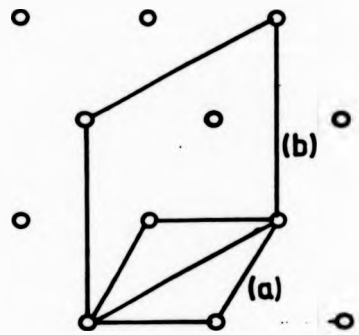

Figure 4.1 The Cu(111)[$\sqrt{3}$x$\sqrt{3}$]R30°-Cl structure, showing the relationship between the substrate mesh (a) and the overlayer mesh (b).

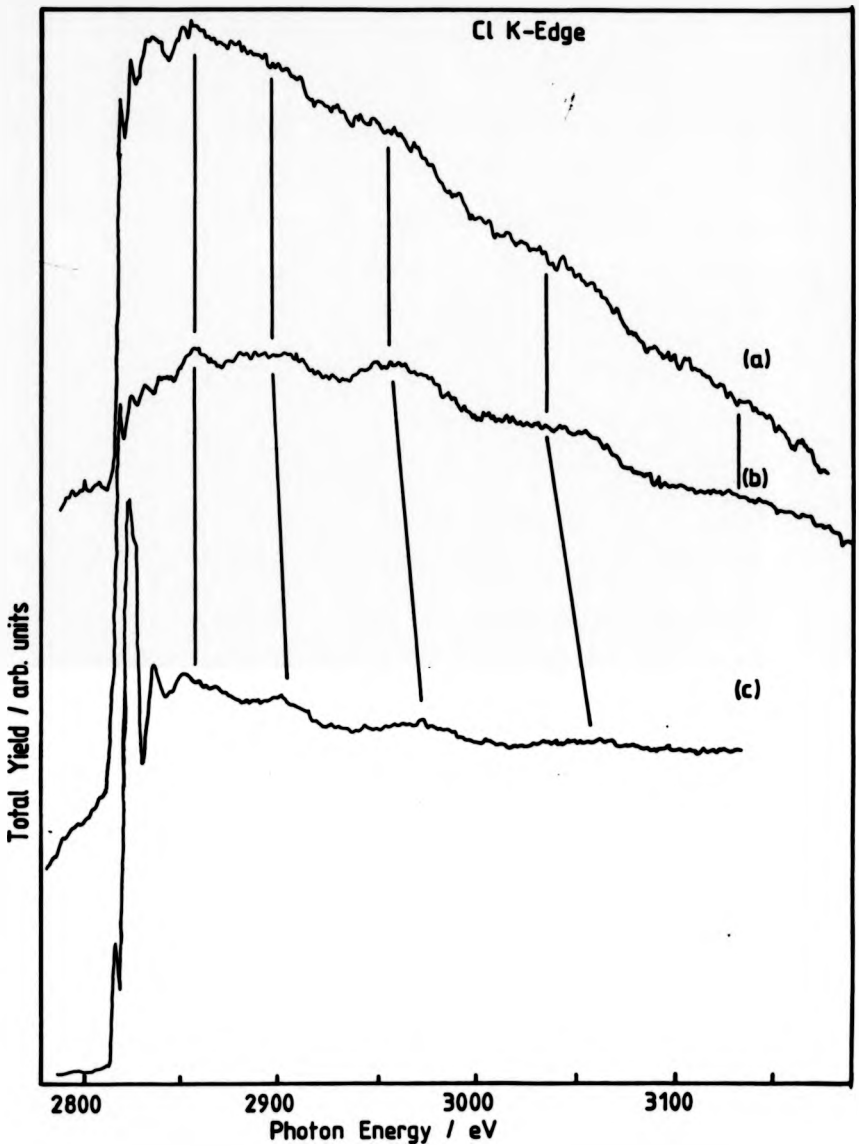

Figure 4.2 EXAFS from the Cu(111)[$\sqrt{3}$x$\sqrt{3}$]R30°-Cl at incidence angles of 60° (a) and 35° (b) and from bulk CuCl (c).

the bulk separation of 2.34Å. It should be noted that the amplitude variation between 60° and 35° (larger EXAFS at 35°) rules out the possibility of the central chlorine atom being co-planar with the copper scattering atom. This eliminates the mixed layer model, and so indicates that the system must be a simple overlayer.

4.4 ANALYSIS: SINGLE SHELL METHOD

The surface EXAFS was analysed using the single shell, Fourier filtering method. $\chi(k)$ was extracted by fitting a cubic spline to the EXAFS and normalising the modulations to the edge step. Fig. 4.3 shows the Fourier transforms of $k.\chi(k)$ using an E_0 of 2820eV. All three transforms are dominated by a peak at about 1.9Å, which corresponds to scattering from the nearest (copper) atom. The nearest neighbour contribution was isolated by multiplying by a window function and the product was back-transformed. Fig. 4.4 shows the back transform superimposed on the raw data. The difference in the phase of the inverse transforms of surface and bulk EXAFS, revealed a surface Cl-Cu bond length of 2.39±0.02Å (an expansion of 0.05±0.02Å).

The amplitude of the EXAFS envelope for both surface spectra was extracted and the ratio $N^{\circ}_{35}/N^{\circ}_{60}$ was found to be 1.25±0.05. Comparing this with the ratios of 2.67 for the atop site, 1.81 for the bridge site and 1.19 for the three-fold hollow, it can be seen that the hollow site is the most probable (Fig. 4.5).

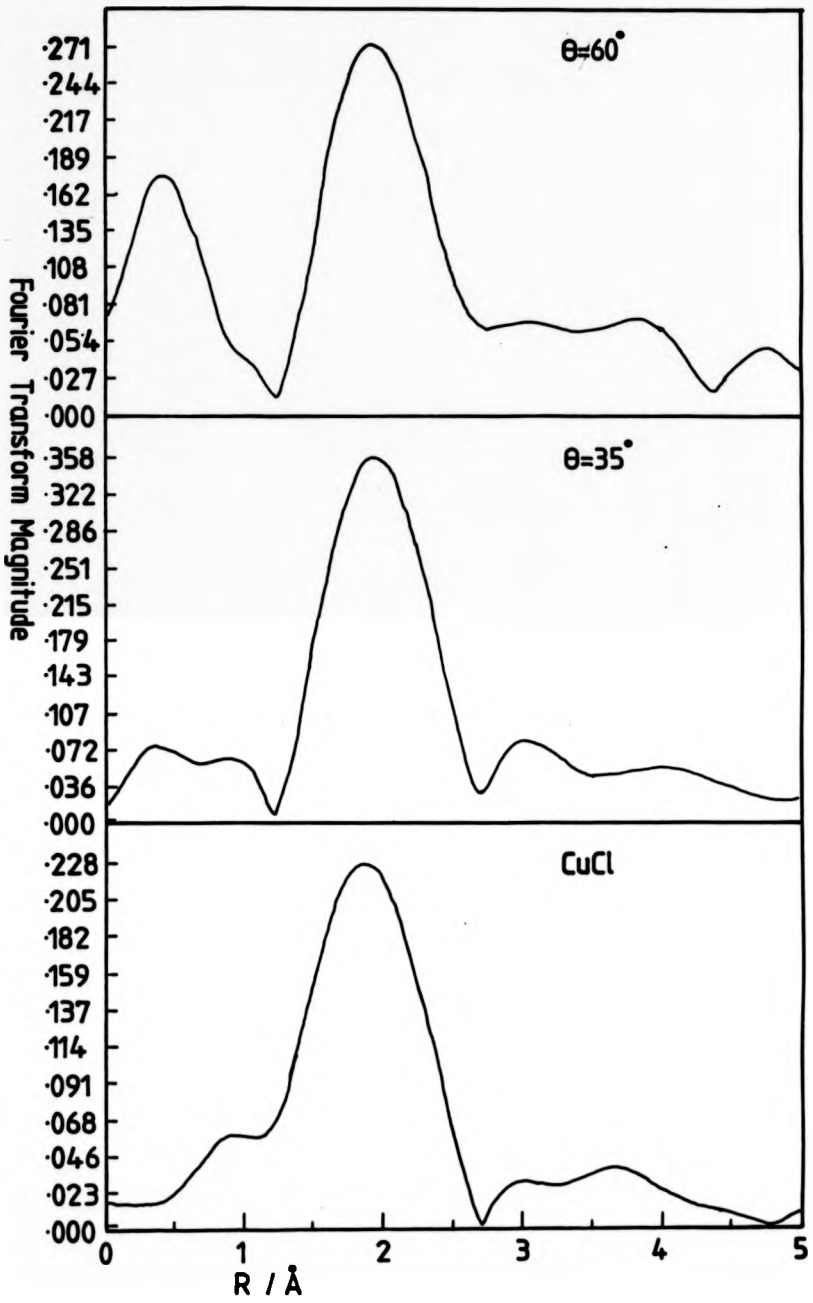

Figure 4.3 Fourier transforms of the EXAFS modulation functions.

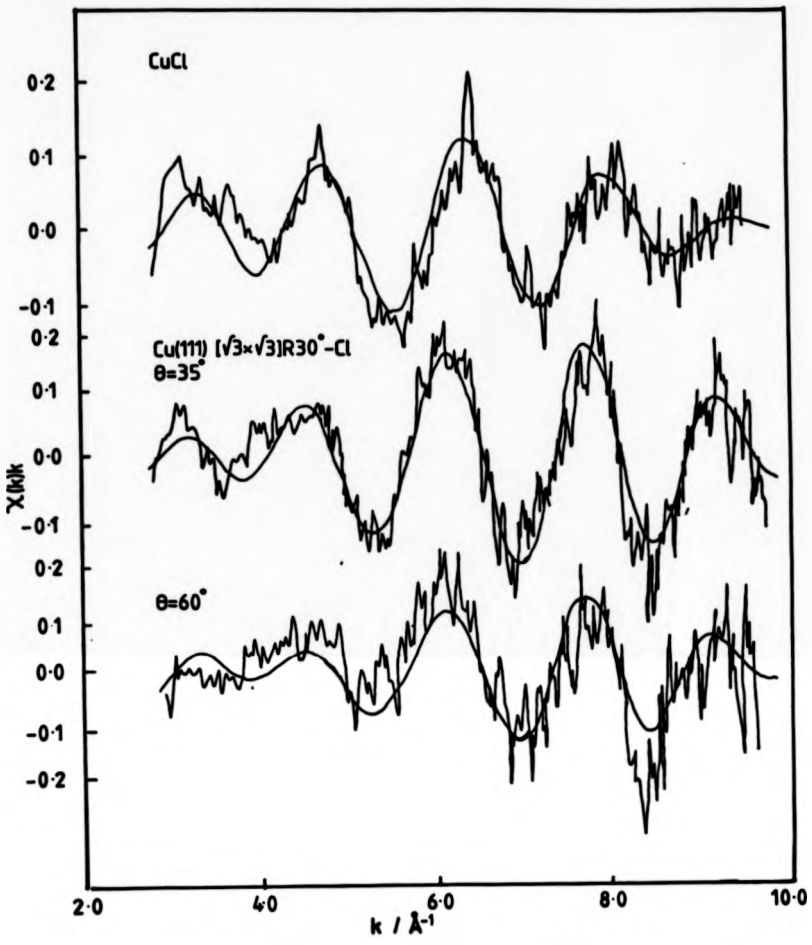

Figure 4.4 Inverse transforms superimposed on the raw data.

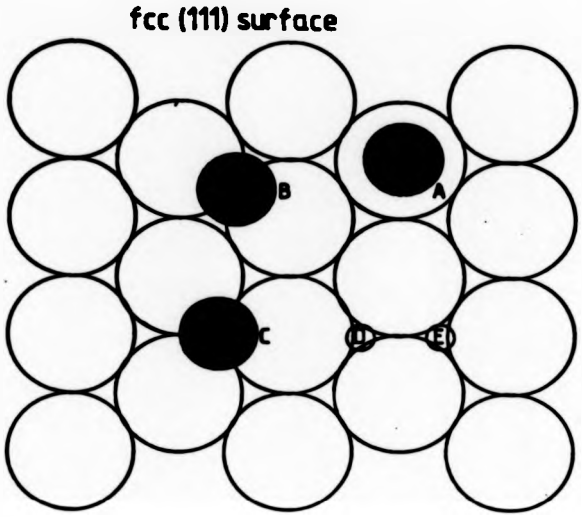

Figure 4.5 The high symmetry adsorption sites on an fcc (111) surface: the atop site (A), the bridge site (B) and the 3-fold hollow (C). Labels D and E indicate the two alternative 3-fold hollows.

4.5 ANALYSIS: MULTI-SHELL METHOD

A multiple shell simulation of the SEXAFS data was carried out in parallel with the single shell analysis. The first step was to simulate the EXAFS of bulk CuCl (zinc blende structure - see Table 4.1) using theoretical phase shifts from the Daresbury EXAFS database[12]. These phase shifts were then modified to obtain a best least mean squares fit to the data. For this simulation, the best fit was obtained with E_0=2818.5eV. The inelastic losses were included by using an imaginary potential, VPI=-5eV, and reductions in amplitude due to central atom relaxation and multi- electron effects[13], were introduced by using an amplitude factor, AFAC=0.6. The Debye-Waller factor used for shells 2-5 was $2\sigma^2=0.06\text{Å}^2$[14]. The value of $2\sigma^2$ used for the first nearest neighbour was 0.02Å^2 (this is less than for the other shells because the thermal vibrations of the central atom and first nearest neighbour will show a much higher degree of correlation than for any of the other central atom - scattering atom pairs)[15]. The three amplitude factors VPI, AFAC and A_j were allowed to vary within sensible limits to obtain the best fit. This best fit to the CuCl data along with the Fourier transform is shown in Fig.4.6.

The phase shifts extracted from the bulk CuCl were then used in simulations of the surface spectra. Model calculations were carried out for all four high symmetry adsorption sites; the atop site, the bridge site and the two possible three-fold hollows. The two hollow

TABLE 4.1 INTERATOMIC SEPARATIONS, ATOM TYPE AND COORDINATION NUMBERS FOR THE FIRST FIVE SHELLS OF BULK CuCl (ZINC BLENDE STRUCTURE)

ATOM TYPE	INTERATOMIC SEPARATION/Å	N
Cu	2.34	4.0
Cl	3.83	12.0
Cu	4.49	12.0
Cl	5.41	6.0
Cu	5.89	12.0

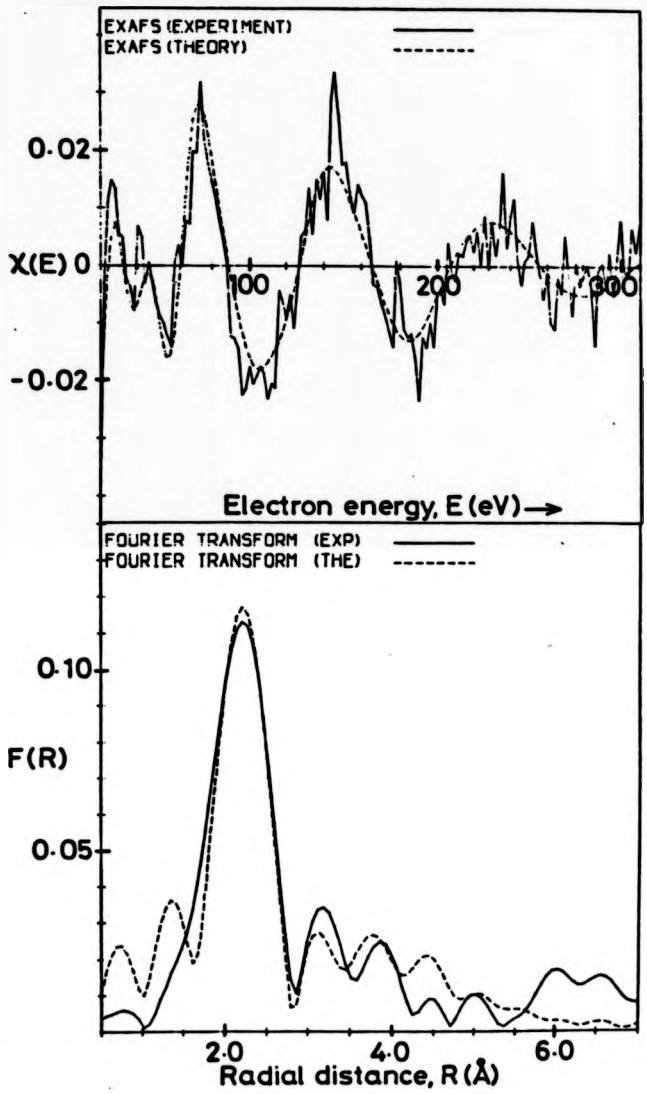

Figure 4.6 Theory/experiment comparison for bulk CuCl.

sites correspond to the Cl atom, either adsorbing in the site where a Cu atom would have been present in the next layer (ABCA packing), or in the alternative three-fold site (ABA packing). These two three-fold sites differ only in the neighbours in the second layer of Cu atoms: the ABA site has a Cu atom directly below the Cl atom, whereas the ABCA site has a vacancy. Table 4.2 shows the bond lengths and effective coordination numbers for each of these sites.

The amplitudes of the surface EXAFS were found to be much larger than those of the bulk EXAFS. This could either be due to a real physical effect (such as different Debye-Waller factors), or to other effects such as radiation damage to the CuCl or non-stoichiometry of the portion of the bulk compound studied. The amplitudes of the SEXAFS were fitted by varying the amplitude related factors, within sensible limits, to obtain a best least mean squares fit. The values used in simulations shown in Figs. 4.7-4.10 were VPI=-4V, AFAC=0.7 and $2\sigma^2$(1st shell)=0.007Å^2 and $2\sigma^2$(higher shells)=0.02Å^2. In principle, the fit is sensitive to all the amplitude factors because of their different energy dependence (AFAC independent of E, inelastic scattering amplitude factor $\exp(-2VPI*R_j/k)$ and amplitude effect of thermal vibrations $\exp(-A_jk^2)$), but there is a significant amount of coupling which creates a large amount of uncertainty in the determination of these parameters. This uncertainty, along with other possible effects on the amplitudes for the bulk phase, means that the reliability of the comparison of bulk and surface Debye-

TABLE 4-2 INTERATOMIC SEPARATIONS AND EFFECTIVE COORDINATION NUMBERS FOR THE HIGH SYMMETRY SITES OF Cu(111)

SITE	INTERATOMIC SEPARATION/Å	N^*_{35}	N^*_{60}
	2.39	2.01	0.75
ATOP	3.50	7.21	5.70
	4.72	5.59	2.36
	2.39	3.15	1.72
BRIDGE	3.00	2.36	1.91
	4.17	1.97	0.76
	3.94	3.57	4.11
	2.39	4.30	2.68
3-FOLD HOLLOW	3.50	2.79	3.05
(ABCA)	4.34	4.67	6.32
	4.23	5.50	2.39
	2.39	4.30	2.68
3-FOLD HOLLOW	3.50	2.79	3.05
(ABA)	4.34	4.67	6.33
	3.97	2.01	0.75

Waller factors is limited. There is, however, a significant difference in the shape of the EXAFS amplitude envelope between surface and bulk spectra which indicates that the magnitude of thermal vibrations of the surface species is smaller than that for the bulk species, although it may not be as large as that indic-indicated by the 'best fits'.

In simulating the surface spectra, the bond lengths and E_0 were allowed to vary to obtain the best fit to both 35° and 60° spectra. The fit was found to be sensitive to the first two copper shells for both angles of incidence, but was found to be insensitive to higher copper shells and to the nearest chlorine neighbours. The iterations to a best fit were carried out using the effective coordination numbers for all sites as starting points. In each case, and for both angles of incidence, the nearest neighbour bond length was found to be 2.39±0.02Å (the same as for the single shell analysis) and the second neighbour distance extracted was 3.50±0.08Å. This second shell distance rules out the possibility of the bridge site, which has second and third nearest neighbours at 3.00Å and 4.17Å, respectively. Both the three-fold hollows, however, should have a neighbour at 3.50±0.015Å (based on the nearest neighbour distance of 2.39±0.02Å) and the atop site would have a neighbour at 3.50±0.015Å. The simulations for all four sites, based on the nearest neighbour distance of 2.39Å, are shown in Figs. 4.7-4.10, along with the Fourier transforms. It can be seen that the atop site can be ruled out because of the relative amplitudes of the first and second

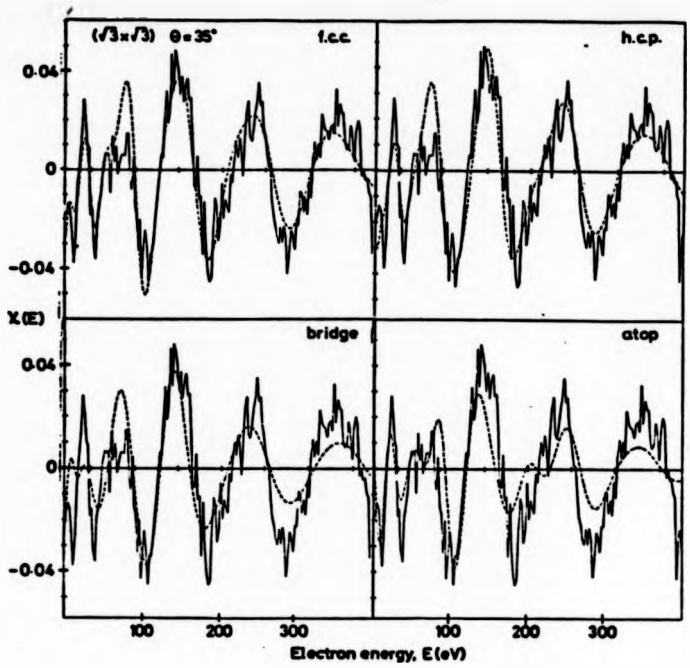

Figure 4.7 Theory/experiment comparison for high symmetry sites: $\chi(E)$ for 35° data

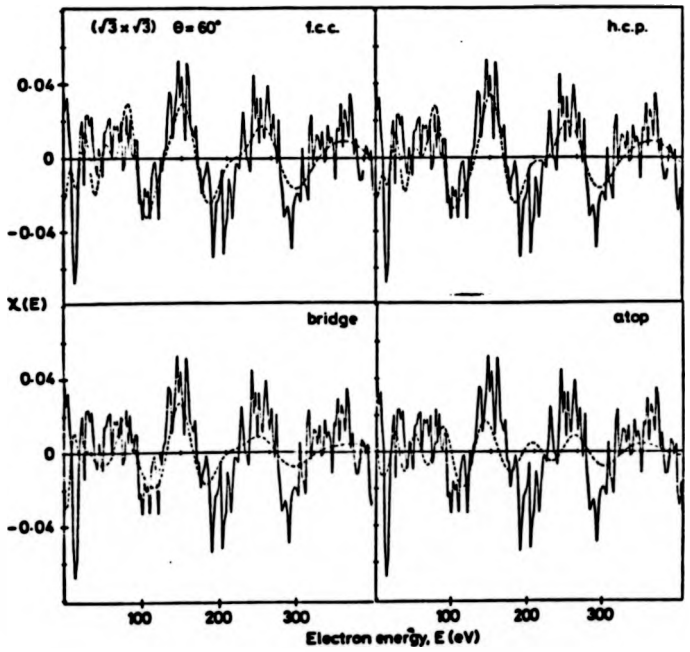

Figure 4.8 Theory/experiment comparison for high symmetry sites: $\chi(E)$ for 60° data.

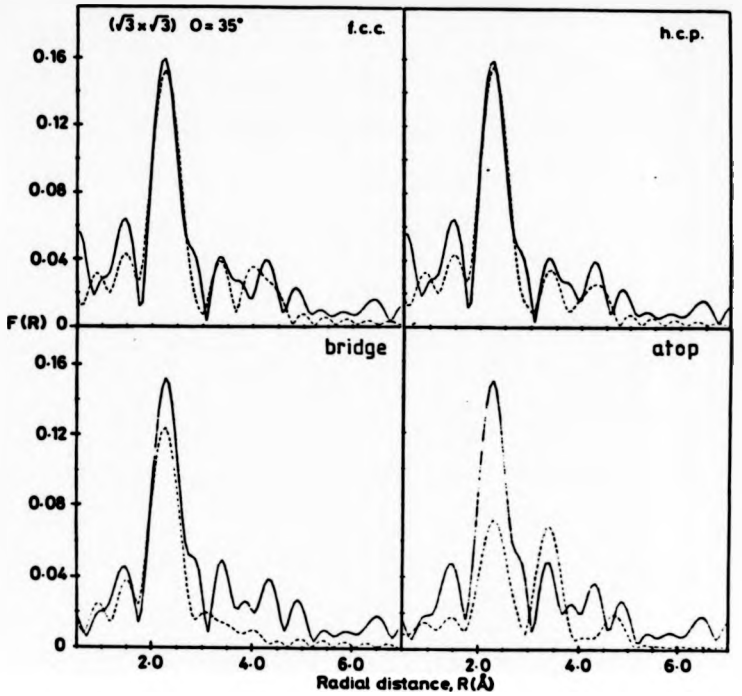

Figure 4.9 Theory/experiment comparison for high symmetry sites: Fourier transforms of 35° data.

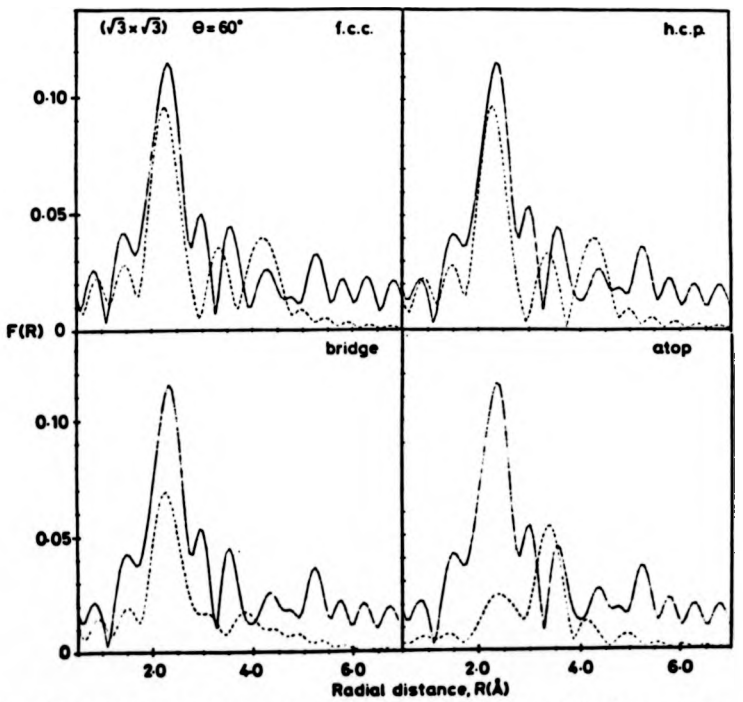

Figure 4.10 Theory/experiment comparison for high symmetry sites: Fourier transforms of 60° data.

shells. The presence of the second shell introduces 'extra structure' which is not seen in the experiment. The simulations for the atop site can be made to fit the data only by changing the Debye-Waller factors to physically unrealistic values (ratios of $2\sigma^2$ for first to second shells of $1:10^3$). The bridge and atop sites can also be ruled out by the amplitude variation shown between the 60° and 35° data (as seen in the single shell analysis). Although all simulations shown here have the same AFAC and VPI parameters, before the bridge and atop sites were ruled out using the SEXAFS amplitude, the effect of varying these parameters was investigated. It was found that even when these parameters were optimised for each site (AFAC=0.9 and VPI=-4eV for the bridge site and AFAC=1 and VPI=-2eV for the atop site) these two sites still could not be used to simulate the data.

Having eliminated the atop and bridge sites, the remaining question is which of the two three-fold hollows is the Cl atom chemisorbed in. The two sites differ only by third and fourth neighbours (Table 4.2). From the simulations shown in Figs. 4.7 and 4.8, it can be seen that the difference in EXAFS for these two sites is very small, and the sites cannot be distinguished without a considerable increase in signal to noise ratio over the data presented here.

4.6 NPD/OPD

The photoelectron diffraction data were obtained in

the form of a thirty point scan at 1eV increment across the Cl 1s photoemission peak at each photon energy, and the photon energy was varied in increments of 2eV in a range equivalent to an electron kinetic energy of 100-400eV. A major problem encountered in the extraction of a photoelectron diffraction 'fine structure function' from this data was the intrusion of the Cl $L_{2,3}VV$ Auger peak into the energy window at 180eV. To overcome this problem, a novel background subtraction algorithm was developed. Each scan of the photoemission peak covered 30eV and, since these were taken in 2eV (photon energy) increments, there was a substantial overlap of electron energy points. The count rates for channels of the same electron energy were summed for all channels which did not include the photoemission peak. In this way, an electron energy distribution curve was extracted which included the Auger peak. By subtracting the relevant part of this curve from each scan, it was possible to generate a 'fine structure function' which was free of the effects of the Auger peak. Fig. 4.11 shows the photoelectron diffraction spectrum for emission along the [111] surface normal. Shown along side this are the spectra, calculated by D.P. Woodruff using phase shifts derived from muffin-tin potential calculations and including only the effects of single scattering, for the four sites: the atop and bridge sites and both 'fcc' (ABCA) and 'hcp' (ABA) three-fold hollows. It can be seen that it is not possible to distinguish between the two sites using the NPD data (although calculations for the atop and bridge sites did not fit the data at

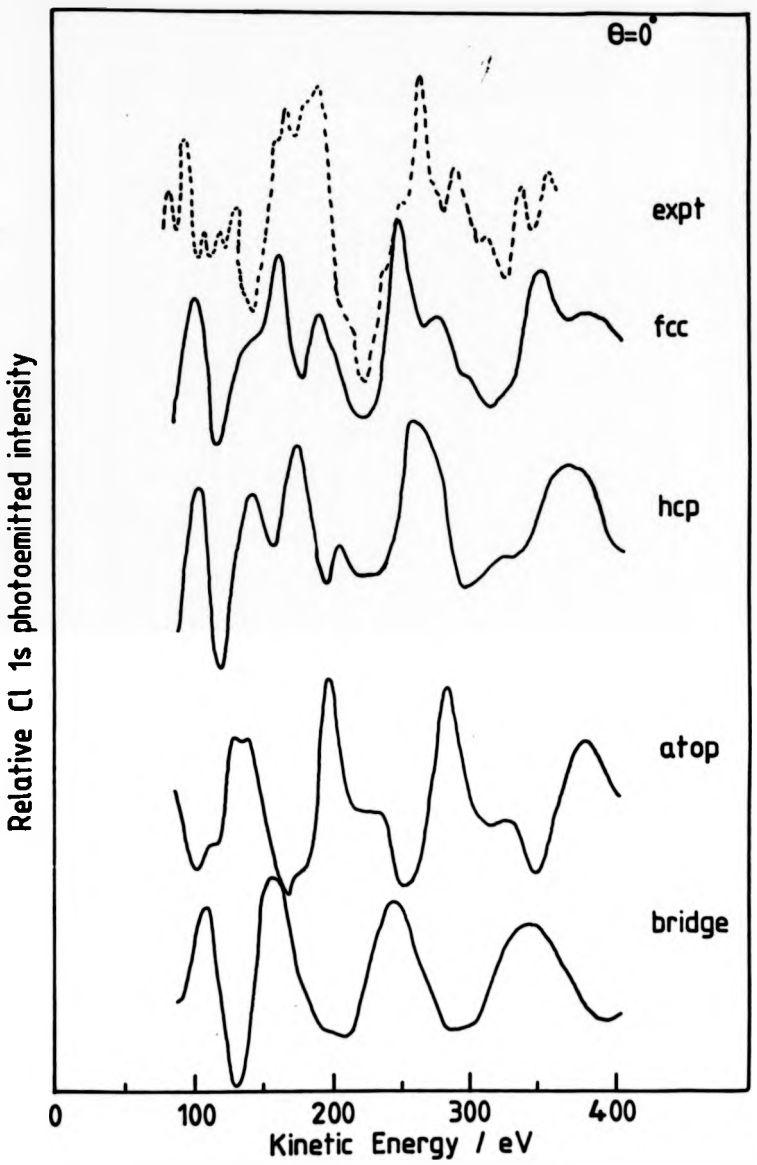

Figure 4.11 Theory/experiment comparison for photoelectron diffraction spectra collected at normal emission.

all). The photoelectron diffraction spectrum for emission at 35° from the surface normal along the [110] direction is shown in Fig. 4.12. There is a gap in this spectrum between 180eV and 230eV due to structure introduced by Bragg reflection off the [111] planes, since in this geometry, the X-ray incidence is only 10° off normal. The calculated spectra for the two hollow sites are very different because the 'fcc' site has a nearest neighbour directly behind the emitting atom (with respect to the detector) whereas the 'hcp' site does not. This alignment of a neighbour will show up clearly in photoelectron diffraction, because of the strong peaking in the back-scattering magnitude around 180° for electrons with kinetic energy in this range. Comparison of the theoretical spectra for both hollows with the experimental spectrum shows clearly that the chlorine atom is chemisorbed in the 'fcc' (ABCA) hollow: that is the chlorine atom occupies the site that would have been taken by copper atoms in the next layer.

4.7 CONCLUSION

The Cl-Cu bond length for the Cu(111)-($\sqrt{3}\times\sqrt{3}$)R30°-Cl system is 2.39±0.02Å (an expansion of 0.05±0.02Å from bulk CuCl). This expansion is, within experimental error, of the same sign and size as that found for the Cu(100)-c(2×2)Cl system using both SEXAFS (2.37±0.02Å) and LEED (2.41±0.02Å). This excellent agreement indicates not only the trend for chlorine adsorbed on copper but also that two major techniques for surface structure

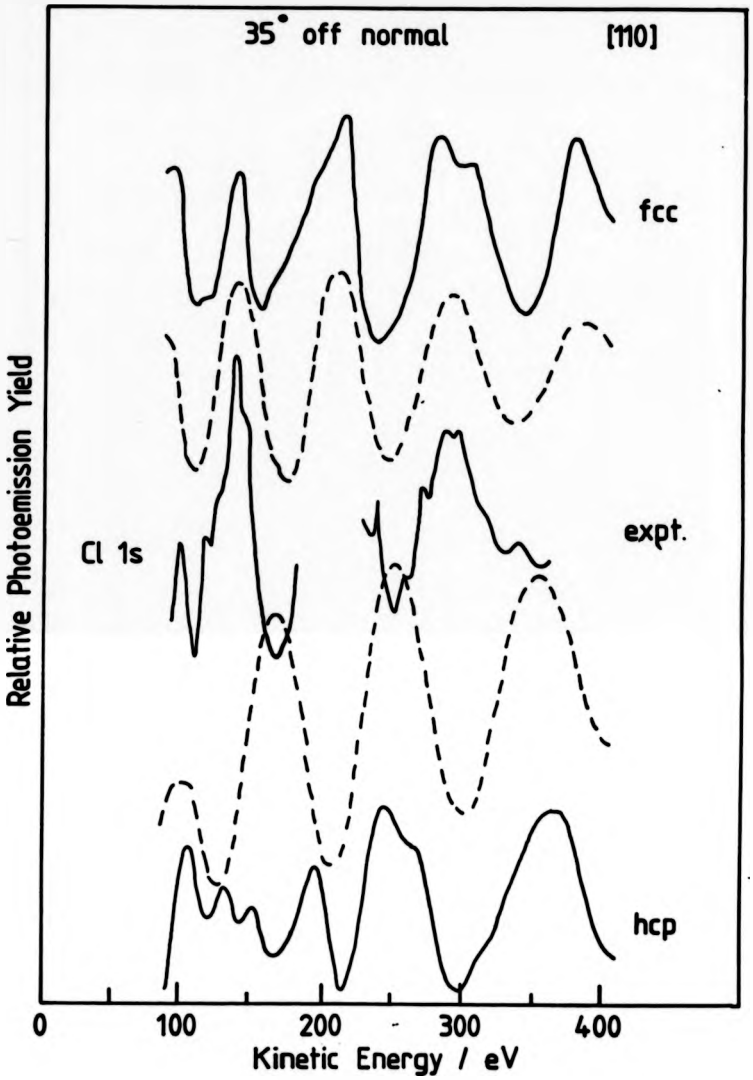

Figure 4.12 Theory/experiment comparison for photoelectron diffraction spectra collected at 35° off normal in the [110] azimuth. The broken lines are the simulation including only the nearest neighbour shell.

determination give essentially the same answer.

It was shown that SEXAFS can identify the adsorption site both directly, using the amplitude of the nearest neighbour peak as a function of angle of incidence, and indirectly, using the modelling technique. The agreement of the two analysis methods shows that for a simple, high symmetry chemisorption system, like the one studied here, the single shell, Fourier filtering method of analysis is adequate. In some low symmetry, multiple bond length situations this may not be the case. Although the Fourier filtering method revealed the bond length and site, the simulation technique revealed more information about the adsorption system, in particular the magnitude of the thermal vibrations of the chemisorbed chlorine atom: the $2\sigma^2$ factor for the surface species was found to be about one third of that for the bulk species.

Although the SEXAFS measurements showed that chemisorption occured in three-fold hollow sites, it could not identify which of the two hollow sites was involved. The NPD/OPD measurements, however, revealed that the adsorption site was the ABCA (fcc-like) three-fold hollow, despite the approximate theoretical treatment used in the simulations. This shows that the NPD/OPD combination is a very useful tool for site determination. It should be noted, however, that the photoelectron diffraction spectra were found to be a less reliable measure of bond length than SEXAFS because of the uncertainties in the theory/experiment comparison and the approximations (theoretical phase shifts and single scattering) used in the calculations.

CHAPTER 4: REFERENCES

1) E. Zanazzi, F. Jona, D.W. Jepson and P.M. Marcus, Phys. Rev. B14, 432-440 (1976).

2) H.S. Greenside and D.R. Hamman, Phys. Rev. B23, 4879-4887 (1981).

3) G. Rovida and F. Pratesi, Surf. Sci. 57 270-282 (1975).

4) M. Bowker and K.C. Waugh, Surf. Sci. 134, 639-664 (1983).

5) P.H. Citrin, D.R. Hamman, L.F. Mattheiss and J.E. Rowe, Phys. Rev. Lett. 49, 1712-1715 (1982).

6) D. Westphal, A. Goldmann, F. Jona and P.M. Marcus, Sol. State Commun. 44, 685-686 (1982).

7) D. Westphal and A. Goldmann, Surf. Sci. 131, 113-138 (1983).

8) F. Jona, D. Westphal, A. Goldmann and P.M. Marcus, J. Phys. C 16, 3001-3010 (1983).

9) G. Lamble and D.A. King, Proc. Roy. Soc. in press.

10) P.J. Goddard and R.M. Lambert, Surf. Sci. 67, 180-194 (1977).

11) R.W.G. Wyekoff, "Crystal Structures", Vol. 1, Interscience Publishers Ltd., (1948).

12) E. Pantos and G.D. Firth, Daresbury Laboratory technical memorandum DL/CSE/TM21 (1982).

13) E.A. Stern, B.A. Bunker and S.M. Heald, Phys. Rev. B21, 5521-5539 (1980).

14) B. Prevot, B. Hennion and B. Dorner, J. Phys. C 10, 3999-4011 (1977).

15) E.A. Stern, D.E. Sayers and F.W. Lytle, Phys. Rev. B11, 4836-4846 (1975).

CHAPTER 5 MOLECULAR ADSORPTION SYSTEMS

5.1 INTRODUCTION

The techniques of NEXAFS and SEXAFS have been applied to several molecular adsorption systems; namely formate and ethoxy on Cu(110). In particular, the orientation of the formate intermediate has been found using NEXAFS and the adsorption site has been determined using single shell SEXAFS analysis. The result for formate on Cu(100), as found by other workers, has been compared with this and discrepancies in interpretation have been resolved using multi-shell analysis. The technique of NEXAFS has also been used to study the reaction of ethanol with oxygen on Cu(110) to produce the ethoxy intermediate.

5.2 PREVIOUS STUDIES OF FORMIC ACID ADSORPTION ON Cu(110)

As has already been stated, one of the areas in which SEXAFS appears to have a promising future is the study of adsorbed molecules. These systems often have no long range order, which rules out structure determination by the more usual diffraction techniques[1]. Molecular adsorption systems are more commonly studied using vibrational techniques such as Electron Energy Loss Spectroscopy[2] (EELS) and Infra-red Reflection Absorption Spectroscopy[3] (IRAS). Work using these techniques has concentrated more on the nature of the surface species and molecular orientation, rather than the adsorption site. This so called 'active' site is thought to be of

great importance in the understanding of chemical reactions on surfaces.

A molecular adsorption system which has received much attention in recent years is the decomposition of formic acid on Cu(110). This was initially characterised by observation of the desorbing products, using Temperature Programmed Reaction Spectroscopy (TPRS)[4]. In this study, formic acid was adsorbed at 190K and then the sample was heated slowly. At about 273K a large H_2 desorption peak was seen and at 473K both H_2 and CO_2 were found to evolve. This showed clearly that the decomposition occured by dehydrogenation (i.e. $HCOOH \rightarrow H_2 + CO_2$) and not by dehydration ($HCOOH \rightarrow H_2O + CO$) as had been found on many oxide surfaces. The desorption peak at 273K was attributed to the loss of the alcohol hydrogen from the formic acid molecule (identified by isotopic labelling) to produce the formate ion (HCOO-). The desorption peaks at 473K are from the breakdown of this formate ion into CO_2 and $\frac{1}{2}H_2$.

A subsequent study of this system by Bowker and Madix[5] involved the use of Ultraviolet and X-ray Photoelectron Spectroscopy (UPS and XPS) along with TPRS. They formed the formate intermediate both by adsorption at low temperatures (140K) and heating, and by adsorption at 400K. Observation of the oxygen 1s XPS peak revealed that only one type of oxygen atom was present on the surface. They concluded that the formate ion was bonded to the surface through the oxygen atoms and that both oxygen atoms were in equivalent sites.

A study of the formate intermediate using Infrared

Reflection Absorption Spectroscopy (IRAS) by Hayden et al.[6] confirmed that both oxygens were completely equivalent, and it was concluded that the molecular plane of the molecule was essentially perpendicular to the surface. It was also shown that the formate ion could be formed by adsorption of formic acid at room temperature.

It was the intention of this study to extract two more structural parameters of the formate/Cu(110) system; the precise molecular orientation (including the azimuthal orientation) and the adsorption site. This was achieved by the combination of the two X-ray absorption techniques, NEXAFS and SEXAFS.

5.3 NEXAFS RESULTS

The near-edge spectra are shown in Figs. 5.1 and 5.2. The near-edge region is dominated by two resonances which have previously been identified. The sharp feature approximately 5eV above the absorption threshold corresponds to an excitation of an electron from the (spherically symmetric) 1s level to an unoccupied anti-bonding orbital of π-symmetry: hence this is known as a π-resonance[7]. The broader feature, centred around a photon energy of 545eV, results from a multiple scattering resonance of the photoelectron between the carbon and oxygen atoms; this is known as the σ-resonance[7] (as the final state has σ symmetry).

The study of the variation of the intensity of these resonances with polarisation direction can reveal the molecular orientation using the known selection rules.

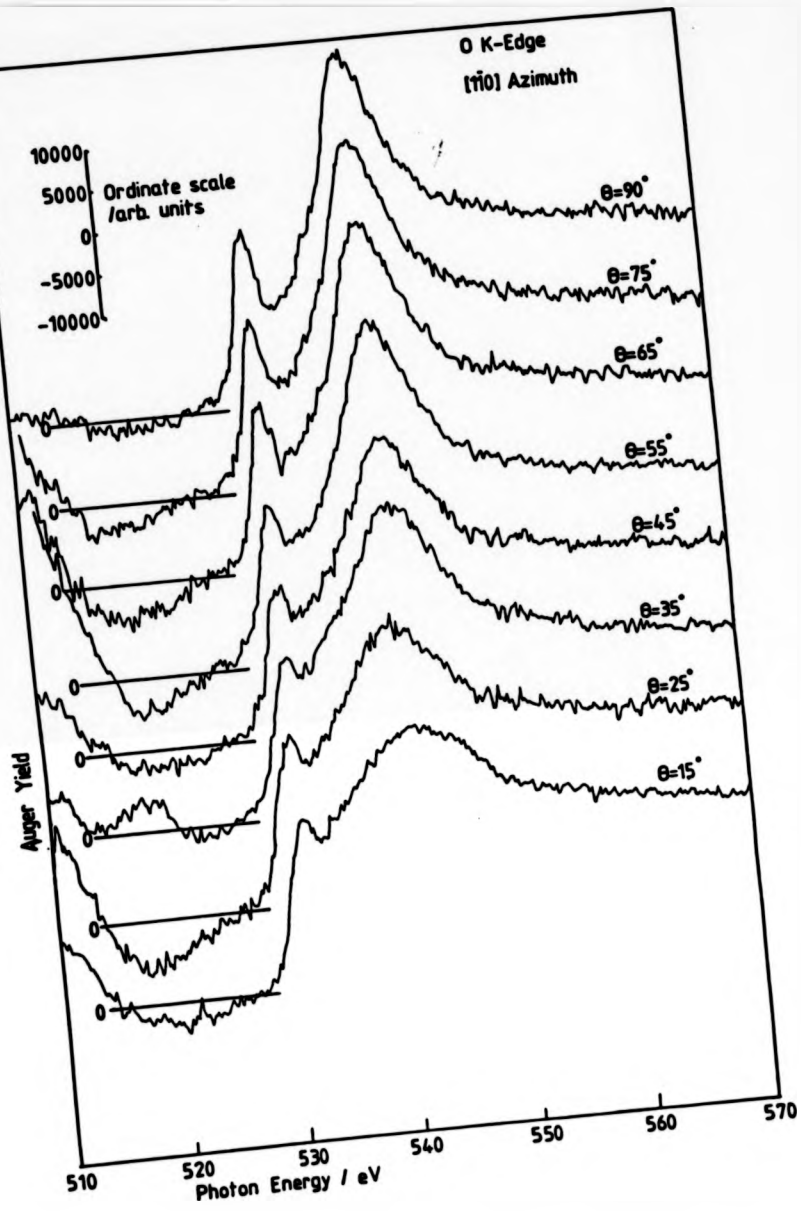

Figure 5.1 NEXAFS spectra with the electric vector in the [1$\bar{1}$0] azimuth.

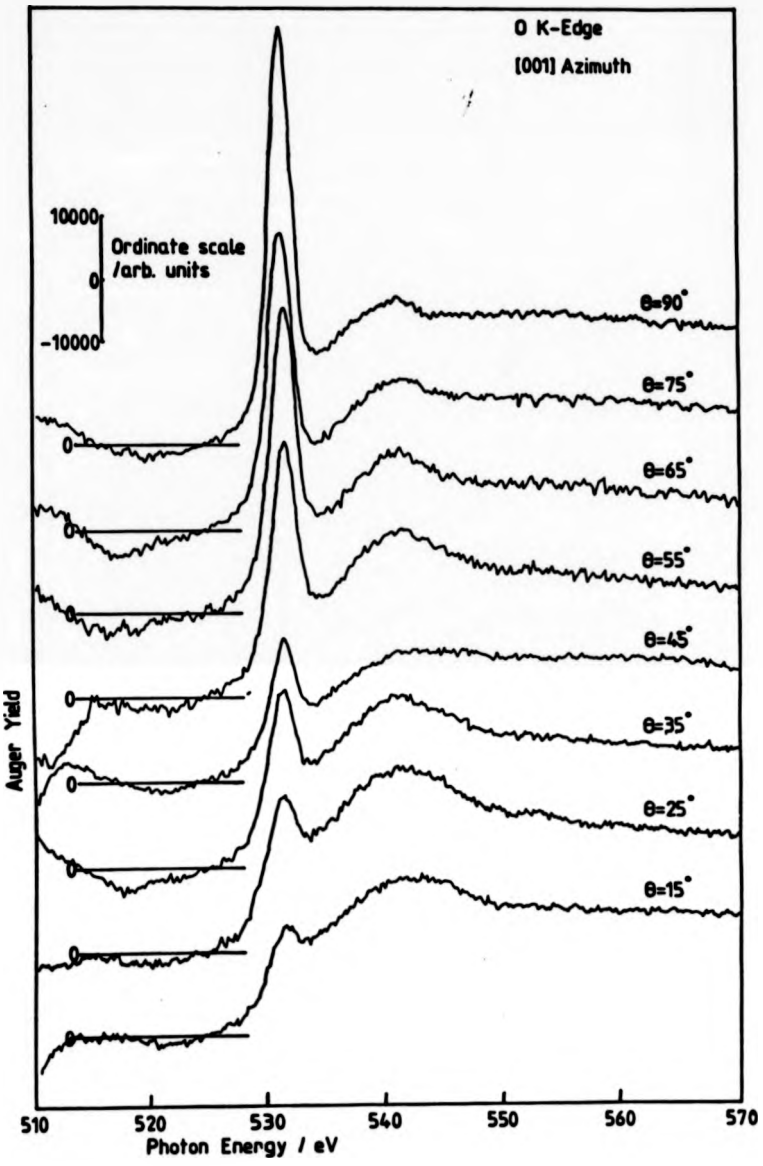

Figure 5.2 NEXAFS spectra with the electric vector in the [001] azimuth.

The anti-bonding or π^* orbitals of the formate ion are anti-symmetric with respect to the molecular plane. Hence, the intensity of the π-resonance varies as $\cos^2\theta$, where θ is the angle between the electric vector and the normal to the molecular plane. The σ-resonance is a quasi-bound multiple scattering resonance of the photoelectron along the axis of the C-O bond. Hence, the magnitude of the σ-resonance varies as $\cos^2\theta$ where, in this case, θ is the angle between the electric vector and the O-C bond direction.

Bearing these rules in mind, an inspection of the NEXAFS at normal and grazing incidence, with the electric vector in each of the principle azimuths reveals the major features of the molecular orientation. With the polarisation vector in the $[1\bar{1}0]$ azimuth, the resonance is weak at all angles, whereas it is strong at normal incidence and weak at grazing incidence when the electric vector lies in the [001] azimuth. This indicates that the molecular plane is parallel to the $[1\bar{1}0]$ azimuth, and perpendicular to the surface. The variation of the σ-resonance (i.e. strong with the electric vector in the $[1\bar{1}0]$ azimuth and weak when it is in the [001] azimuth) confirms this conclusion. It should be noted that the variation of the σ-resonance intensity in the $[1\bar{1}0]$ azimuth (i.e. strong at normal incidence and weaker at grazing incidence) confirms the earlier supposition[4] that the O-C-O bond angle is large.

Accepting this interpretation (which involves an orientation which is essentially the same as that for

HCOO- adsorbed on Pt(110) as found by EELS[9]) it must be concluded that the small π-resonance peaks in the [1$\bar{1}$0] azimuth and the small σ-resonance at normal incidence in the [001] azimuth must be due to incomplete polarisation of the X-rays.

5.4 QUANTITATIVE INTENSITY ANALYSIS

In the previous section, a qualitative interpretation of the NEXAFS resonances has been given in terms of the molecular orientation. In order to set limits of confidence on the parameters defining this orientation, a quantitative analysis of the resonance intensities as a function of azimuthal and incidence angles was carried out.

A major problem encountered was the selection of a suitable background. It seemed reasonable to use a straight line background on the π-resonance both because of its small width and because it lies in an energy region where there are not likely to be any structures resulting from scattering from the substrate[8]. The σ-resonance proved more difficult, however, because of its large width and because of the lack of knowledge about any absorbate-substrate scattering features in the same energy region. The applicability of several different types of background (including quadratic and cubic polynomials, cubic splines and a Shirley[10] type background used in XPS data analysis) was investigated but it was decided that the use of these could not be justified any more than a linear background and since

the latter can be fitted more simply and repeatably, it was this that was employed. Following background subtraction, the area of each resonance was measured and normalised to the edge jump to eliminate the effect of angular variation in total X-ray absorption and to allow for any possible differences in coverage.

The π^* orbital responsible for the π-resonance is antisymmetric with respect to the molecular plane[11], hence the intensity of the resonance will vary as the cosine squared of the angle between the electric vector and the normal to the plane[8]. Studies of diatomic molecules have shown that the shape resonance is associated with the axis between the two atoms and is very insensitive to the presence of other atoms in the vicinity[8] (except in the case of colinear neighbours). Therefore, it seems reasonable that the shape resonance has σ-symmetry about each O-C bond in the formate ion, and that it is relatively unaffected by the other C-O bond. Using this assumption it can be seen that the intensity of the σ-resonance is proportional to $\cos^2\theta_1 + \cos^2\theta_2$ where θ_1 is the angle between one O-C axis and the electric vector, and θ_2 is the angle to the other O-C axis. Using these relationships the variation of the resonances with the polar angle of incidence and the azimuthal angle was modelled and fitted to the data using a least mean squares iterative process.

Fig. 5.3 shows the best fit (continuous line) assuming the molecule to be perpendicular to the surface and aligned with the [1$\bar{1}$0] azimuth. The two parameters in this model (apart from μ_σ^0 and μ_π^0, the absolute

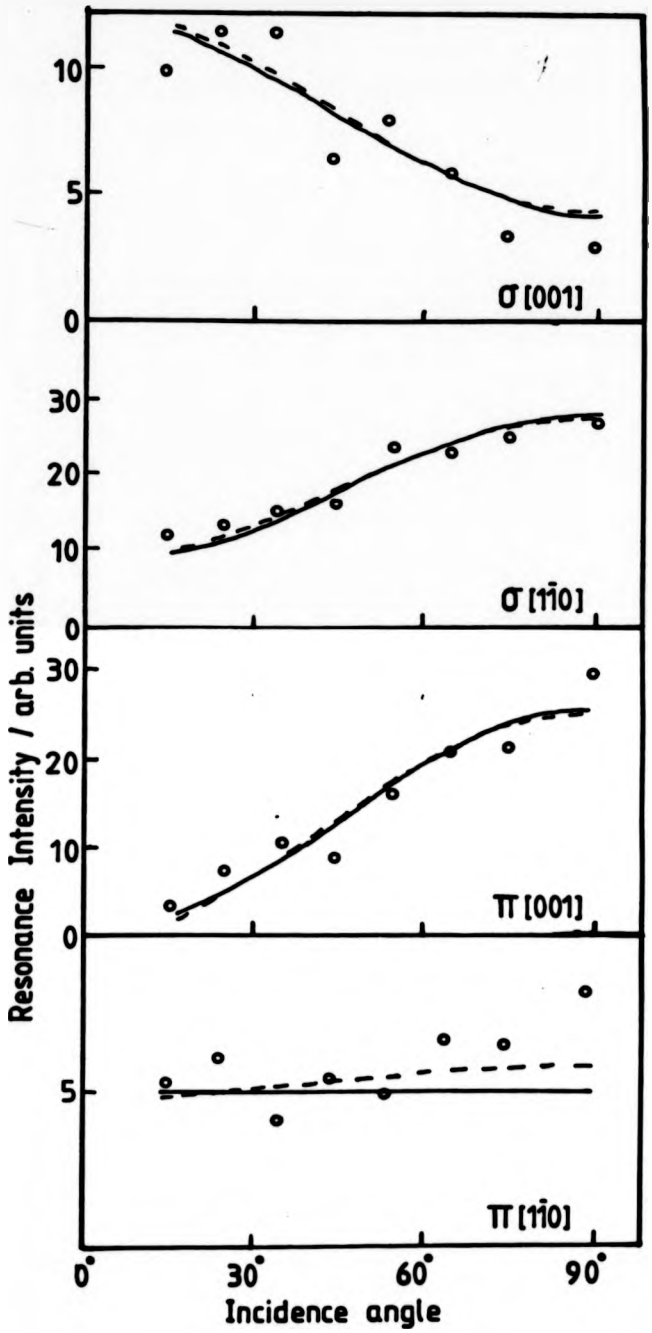

Figure 5.3 Comparison of experimental NEXAFS intensities with those expected for the proposed models.

resonance cross sections) are α, half angle in the O-C-O bond, and P, the fraction of polarisation in the horizontal plane. The relationship between these parameters and the intensities is given in equation (5.4.1).

$$[110]\quad \mu_\sigma = \mu_\sigma^0 P[\cos^2(\alpha-\theta)+\cos^2(\alpha+\theta)]$$
$$\mu_\pi = \mu_\pi^0 2(1-P)$$

$$[001]\quad \mu_\sigma = \mu_\sigma^0[(1-P)\sin^2\alpha + P\cos^2\alpha\cos^2\theta]\times 2$$
$$\mu_\pi = \mu_\pi^0 2P\sin^2\theta \qquad (5.4.1)$$

This model gives a best fit with $\alpha=62^\circ$ and P=0.87 (which is reasonable for this monochromator).

To check the confidence limits of this model the effect of allowing small twists (i.e. misalignment with the $[1\bar{1}0]$ azimuth) and tilts (i.e. deviations of the molecule from the perpendicular) was investigated. Study of the π-resonance intensities in the $[1\bar{1}0]$ azimuth shows a small systematic increase towards normal incidence, although, for our model, this should be constant at all angles because it is due only to the incomplete polarisation. This may be due to systematic problems in the background subtraction or it can be accounted for by small twists or a crystallographic misalignment with the incidence plane. The effect of such misalignments and the possibility of a second formate species orthogonal to the first was also examined. The dependence of the resonance intensities to these parameters was investigated using a computer

modelling program based on the equations given in the following text. The intensity of the resonances as a function of β the tilt of the molecule away from the surface normal, γ the twist angle of the molecular plane from the [1$\bar{1}$0] azimuth, Θ the angle between the main component of the polarisation and the surface normal and ϕ the angle between the main component of the polarisation and the [1$\bar{1}$0] azimuth are given in equations (5.4.2) and (5.4.3). P, α, μ_{π}^{0} and μ_{σ}^{0} have the same meaning as previously.

$$\mu_{\pi} = 2\mu_{\pi}^{0}\left[P(\hat{\underline{p}}.\hat{\underline{A}}_{\parallel})^{2} + (1-P)(\hat{\underline{p}}.\hat{\underline{A}}_{\perp})^{2}\right] \qquad (5.4.2)$$

$$\mu_{\sigma} = 2\mu_{\sigma}^{0}\left[P(\hat{\underline{s}}_{1}.\hat{\underline{A}}_{\parallel})^{2} + P(\hat{\underline{s}}_{2}.\hat{\underline{A}}_{\parallel})^{2} + (1-P)(\hat{\underline{s}}_{1}.\hat{\underline{A}}_{\perp})^{2} + (1-P)(\hat{\underline{s}}_{2}.\hat{\underline{A}}_{\perp})^{2}\right] \qquad (5.4.3)$$

where the unit vector defining the normal to the molecular plane is

$$\hat{\underline{p}} = \begin{pmatrix} \sin(\pm\gamma)\cos(\pm\beta) \\ -\cos(\pm\gamma)\cos(\pm\beta) \\ \sin(\pm\beta) \end{pmatrix}$$

the two unit vectors defining the O-C bond axes are

$$\hat{\underline{s}}_{1} = \begin{pmatrix} -\cos\alpha\sin(\pm\beta)\sin(\pm\gamma) + \sin\alpha\cos(\pm\gamma) \\ \cos\alpha\sin(\pm\beta)\cos(\pm\gamma) + \sin\alpha\sin(\pm\gamma) \\ \cos\alpha\cos(\pm\beta) \end{pmatrix}$$

$$\hat{\underline{s}}_{2} = \begin{pmatrix} -\cos\alpha\sin(\pm\beta)\sin(\pm\gamma) - \sin\alpha\cos(\pm\gamma) \\ \cos\alpha\sin(\pm\beta)\cos(\pm\gamma) - \sin\alpha\sin(\pm\gamma) \\ \cos\alpha\cos(\pm\beta) \end{pmatrix}$$

and the vectors defining the major component of the polarisation, $\hat{\underline{A}}_{\parallel}$, and the minor component, $\hat{\underline{A}}_{\perp}$ are

$$\hat{\underline{A}}_{\parallel} = \begin{pmatrix} \sin\theta\cos\phi \\ \sin\theta\sin\phi \\ \cos\theta \end{pmatrix}$$

$$\hat{\underline{A}}_{\perp} = \begin{pmatrix} -\sin\phi \\ \cos\phi \\ 0 \end{pmatrix}$$

where the x components are parallel to the $[1\bar{1}0]$ azimuth, the y components are parallel to the [001] azimuth and the z components are parallel to the surface normal.

The $\pm$ signs indicate the possibility of domains with tilt and/or twist of opposite sign.

It was found that the parameters were coupled to a certain extent but the fit was sensitive to all parameters. The variation of the π-resonance in the $[1\bar{1}0]$ azimuth could be explained by a 10° misalignment of the crystal which though quite large is reasonably acceptable. Tilts and twists of more than a few degrees were found to be unlikely, and no evidence of a second species was found. A typical 'best fit' is shown in Fig. 5.3 (broken line) using a misalignment of 10°. The model defines α and P to within about 5%.

These statements of precision refer to the modelling of the intensities alone, and do not take into account inaccuracies in the extraction of these. As has been

stated, there were problems in the fitting of a suitable background to the σ-resonance and the intensity of this was found to be sensitive to the procedure used. The measurement of the edge-jump, which was used to normalise the intensities, was also difficult to measure because it was often small compared to the resonances and was superimposed on a sloping background. Thus this (necessary) normalisation was as great a source of error as the measurement of the resonances.

Including these errors of measurement the true precision of the of the calculations is much worse than that implied by the quality of the fits. It was concluded that the uncertainty in α was at least $\pm 5^{\circ}$ and may be as large as $\pm 10^{\circ}$. The results do exclude the possibilities of large average tilts or twists (and so any large amplitudes of vibration of the molecule in these directions) and exclude the possibility of any second formate species in significant amounts (<5%).

5.5 O-C Bondlength

It has been shown that the position of the σ-resonance with respect to the 1s binding energy is dependent upon the distance between the two (low Z) atoms of diatomic molecules[12]. This relationship has been studied empirically for several gas phase molecules containing various low Z atoms[11], and for small O and C containing molecules chemisorbed on Cu(100)[7]. The study of the gas phase molecules has shown that the difference in energy between the σ-resonance and the 1s bind-

ing energy is a linear function of the bondlength for molecules with atom pairs of the same total Z (e.g. bondlengths can be compared using this method for the molecules CO and N_2 for which the total Z=14).

Using these ideas it should, in theory, be possible to measure intra-molecular bondlengths for chemisorbed species by comparing results with the gas phase data. This is a non-trivial exercise, however, because in general chemisorption induces a change in the 1s binding energy and may also perturb the molecular potential. This principle has been applied to the chemisorption of hydrocarbons by Stöhr et al.[14]. They related the energy separation for the chemisorbed species to the gas phase species as follows:

They defined the separation δ as.

$$\delta = e - E \qquad (5.6.1)$$

where e is the energy of the σ-resonance and E is the 1s binding energy. Thus

$$\delta_s - \delta_g = (e_s - e_g) - (E_s - E_g) \qquad (5.6.2)$$

where the subscripts s and g denote the surface and gas phase respectively.

They then made the assumption that $e_s = e_g$ [which for hydrocarbons is a fair assumption].

This then gives

$$\delta_s = \delta_g - (E_s - E_g) \qquad (5.6.3)$$

which effectively gives

$$\delta_g = e_s - E_g \qquad (5.6.4)$$

relating δ to the difference between the surface species resonance and the gas phase binding energy.

The assumption $e_s = e_g$ will not, however, be a good one

for the formate species. The gas phase O 1s binding energies of formic acid are 538.75 eV for the carboxyl oxygen and 540.45 eV for the hydroxl oxygen[15] (relative to the vacuum level) whereas for the chemisorbed formate ion, the 1s binding energy is 531.5±0.2 eV[5] relative to the Fermi energy. The work function of Cu(110) is about 5eV[16] so that there must also be a shift of binding energy, due to the change in chemical nature of the species and (predominantly) extramolecular relaxation. The position of the σ-resonance for this system is 545.0±0.8 eV. Thus referencing to the 1s binding energy corrected for the work function we get δ=8.5±1.0 eV. This gives an O-C bondlength of 1.12± 0.03 Å (using the relationship found by Sette et al.[13] for $Z_1+Z_2=14$). Alternatively, referencing to the gas phase binding energy we get a bondlength of 1.28±0.05 Å (compared with an expected bondlength of 1.25±0.02 Å[17]).

It can be seen, therefore, that although the position of the σ-resonance gives an indication of the intramolecular bond length, the application of this to a chemisorbed species causes many problems because of the large number of unknowns.

5.6 SEXAFS Results and Single Shell Analysis

Surface EXAFS spectra for normal and grazing incidence in both principle azimuths are shown in figure 5.4. The data is truncated at approximately 700eV photon energy due to the intrusion of photoelectrons from the carbon 1s level into the partial yield detector.

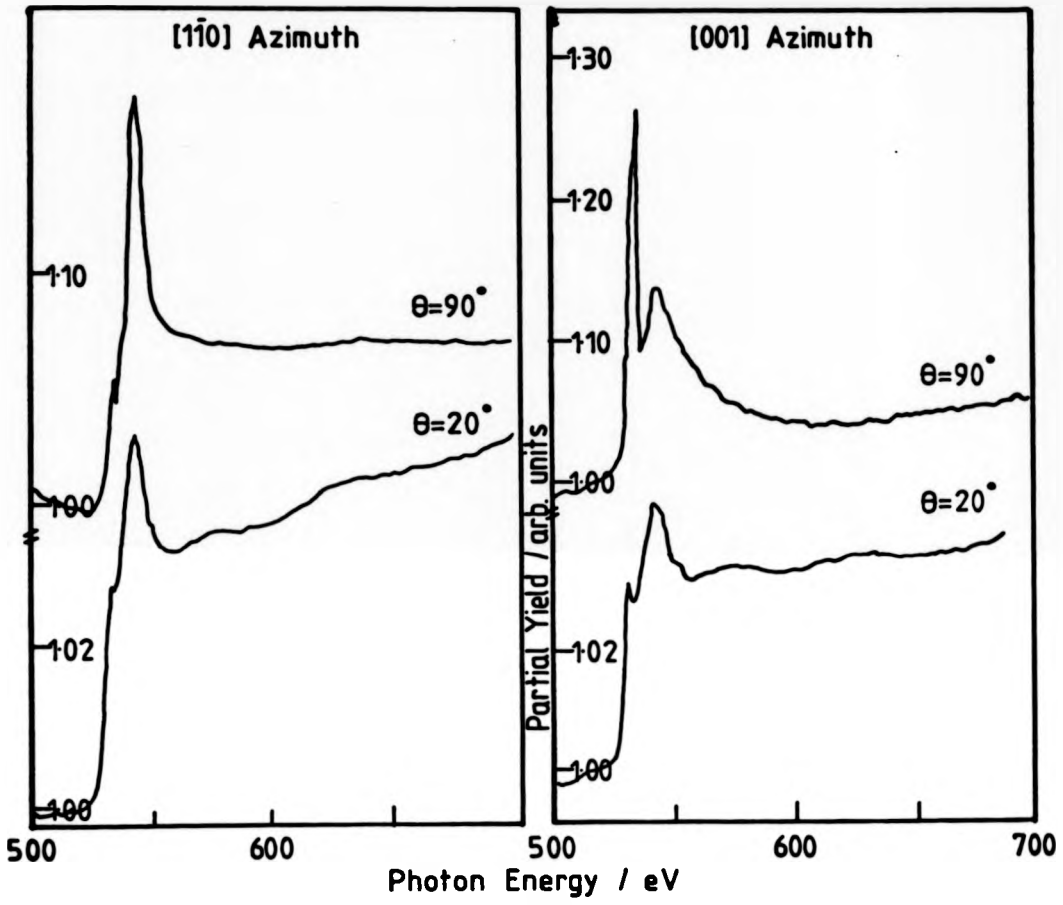

Figure 5.4 SEXAFS spectra collected at normal and grazing incidence in both principle azimuths.

This restriction in the data range decreases the accuracy of the bond length determination.

The EXAFS of this system will be dominated by scattering from the nearest copper atoms which have a far higher scattering cross-section than the lighter carbon, oxygen and hydrogen atoms. This means that the effect of the carbon, which is very close (1.25 Å) to the oxygen, will be negligible except at very low photoelectron energies. Thus a single shell analysis of the EXAFS should reveal the O-Cu bond length.

Single shell analysis, carried out by Dr.J.Haase using Cu_2O as the model compound, gives a bondlength of 1.98±0.07 Å (fig. 5.5). This is consistent with anhydrous copper formate[18] [$Cu(HCOO)_2$] which has four oxygen atoms spaced at between 1.93 and 1.99 Å from the central copper atom. The result is also in excellent agreement with a bidentate formate bonded to a bi-nuclear cluster[19], which gives a bondlength of 1.98 Å.

Using the bondlength obtained from the SEXAFS measurements, and the molecular orientation determined by NEXAFS, there are four possible high-symmetry sites; with the formate molecule sitting in the atop site or bridge site with respect to copper atoms both on the 'ridge' and in the 'trough' (see figure 5.6). The absence of observable EXAFS for normal incidence in the [001] azimuth rules out either of the 'trough' sites. Of the two remaining sites, the bridging site would result in the oxygen atoms being almost in atop sites. This would lead to the EXAFS being negligible

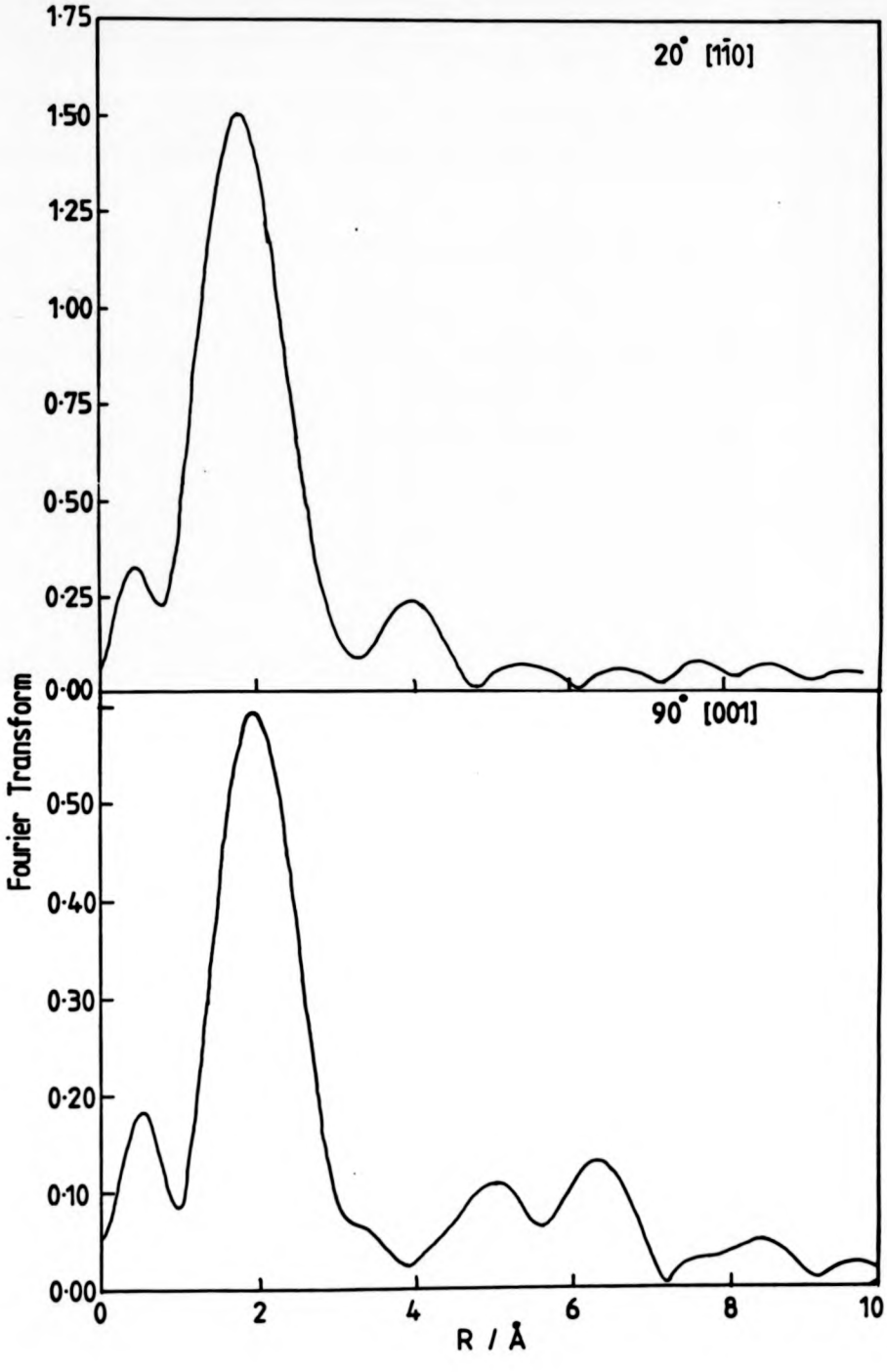

Figure 5.5 Fourier transforms for formate on Cu(110).

for normal incidence in the [1$\bar{1}$0] azimuth; this is not the case. Table 5.1 shows the relative amplitudes of the EXAFS, normalised to grazing incidence in the [1$\bar{1}$0] azimuth, and it is clear that the formate must sit in the atop site, with the oxygen atoms in bridge like sites. Given the O-C bond length (1.25 Å), the O-Cu bond length (1.98 Å) and the O-C-O bond angle (62°) it is not possible for the oxygen atoms to be in the high symmetry sites (even allowing for the maximum possible error in all the parameters), so the 1.98 Å must be an average between two different bondlengths (see Fig. 5.6b).

5.7 STRUCTURE OF FORMATE ON Cu(110) AS DETERMINED BY NEXAFS AND SINGLE SHELL SEXAFS ANALYSIS

Using the combination of NEXAFS and SEXAFS, a detailed structural analysis of the formate intermediate on Cu(110) has been carried out. The molecular orientation found by NEXAFS is in broad agreement with that found in an EELS study of formate on Pt(110): the formate ion was found to align with the [1$\bar{1}$0] azimuth on this surface although the adsorption site was not found. The EELS measurements of this system, however, implied a small tilt in the molecule within the plane defined by the [1$\bar{1}$0] azimuth and the surface normal. This possibility was not considered in the study on Cu(110) because previous XPS[5] and IRAS[6] measurements had shown that the oxygen atoms were in completely equivalent sites.

The bond length found in the SEXAFS measurements

TABLE 5.1

THEORETICAL AND EXPERIMENTAL SEXAFS AMPLITUDE RATIOS FOR DIFFERENT INCIDENCE DIRECTIONS.

The theoretical amplitudes were calculated using the models shown in Fig. 5.6. The amplitudes are normalised to that for 20° incidence angle in the [1$\bar{1}$0] azimuth.

AZIMUTH	θ	MODEL 5.6(a)	MODEL 5.6(b)	EXPT.
[1$\bar{1}$0]	20°	1.0	1.0	1.0
	90°	0	0.7	0.6±0.2
[001]	20°	1.0	1.0	1.0±0.2
	90°	0	0	0

TABLE 5.2

FIRST THREE NEAREST NEIGHBOUR SHELLS FOR Cu_2O.

ATOM TYPE	R/Å	N*
Cu	1.85	4
Cu	3.54	12
O	3.70	8

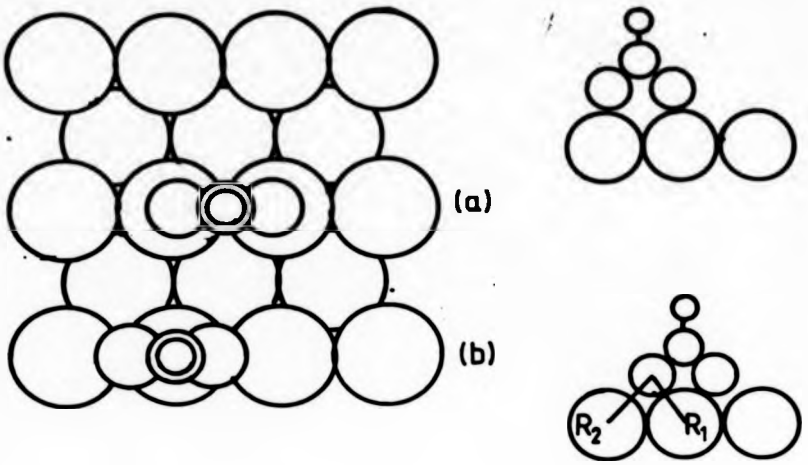

Figure 5.6 The possible adsorption sites for formate on Cu(110).

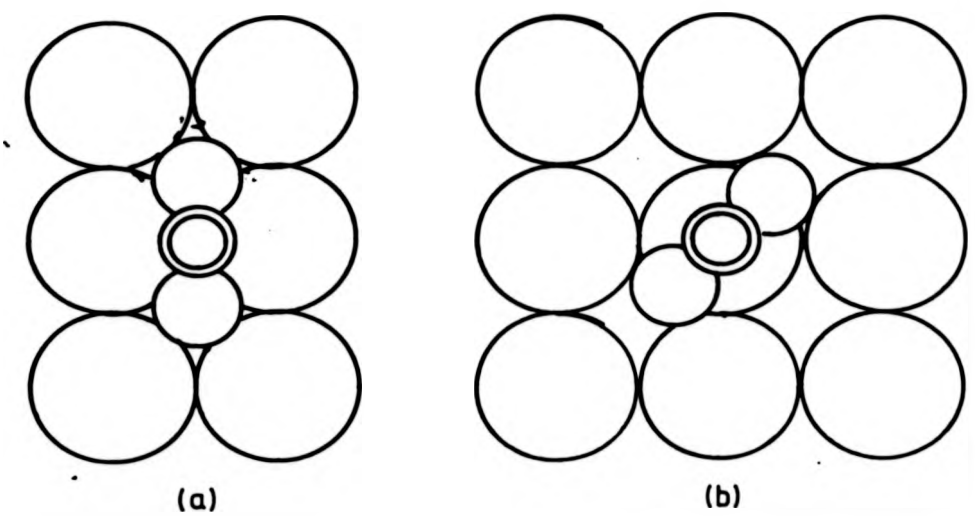

Figure 5.7 Formate on Cu(100): the site proposed by Outka et al. (a) and the site proposed here (b).

(1.98±0.07 Å) is in agreement with that for bulk copper formate and is slightly larger than that for atomic oxygen on Cu(110) (1.84±0.02 Å). The dependence of the SEXAFS amplitudes on polarisation direction has allowed the unambiguous determination of the adsorption site which is shown in Figure 5.6(a).

5.8 COMPARISON OF FORMATE ON Cu(110) AND Cu(100)

The structure which has been found here for the adsorption of the formate ion on Cu(110) is radically different from that found for the Cu(100)[20,21] surface. This was also studied using NEXAFS and single shell EXAFS analysis. The variation of the NEXAFS intensities with incidence angle yielded the same result as was found for Cu(110) i.e. the molecular plane is essentially perpendicular to the surface. The increased symmettry of this surface with respect to the (110) surface precluded the determination of the azimuthal orientation. however. Single shell SEXAFS analysis. however. gave a bond length of 2.38±0.03 Å and the variation in amplitudes with angle indicated a different adsorption site: the formate in the bridge site with the oxygens sitting above the four-fold hollows (Figure 5.7(a)). The authors of this paper (Outka et al.) associated this unusual lengthening of the surface bond (which is 0.4 Å longer than any other known O-Cu bond) with steric considerations. With adsorption in this 'cross bridge' site. if the O-Cu bond length were 1.98 Å (as found on the (110) surface) then the carbon

atom would be about 2 Å from the copper atoms (in the site proposed for the (110) surface this would be 2.17 Å). Outka et al. claim that it is this C-Cu interaction which forces the formate to 'sit higher' on the surface, leading to the anomalously long O-Cu bond length. If the formate ion sits in the site proposed by Outka et al. then it would not be possible for the oxygen atoms to sit exactly in the four-fold hollows without severely distorting the molecule. This means that there must be two bond lengths contributing to the EXAFS. Outka et al. set a limit on the difference in these of 0.15 Å since no beating is observable in the data. This leads to a suggested pair of Cu-O distances of 2.30 and 2.44 Å.

Using these ideas, Upton[22] has carried out calculations for the formate ion bonded to the Ni(100) surface, and has found that with the formate ion in this bridge site, the most favourable configuration is with this expansion of the adsorbate-surface separation. These calculations reveal a Ni-O separations of 2.22 Å and 2.35 Å. This expansion in bondlength is similar to that measured on Cu(100) (taking into account the Ni-Ni separation of 2.49 Å compared with the Cu-Cu seperation of 2.56 Å). This similarity in results for the two surfaces appears rather conclusive on first sight, but it should be noted that no other site was considered in the calculations.

It would seem unusual that the formate should adsorb in a site where there was such an unfavourable C-Cu interaction when the site which was identified on the

(110) surface is availaible and has, apparently, no similar problem (as witnessed by the average bond length 1.98±0.07 Å). The (100) surface is more closely packed than the (110), so it is possible that several similar interatomic seperations contribute to the EXAFS in this system. The possibility of a superposition of several shells contributing to the EXAFS and so causing an anomalous result in the single shell analysis was therefore investigated using the multi-shell simulation package EXCURVE.

5.9 MULTI-SHELL SIMULATIONS OF FORMATE ADSORPTION

The phaseshifts to be used in the surface simulation were extracted by fitting EXAFS data[23] of Cu_2O (cubic structure[31] see Table 5.2) in which the central oxygen atom has four copper neighbours at 1.85 Å, a further twelve at 3.54 Å and eight oxygen neighbours at 3.70 Å. Four of the nearest oxygen atoms are shadowed by the nearest neighbour copper atoms, and so it is not possible to extract reliable backscattering phaseshifts for oxygen from this system for the reasons outlined in chapter 2. The best fit for this data was obtained with E_0=526 eV, VPI=-4 eV, AFAC=0.7, and $2\sigma^2$ for the nearest neighbour of 0.025 Å^2 (correlated value). This fit is shown in Figure 5.8.

Before attempting to investigate possible models for the anomalous HCOO-/Cu(100) system, it was necessary to confirm the model proposed for the (110) surface on the basis of a single shell analysis. Simulations were

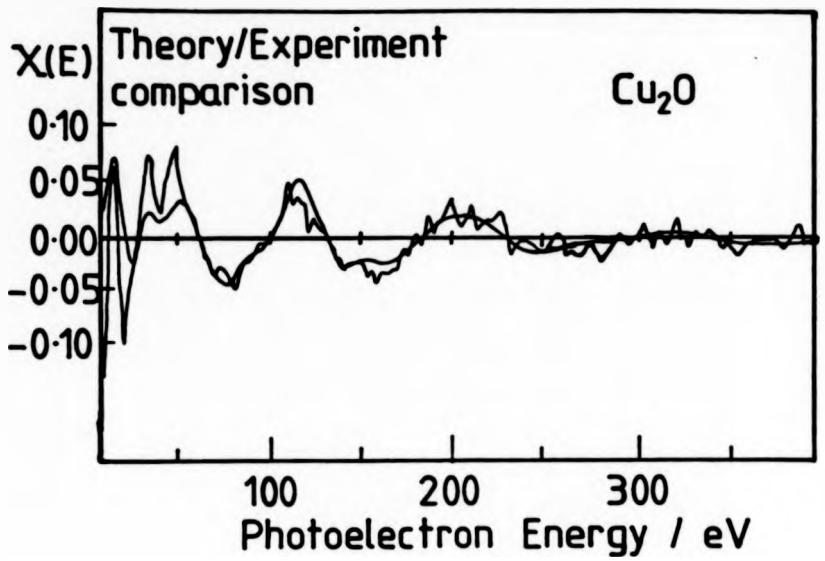

Figure 5.8 Comparison of experimental with simulated EXAFS used to extract the phase shifts: E_0=526eV.

carried out for the three data sets with observable EXAFS: 20° incidence angle, both azimuths, and normal incidence in the [1$\bar{1}$0] azimuth. The simulations for the two possible high symmetry sites on the 'ridges' with the molecular orientation found using NEXAFS are shown in Figures 5.9 and 5.10. These and subsequent simulations use $2\sigma^2=0.03\text{Å}^2$ for the nearest neighbour (and for the second nearest neighbour if this is at a similar distance to the first) and $2\sigma^2=0.06\text{Å}^2$ for neighbours at a significantly greater distance. As can be seen from the simulations, only the model previously proposed was found to fit the data fairly well and the best fit for the two O-Cu distances was found at $R_1=1.94$Å and $R_2=2.15$Å (this puts the O-O distance at 2.22Å as would be found for an internal O-C-O angle of 125° and an O-C distance of 1.25Å).

Having confirmed the model proposed for the (110) surface, the Cu(100) system was investigated. The data presented by Outka et al.[21] were digitised in the background subtracted form. This ruled out the possibility of effects due to different background subtractions. The simulations for their model (Fig. 5.6a) with a $\Delta E_0=0$ev are shown in Fig. 5.11. It can be seen immediately from the 15° incidence angle theory/experiment comparison that something is seriously wrong with this model. The peaks in the simulation are approximately out of phase with the peaks in the experimental data and, interestingly, more or less in phase for the 90° case. The best fit for the 15° data occurs with a $\Delta E_0=19$eV whereas a $\Delta E_0=6$eV fits the 90° data. The ΔE_0

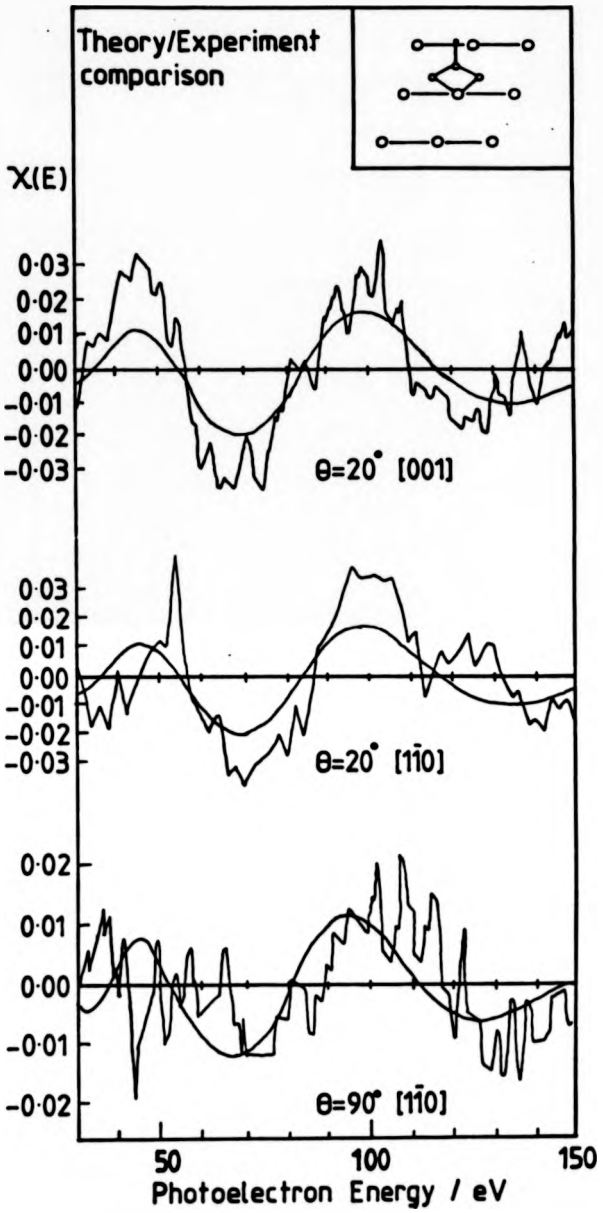

Figure 5.9 EXAFS simulations for the site proposed for the Cu(110) surface.

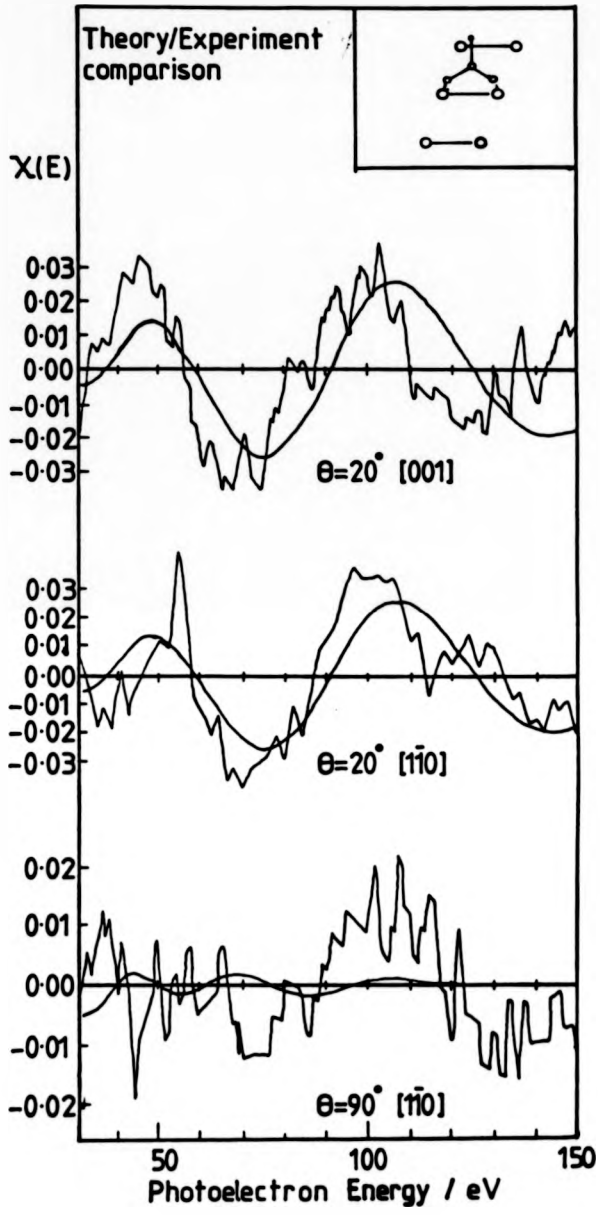

Figure 5.10 EXAFS simulations for the other possible site for the Cu(110) surface.

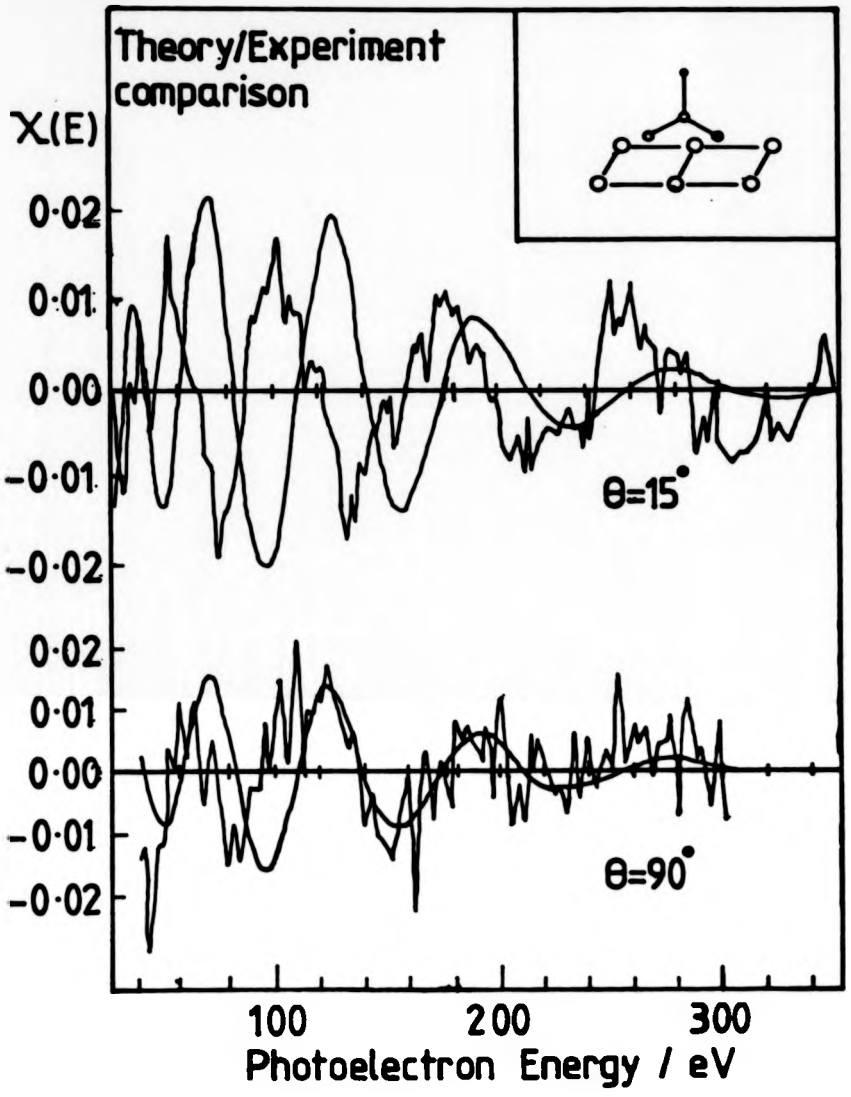

Figure 5.11 EXAFS simulations for the model proposed by Outka et al. for formate on Cu(100).

value for the 15° data is far too large to be justifiable in the general scheme of EXAFS. Small E_0 shifts are usually required in the analysis to account for changes in the phase shifts between model and unknown compound due to chemical influences on scattering from valence electrons. These changes in E_0 are commonly limited to a few ($\lesssim 5$) electron volts. The large discrepancy between the ΔE_0 values for the 15° and 90° data cannot be justified in terms of phase shift changes because if this were the case, the effect should be independent of angle. The site proposed by Outka et al. cannot be made to fit the data even if the anomalously long bond length is shortened to 1.94Å, as found on Cu(110). This would remove the need for a large E_0 shift for the 15° data, but would introduce a very strong amplitude minimum into the data at an electron energy of 230eV which is not seen in the SEXAFS. This reduced bond length would also result in very different effective coordination numbers which leads to an incorrect amplitude ratio for 15° to 90° (see Fig. 5.12). The thing which most strongly discounts the possibility of the 'Outka' site with $R_1 = 1.94$Å is that it introduces a phase mismatch between theory and experiment for the 90° data. This would introduce the need for a fairly large (15eV) ΔE_0 for this angle.

Thus, it has been shown that the site proposed by Outka et al. for formate adsorption on Cu(100), which is completely different to that found for Cu(110) and necessarily includes an anomalously long bond length, can be completely ruled out. This being the case, the formate must be adsorbed in another site that generates

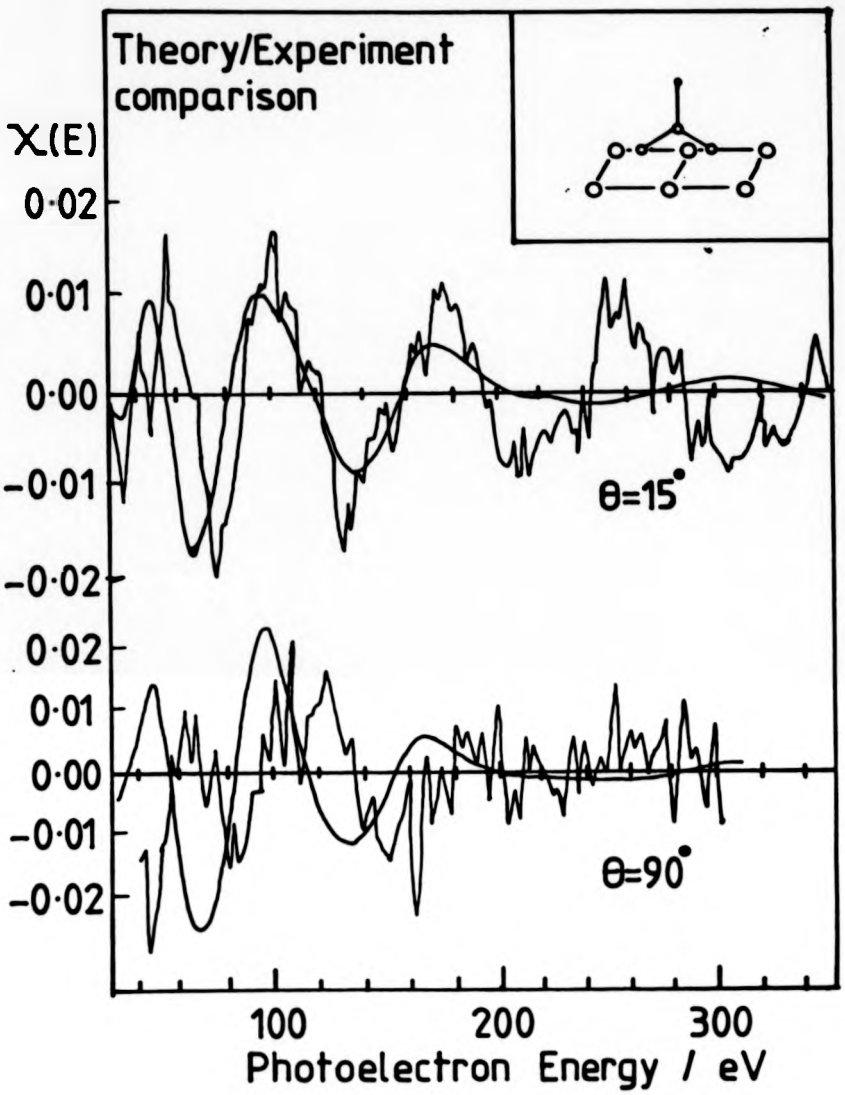

Figure 5.12 EXAFS simulations for the model proposed by Outka et al. with R_1=1.94Å.

EXAFS which lead to misleading results in the single shell analysis. By far the most probable cause of such a problem is the superposition of EXAFS from two similar interatomic separations. An interesting clue to the nature of the real site on Cu(100) is the comparative energy positions of the maxima in the EXAFS for the 90° and 15° data. These maxima do not 'line up', which indicates that these two data sets sample different bond lengths. This indicates that the correct site not only involves two different interatomic separations, but that the ratio of effective coordination numbers for these two distances is very different in the two angles used. One model which fulfils this requirement can be obtained by taking the site found for the (110) surface (with the molecule in the atop site) and rotating the molecular plane by 45° azimuthally (this site is shown in Fig. 5.7b). This 'cross-diagonal' atop site has a ratio of $N_1=N_2$ of 0.79 at grazing incidence (15°) and 0.28 at normal incidence (90°) based on a nearest neighbour distance of 1.94Å (which leads to a second nearest neighbour distance of 2.51Å). The simulations for this site (based on $R_1=1.94$Å and $\Delta E_0=0$) are shown in Fig. 5.13. It can be seen that reasonably good fits can be obtained at both angles without the need for dramatic E_0 changes. An interesting point to note is that the simulation of the first maximum for $\Theta=15°$ contains a double peak which is also seen in the experimental data. The poor fit in the 240-350eV region may be due to slightly incorrect distances or may be an indication that the $\chi(E)$ in this region is not reliable because of the C 1s

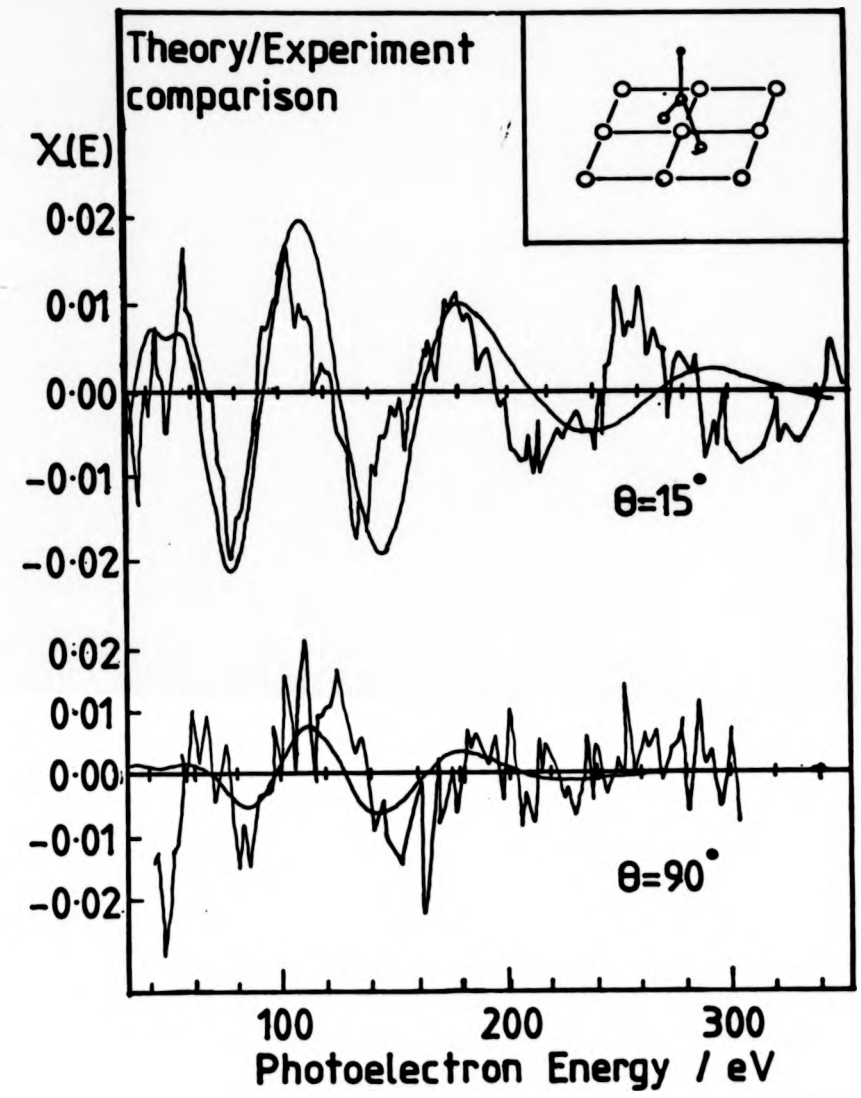

Figure 5.13 EXAFS simulations for the 'diagonal atop site' for HCOO/Cu(100) with R_1=1.94Å.

photoemission peak which enters the analyser at about 214eV photoelectron energy.

Before it can be stated with any certainty that this 'cross-diagonal' atop site is the correct one, it is necessary to check the other high symmetry sites which are available on Cu(100). The simulations for the other sites (including the site extracted for formate on Cu(110)) are shown in Fig. 5.14. It can be seen that all of these can be ruled out by the phase of the EXAFS for either θ=15° or θ=90° and/or by the relative amplitudes for these two angles.

There is one further interesting feature that can be investigated using the multishell simulations; the influence of back-scattering from the other oxygen in the formate ion. If Fig. 5.13 is reexamined, it can be seen that the fit of the 90° data in the 40-80eV region is quite poor. The back-scattering of copper is very weak in this region (Fig. 5.15), and so copper neighbours will introduce little structure here (as can be seen in the simulation). The back-scattering of oxygen, however, which has previously been ignored, is still fairly large and will dominate scattering from copper in this energy regime. Fig. 5.16 shows the simulations for all sites with scattering from the oxygen atom included. Only the 90° data sets are shown since the structure due to scattering from the oxygen will be negligible at θ=15°. It was not possible to use oxygen back-scattering phase shifts extracted from the Cu_2O data because of the shadowing effect of the nearest neighbour copper atom as pointed out previously. The phase shifts used,

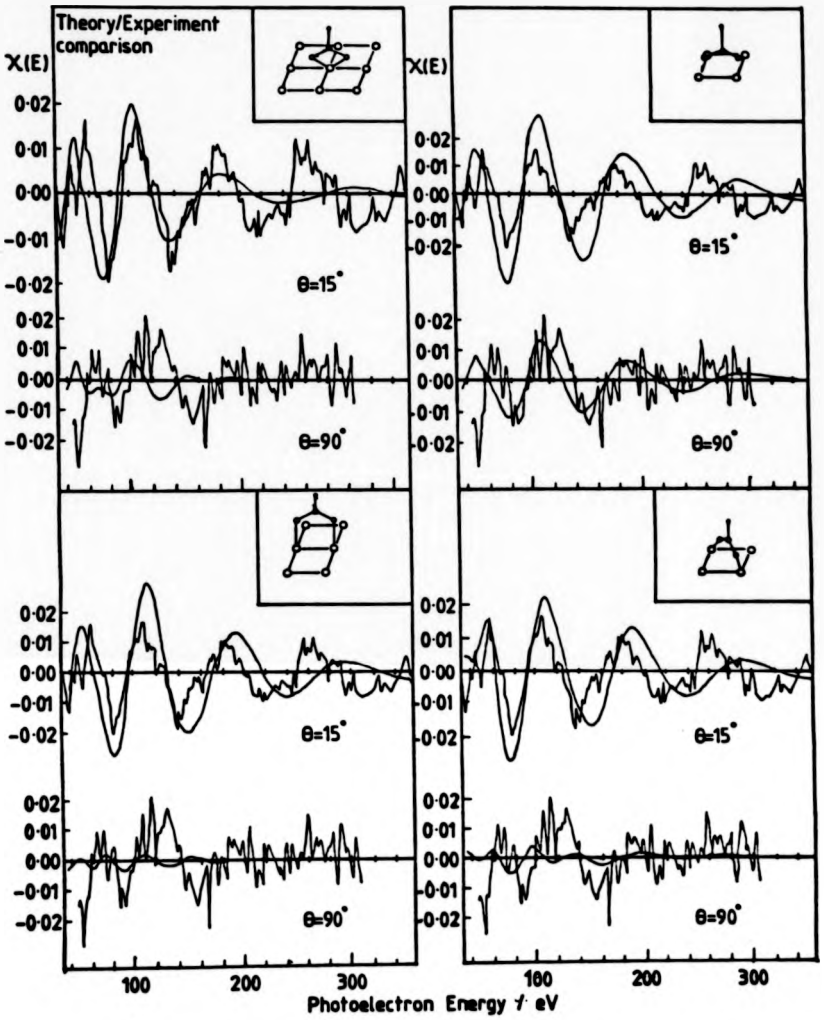

Figure 5.14 EXAFS simulations for all other high symmetry sites for HCOO/Cu(100) with R_1 = 1.94Å.

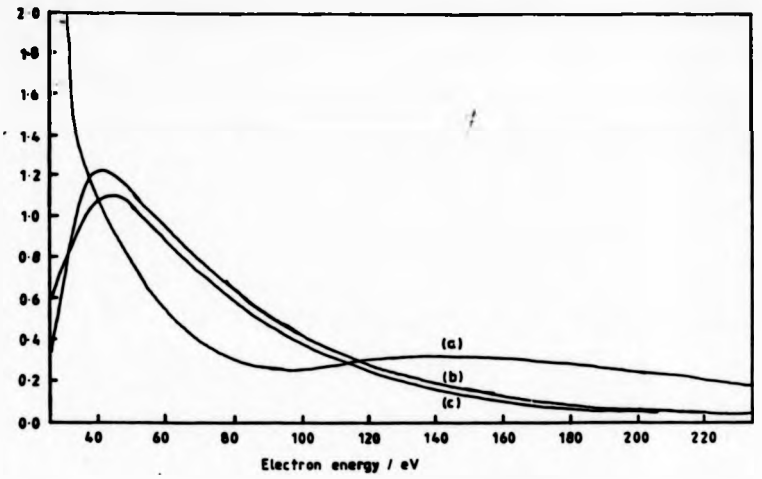

Figure 5.15 Backscattering magnitudes of Cu (a), O (b) and C (c).

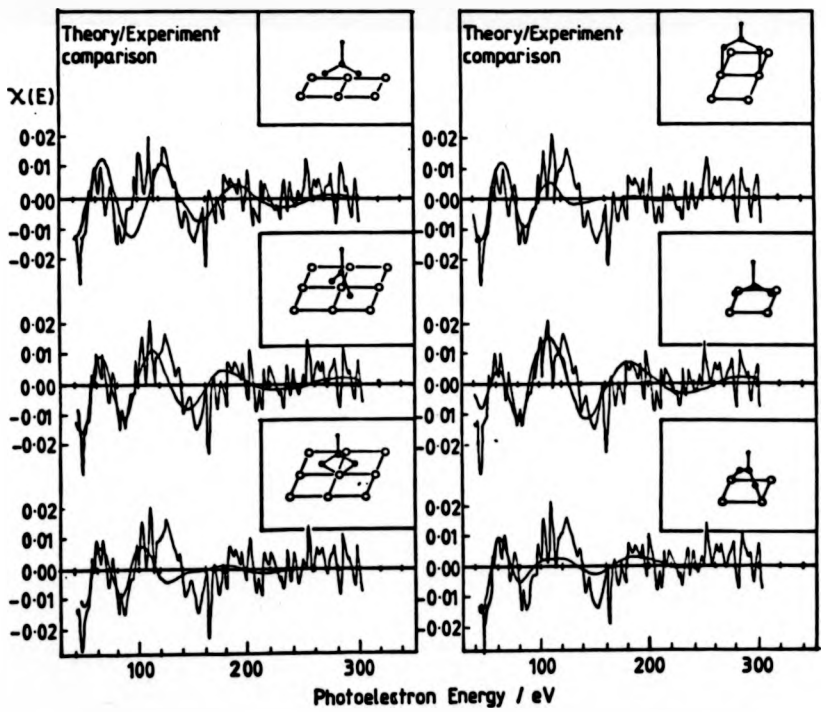

Figure 5.16 EXAFS simulations for all high symmetry sites for normal incidence with the effects of the oxygen neighbour taken into account.

obtained from the EXAFS data base[24], are from muffin-tin potential calculations for NiO. To get a good fit to the first EXAFS wiggle (which is the only one to which the oxygen makes a significant contribution) it was necessary to use an oxygen-oxygen separation of about 2.45Å for all sites. This apparent expansion in bond length over the expected separation of 2.22Å is more likely to be an indication of the inaccuracy of the phase shifts or an indication of a difference in E_0 for intra- as opposed to inter- molecular scattering (these two possibilities are essentially the same thing) rather than a real structural effect (and, indeed, the result may be due to a combination of these effects). It can be seen from the simulations that the only site which cannot be ruled out, either by phase problems or by the relative amplitudes for the two angles, is still the 'cross-diagonal' atop site. Thus, this refinement in the models has not changed the conclusion.

The vast improvement in fit (for all sites) when the oxygen scattering is introduced is a strong indication that the effect is real and that any SEXAFS studies of similar systems, which involve low photoelectron energies, must take it into account. The possible effect of scattering from the oxygen atom on the conclusions reached for the study of formate on Cu(110) were investigated. Fig. 5.17 shows the simulations for both possible sites with the oxygen taken into account (for $\Delta E_0=0$ and Roxygen=2.45Å). It can be seen that this effect does not change the conclusion that the formate is adsorbed with the molecule in the atop site (and the

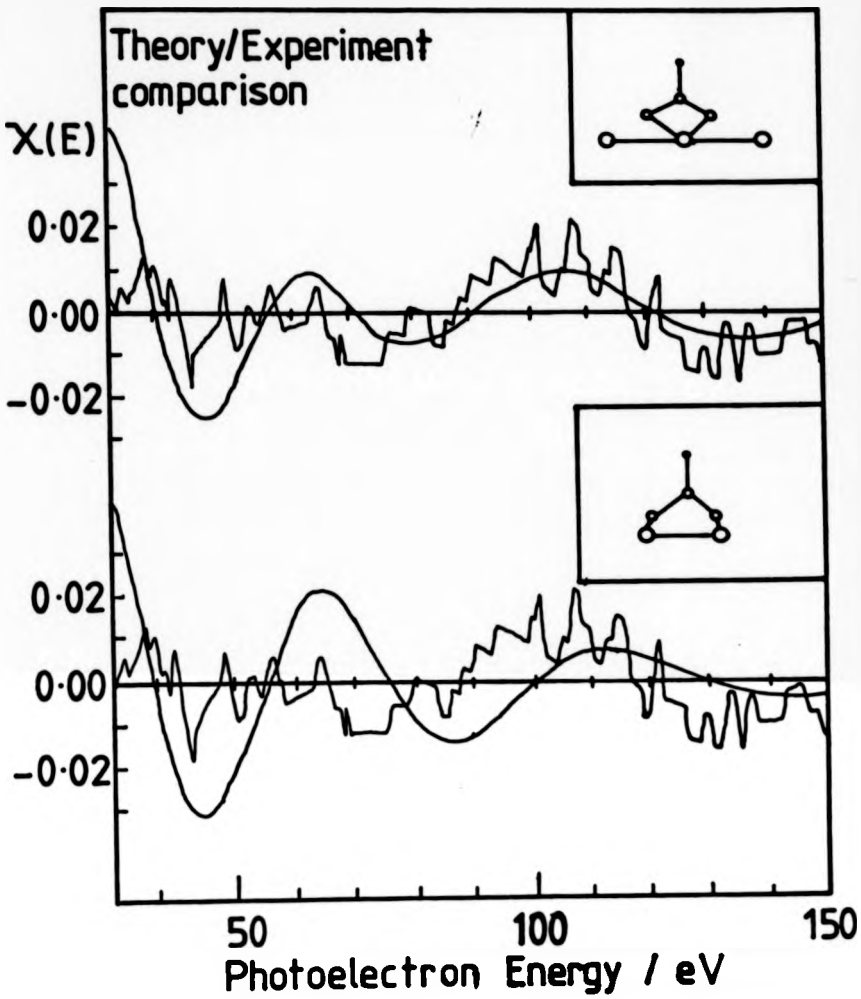

Figure 5.17 EXAFS simulations at normal incidence for both possible sites on Cu(110) with the effect of the oxygen neighbour taken into account.

oxygen atoms in the pseudo bridge sites). The poor fit in the 30-40eV region is most likely an indication that real EXAFS structure has been removed by the background subtraction.

Using the 'cross-diagonal' atop site, which has been established for the Cu(100), confidence limits were set on the value of R_1. Based on both the quality of the fit obtained for different bond lengths and the E_0 necessary to obtain this fit (ΔE_0 should be less than about 5eV) the value of R_1 was found to be 1.99±0.10Å. Fig. 5.18 shows the simulations based on this 'best' R_1. Using a similar procedure, the bond length for the Cu(110) surface was found to be 1.94±0.10Å.

5.10 DISCUSSION OF THE FORMATE/Cu(100) SYSTEM

Having established that single shell analysis of the $HCOO^-$/Cu(100) system resulted in the proposal of an erroneous model, it may be informative to examine the procedure which was used, in order to discover exactly what went wrong. The examination of this example of the use of single shell Fourier filtering analysis may yield useful lessons about the pitfalls of the method.

The Fourier transforms and filtered data compared with the raw data is shown in Fig. 5.19. Outka et al. assign the peak in the Fourier transform at about 2Å in each data set to scattering from the nearest copper atom. They rule out the possibility of O-O scattering being important for two reasons: the larger back-scattering amplitude of copper and the amplitude variation

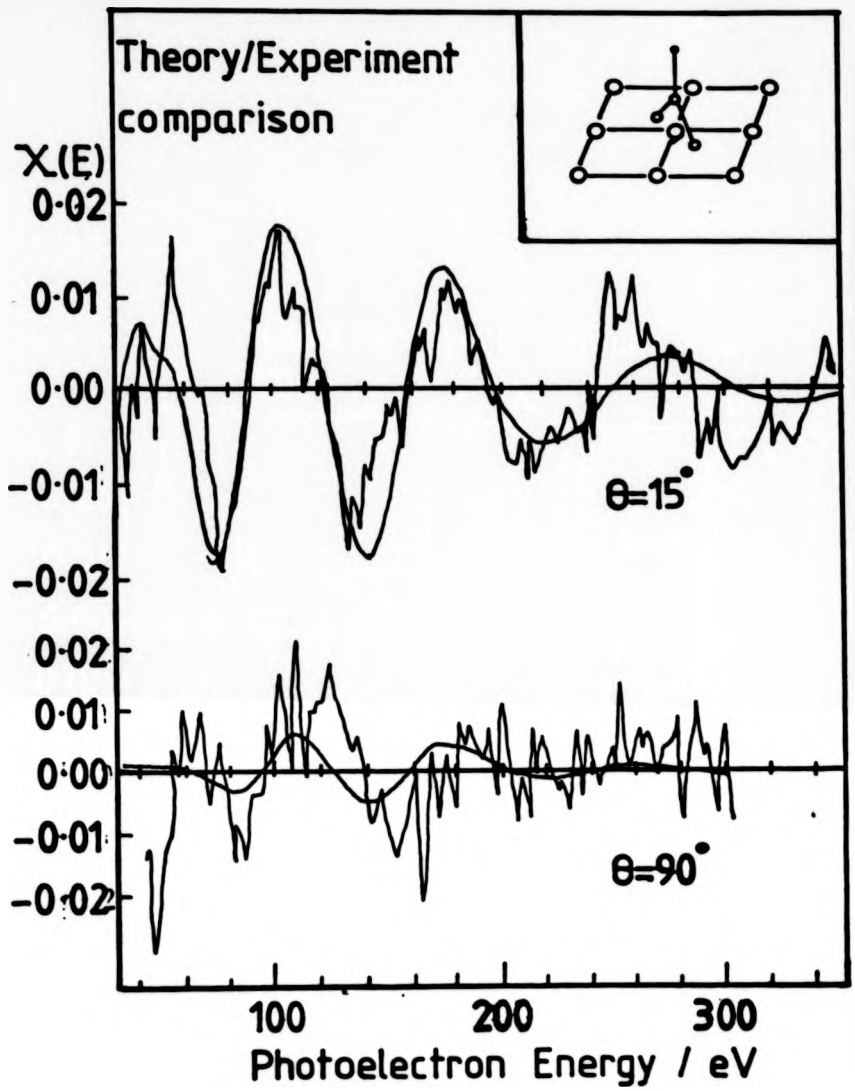

Figure 5.18 EXAFS simulations for the 'diagonal atop site' on Cu(100) with the 'best value' R_1=1.99Å.

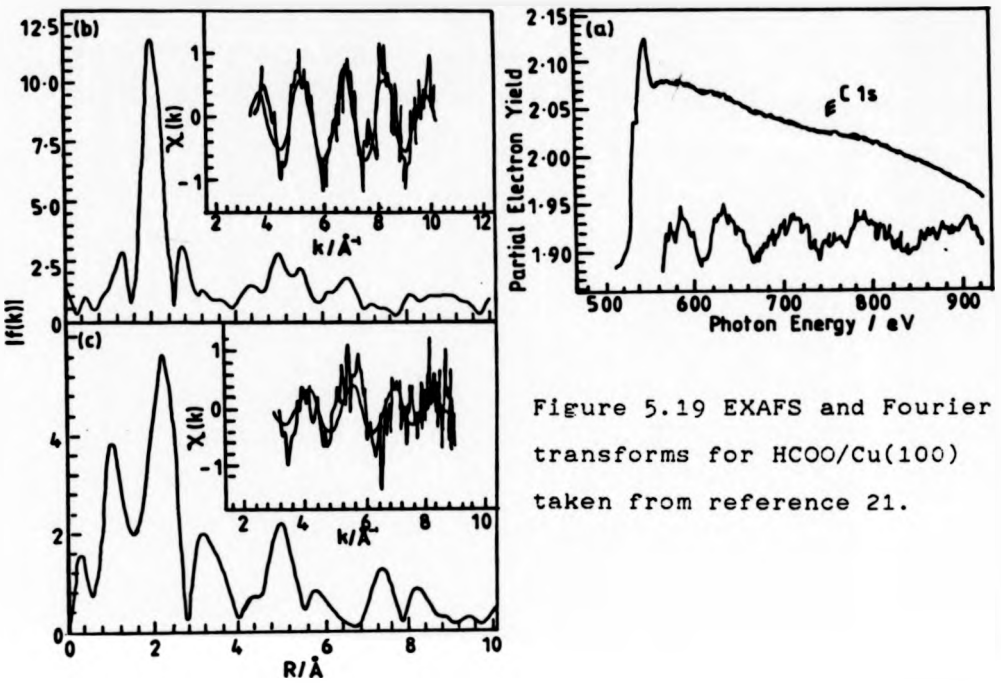

Figure 5.19 EXAFS and Fourier transforms for HCOO/Cu(100) taken from reference 21.

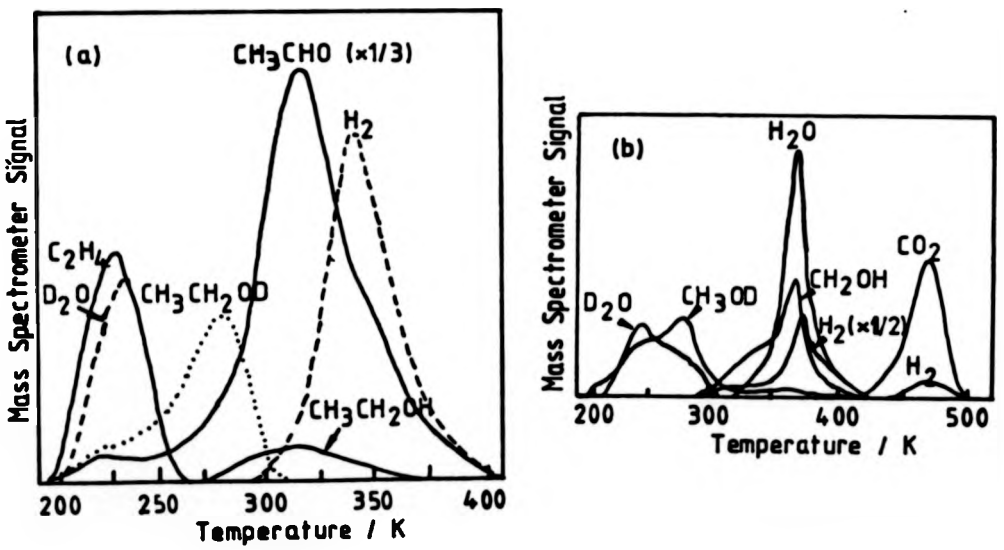

Figure 5.20 TPRS spectra for (a) ethanol and (b) methanol on Cu(110) taken from references 25 and 28.

of the peak with angle of incidence. They argue that if the scattering were dominated by oxygen then the EXAFS amplitude would be greater at normal, rather than grazing, incidence. As we have seen, these arguments are erroneous because they apply only if the amplitudes are averaged over the full data range. In fact, the oxygen scattering is important at low k (but is only seen in the 90° data due to polarisation effects), whereas copper dominates at high k. This means that the amplitude of the Fourier transform is an average of these two contributions. Another point to notice is the difference in peak positions: the 15° data gives a peak at about 2Å whereas the peak for the 90° data is at 2.3Å. This is a strong indication that the two data sets are sampling a radically different bond lengths. Using the backscattering phase shifts of copper (obtained from Cu_2O), they found bond lengths of 2.37±0.02Å for the 15° data and 2.40±0.04Å for the 90° data. No statement is made in the paper regarding the ΔE_0 values used, but single shell analysis carried out in parallel with the multishell analysis presented here and using a similar procedure to that known to be used by Outka et al. could only reproduce this result using ΔE_0 similar to those necessary to make simulations of their model fit the data (15eV for Θ=15° and 3eV for Θ=90°). These numbers are, as has been already pointed out, completely unphysical.

Having determined the (apparent) bond length, Outka et al. set out to find the adsorption site. The ratio of SEXAFS amplitudes 15°:90° was found to be 1.7±0.1

assuming that only one copper shell contributed to the scattering. Using a bond length of 2.38±0.03Å (which they gave as the weighted average of the 15° and 90° results) the only site which gives a similar amplitude ratio is the four-fold hollow (15°:90°=1.86). The two oxygens cannot sit exactly in the four-fold hollows, however, because of the mismatch in the O-O separation (2.22Å) and the interatomic Cu-Cu distance (2.56Å). This means that there must be two different O-Cu distances involved even in the 'cross-bridge' site they propose.

Outka et al. set limits on the maximum separation of these bond lengths as follows. No beating is observed in the data range, so the two interatomic distances must be so close as to drive the first minimum above the high k end of the data. The expression for two superimposed sinusoidal waves of identical amplitude is

$$\chi(k) = A[\sin(2kR_1+\phi) + \sin(2kR_2+\phi)]$$
$$= 2A \sin(k(R_1+R_2)+\phi) \cos(k(R_1-R_2)) \qquad (5.10.1)$$

The cosine term in the equation is the envelope of the oscillation. This has minima at

$$k(R_1-R_2) = k\Delta R = \pi/2, 3\pi/2 \text{ etc.} \qquad (5.10.2)$$

For the first minimum to occur above the high k end of the data, i.e. above 10Å^{-1}, then $\Delta R \lesssim 0.15$Å. Using this maximum difference, the formate can be made to sit in the bridge site, with the oxygens nearly above the

hollows with two O-Cu distances: R_1=2.30 and R_2=2.44 Å.

This argument assumes that the only way to get a 'beat free' data range is if the first beat is beyond the upper end of the spectrum. The data does not start from zero, so it would be possible, in principle, for the first beat to occur below the start of the data and the second beat to lie above the end of the range, thus resulting in a 'beat free' data set. If ΔR were 0.5Å for example, the first beat would occur at 3.1Å^{-1} and the second at 9.4Å^{-1} which lie at either side of the data range. This argument applies to the 'diagonal atop' site proposed here, ΔR is of the order of 0.5Å although the value of this cannot be extracted with a high degree of accuracy. It is also interesting to note that the magnitudes of the two contributions to the EXAFS are quite different (not identical as assumed in the preceeding calculations) which would decrease the effect of the beating and so may reduce the observability of any such feature. Another point which is worthy of note is that the angular dependence of the EXAFS amplitudes gives an indication of the position of the oxygen atoms only: not the position of the molecule. The site proposed by Outka et al. involves the oxygen atoms sitting approximately above the four-fold hollows with a d-spacing above the surface of 1.56Å. The model proposed here also involves the oxygens sitting approximately above the hollows with a d-spacing of 1.59Å.

In summary, the HCOO-/Cu(100) adsorption system has been studied using data simulation techniques and the model proposed by Outka et al., which included a 'novel

chem'sorption bond' has beeen shown to be erroneous. This anomalous result was caused by the superposition of EXAFS from two different interatomic separations, which made the use of the single shell analysis method invalid. That the data analysis should have gone so seriously awry serves as a warning about the applicability of such analysis for similar systems. All the assumptions made in the initial single shell analysis were consistent with the 'current practice' for SEXAFS analysis, so this system gives an indication that SEXAFS analysis may not be as straight forward as is usually claimed. The reason for the failure of the usual principles of SEXAFS analysis in this case, is the unusual bonding configuration. The formate ion bonds to the surface through two atoms of fixed separation. The mismatch of this O-O distance with any of the principle separations on the surface leads to the oxygen atoms sitting in asymmetrical sites which lead to a mixture of Cu-O distances of similar length. The assumptions in EXAFS analysis usually rely on a fairly symmetric system with definite shells at progressively further distances from the absorbing atom. This work highlights the danger of using a direct analysis method without a simulation routine to check the result.

The site proposed by Outka et al. was given support by the calculations of Upton[22] of formate on Ni(100). Although the results of these calculations agree with the result obtained by single shell SEXAFS analysis on Cu(100), the only site that was considered was that proposed by Outka et al. It would be interesting to see

the results of such energy minimisation calculations applied to the site proposed here for Cu(100).

5.11 THE DECOMPOSITION OF ETHANOL ON Cu(110)

The adsorption of ethanol on Cu(110) was first studied by Wachs and Madix[25] using Temperature Programmed Reaction Spectroscopy (TPRS). They adsorbed CH_3CH_2OD at 180K on clean and oxygen pre-dosed copper. Upon heating of the (un-pre-dosed) sample, several desorption peaks were observed (Fig. 5.20a). At about 225K, D_2O and C_2H_4 were evolved: this was associated with the decomposition of a $CH_3CH_2OD_2$ intermediate. A large CH_3CH_2OD desorption peak was observed at 280K, which was thought to be unreacted adsorbate. When the sample was heated to 316K, CH_3CHO and CH_3CH_2OH desorbed simultaneously (in the ratio $CH_3CHO:CH_3CH_2OH$ of 35:1). This was followed by a H_2 peak at 340K. The three higher temperature peaks were interpreted as resulting from the decomposition of an ethoxide (CH_3CH_2O) intermediate on the surface. Pre-dosing the copper crystal with oxygen was found to enhance the formation of ethoxide.

Subsequent studies[26], using TPRS, XPS and UPS, of ethanol absorption on Cu(110) confirmed the existence of the ethoxide intermediate. It was suggested that the ethanol (which was adsorbed at low temperature) had either desorbed or dissociated at 200K. The ethoxy species was said to be stable to 348K. The O 1s binding energies were measured for both species, and were found to be 532.9eV (ethanol) and 531.0eV (ethoxy). This com-

pares with an O 1s binding energy of 530.15±0.20eV for atomic oxygen on Cu(110)[27].

5.12 STUDY OF ETHOXY SPECIES USING NEXAFS

The work discussed in the previous section suggested that the ethoxy species can be found by pre-dosing the surface with oxygen, dosing with ethanol at 160K and then heating to room temperature. This 'recipe' has also been shown to form a methoxy species if methanol is used instead of ethanol[28,29]. The thermal desorption spectrum for methanol on Cu(110) is shown in Fig. 5.20b. In order to facilitate the assignment of near edge features for the ethoxy system, the NEXAFS spectra (at the O K-edge) were collected for atomic oxygen (Fig. 5.21) and molecular ethanol (Fig. 5.22). The spectrum for atomic oxygen (which was formed by adsorption at low temperatures followed by heating to room temperature) is dominated by a very sharp feature at about 531eV. This is likely to be due to adsorbate-substrate scattering. The near-edge region of molecular ethanol (adsorbed and measured at 160K) is dominated by a shape resonance, centred at 538eV.

It can be seen from Fig. 5.20a that the main ethanol desorption peak occurs at about 280K and the ethoxy desorbs at around 316K. So, if it is desired to form the ethoxy intermediate without the presence of any other species, the sample heating phase of the procedure is is very critical. The maximisation of the amount of adsorbed ethoxy may be even more difficult because it

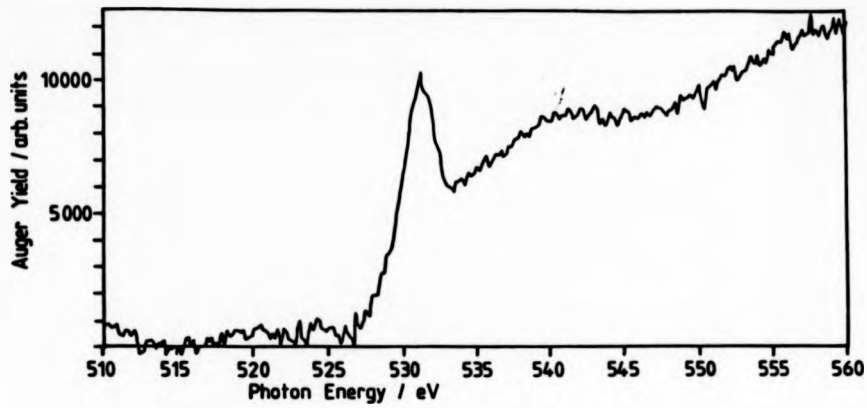

Figure 5.21 O K-edge for atomic oxygen on Cu(110).

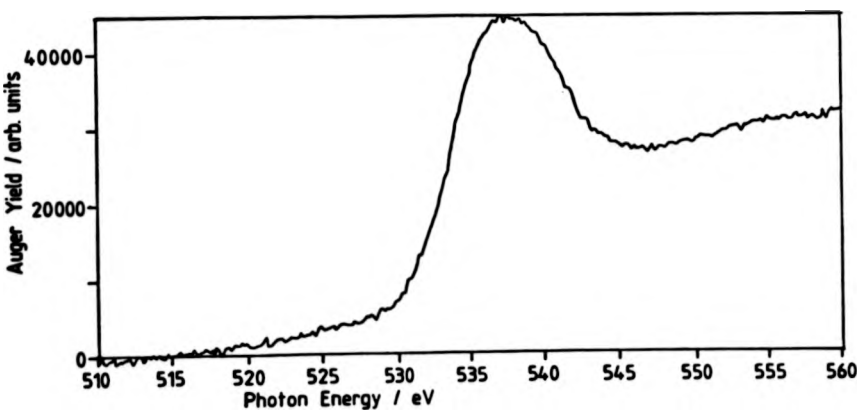

Figure 5.22 O K-edge for molecular ethanol on Cu(110).

has been suggested that the intermediate stabilises the ethanol molecule on the Ag(110) surface[25]. To examine the effect of heating on the formation of the ethoxy intermediate, the crystal was dosed with 0.2L O_2 and 5L CH_3CH_2OH at 160K and NEXAFS measurements were made following heating to successively higher temperatures. Fig. 5.23 shows the oxygen K-edge (collected at normal incidence) after heating to 225K, 265K, 275K and 280K. In each case, following heating, the sample was quickly cooled to 225K and held at this temperature for the duration of the measurements to prevent any further desorption. It can be seen that the near-edge region is dominated by a broad feature which appears to be the sum of two shape resonance-type features. The feature at higher energy (~538eV) dominates at low temperatures whereas the other feature (~536eV) increases in relative intensity as the temperature to which the sample is heated increases. The energy separation of these two features (~2eV) is approximately the same as the energy separation of the O 1s binding energies for ethoxy and ethanol on Cu(110). This similarity, and the fact that the energy position of the higher energy resonance is the same as was found for molecular ethanol, allows the assignment of the resonances to an ethoxy species (536eV peak) and co-adsorbed ethanol (538eV peak). A similar relationship was found for the resonance positions of methoxy and methanol on Cu(100)[30]. A third feature in the spectra is a shoulder at about 530eV. The similarity in energy position of this to that of the strong feature in NEXAFS of atomic oxygen at 531eV raised the question

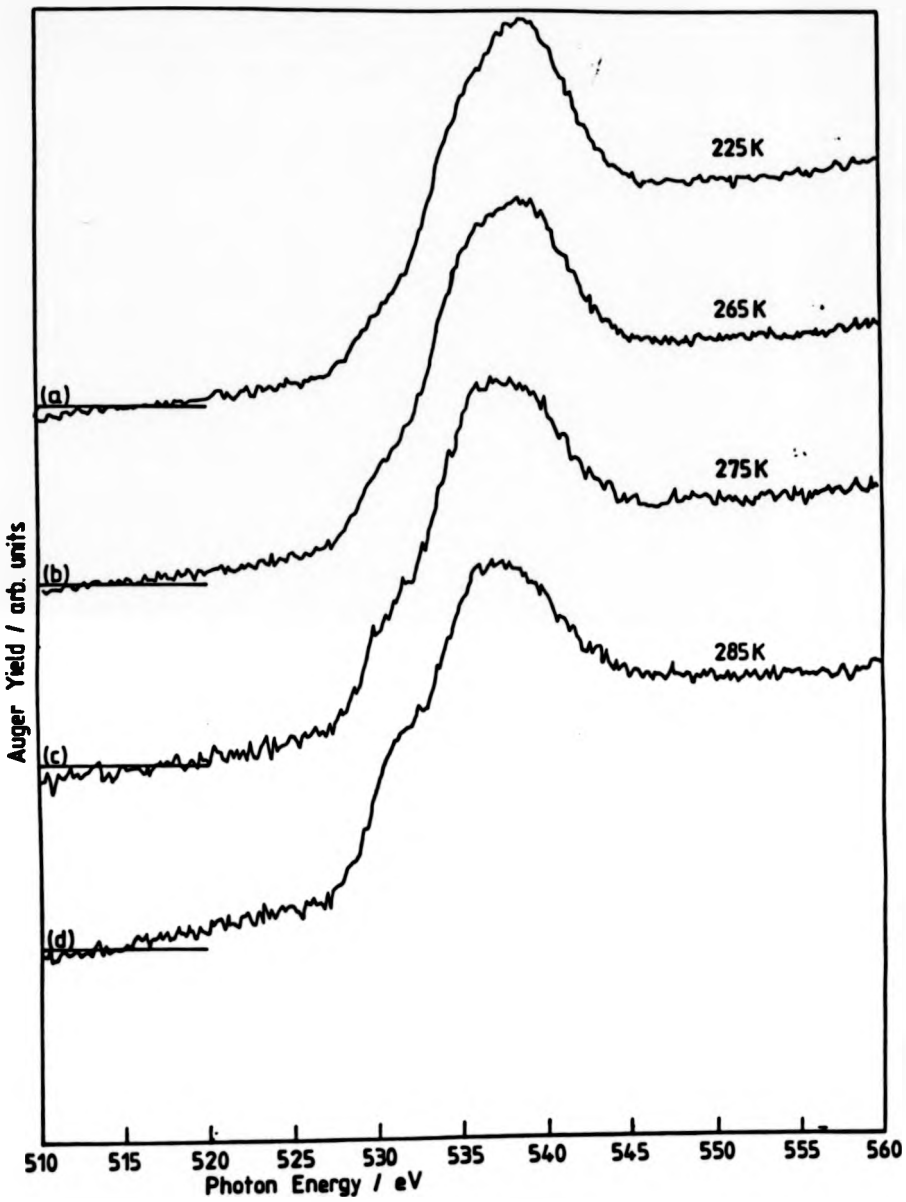

Figure 5.23 O K-edge for ethanol on oxygen predosed Cu(110) following heating to succesively higher temperatures.

as to whether there was atomic oxygen remaining on the surface. This is unlikely, however, because upon further heating to desorb the ethoxy and ethanol species, no residual oxygen was found. It can be seen from the spectra that the intensity of this shoulder is strongly correlated with the intensity of the ethoxy shape resonance which implies that it is also due to the ethoxy species. Indeed, a similar feature can be seen on the absorption spectra of methoxy on Cu(110)[29], where it is more likely that only one species is present (as can be seen from the TPRS spectra).

The overall decrease in absorption intensity with increasing temperature, coupled with the relative intensities of the two shape resonances indicates that both species desorb as the temperature is increased but that the ethanol desorbs at a greater rate than the ethoxy. The effect of holding the crystal at 275K for prolonged periods of time was investigated. Fig. 5.24 shows three spectra separated by approximately four minutes each. This shows a steady decrease in the amount of ethoxy/ethanol on the surface. Based on this knowledge of the rate of ethanol desorption compared with the ethoxy and the time dependent desorption of both species, the following procedure was decided on to maximise the amount of ethoxy present relative to ethanol: the sample was dosed at 160K with 0.2L O_2 and 5L CH_3CH_2OH followed by rapid heating to 275K and immediate cooling to 225K. It should be noted that this procedure always left some ethanol on the surface, which limits the amount of detailed structural information that can be extracted

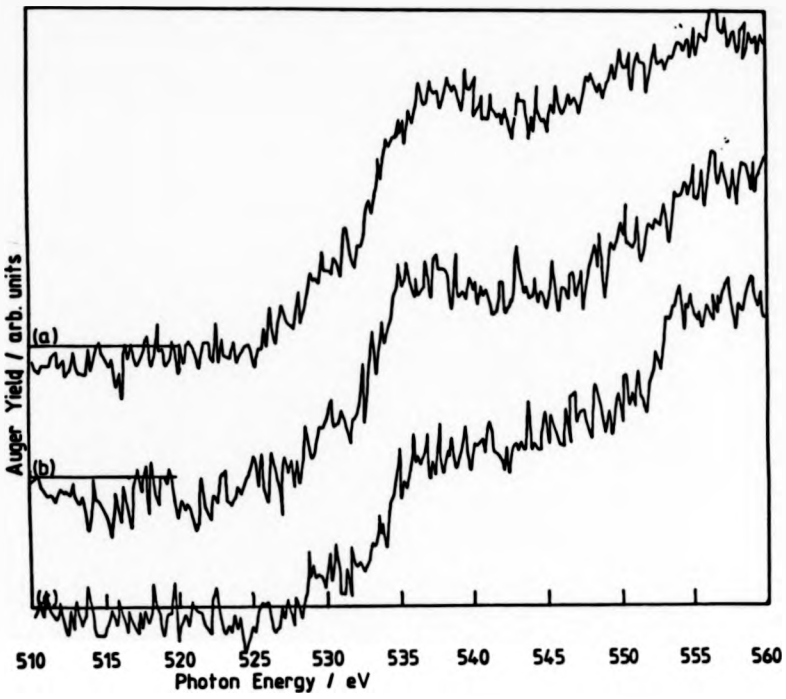

Figure 5.24 O K-edge for ethoxy/ethanol system held at 275 K succecively longer periods of time.

about the ethoxy species. All spectra reported from now on were collected at 225K. This was cold enough to prevent further desorption of ethoxy but not cold enough to allow readsorption of molecular ethanol from the residual gas of the vacuum system. The stability of the surface with time is shown in Fig. 5.25. These two spectra were collected eight minutes apart, at 225K, and show no significant change in either intensity or structure of X-ray absorption.

The intensity of the shape resonances of the adsorption system formed using this method was studied as a function of angle. Fig. 5.26 shows the near edge structure as a function of the angle between the electric vector and the surface normal with the electric vector in the [001] azimuth. It can be seen that the two shape resonances have opposite angular dependencies. The feature at 536eV (associated with the ethoxy species) is strongest at grazing incidence, whereas the feature at 538eV (associated with ethanol) is strongest at normal incidence. This indicates that the ethoxy intermediate is essentially 'standing up' on the surface and the ethanol is lying down. It is difficult to quantify this statement because the significant overlap of the two peaks makes it impossible to measure the resonance intensities with any accuracy. Quantification is further complicated by the availability of data from one azimuth only. If the O-C bond is tilted from the surface normal in any preferred azimuth then it would not be possible to extract this from data collected in one azimuth only. If it is assumed that any such tilt has no azimuthal

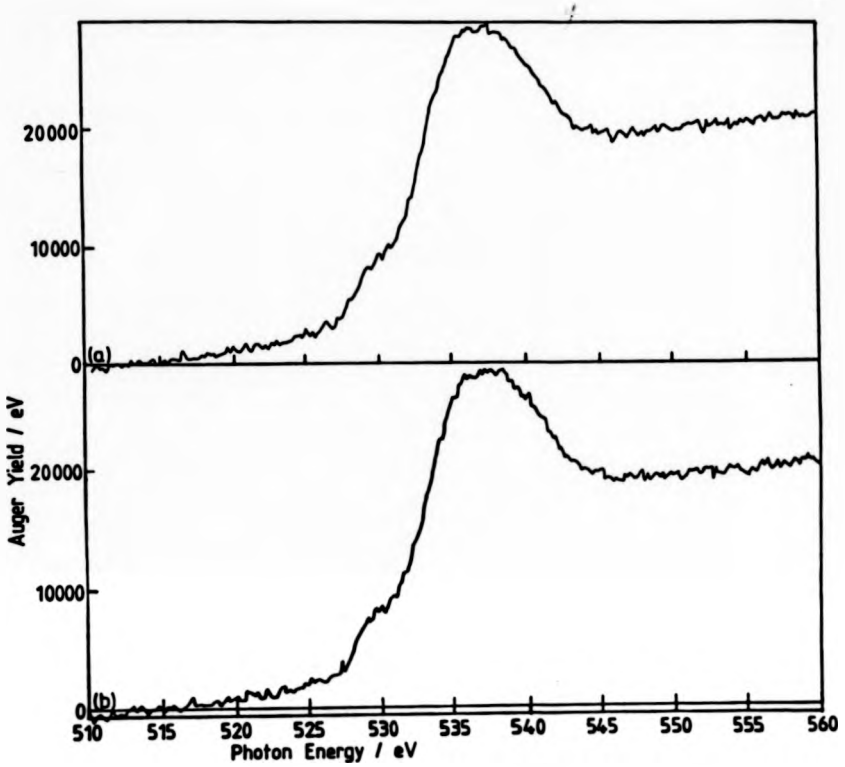

Figure 5.25 O K-edges separated by eight minutes to demonstrate the stability of the ethoxy/ethanol system at 225K.

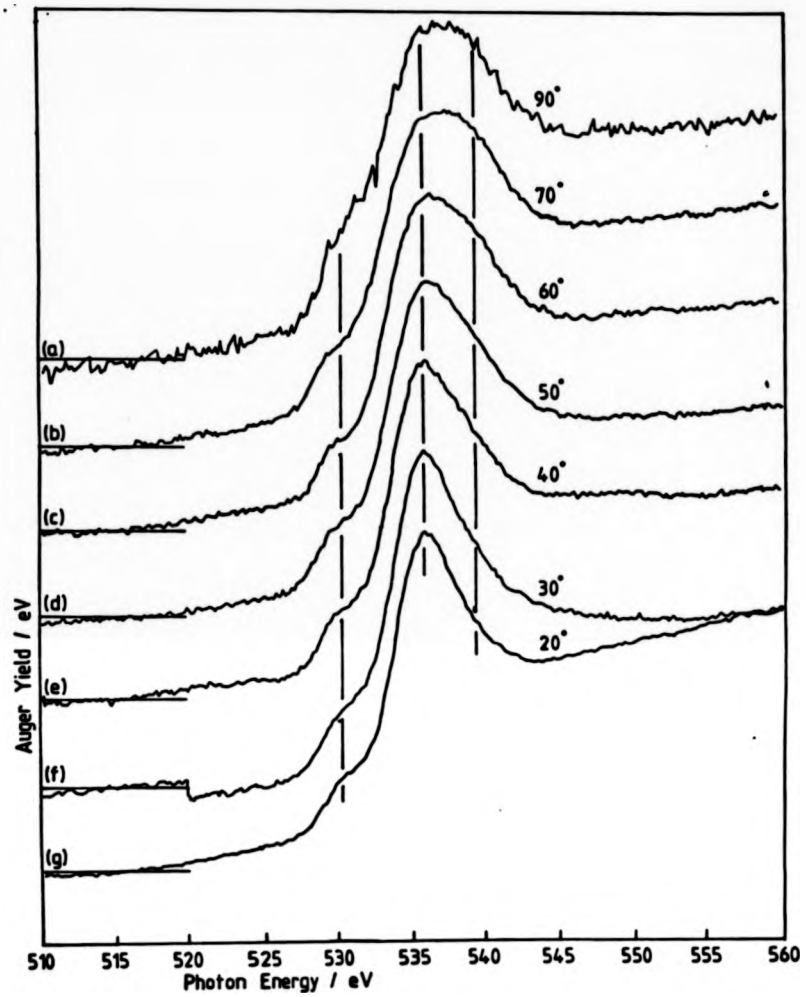

Figure 5.26 NEXAFS spectra for the ethoxy/ethanol on Cu(100) as a function of incidence angle.

preference, then it can be stated that the angle between the surface normal and the O-C bond in ethoxy is less than the 'magic angle' (54.7°) whereas in ethanol the tilt must be more than this angle. This result is similar, in part, to studies of methoxy on Cu(110)[29] where the intermediate is found to have an angle of 36±5° between the surface normal and the O-C axis. No structural parameters for adsorbed methanol were extracted in this work.

An interesting feature of the NEXAFS spectra is that the shape resonance of ethoxy (Fig. 5.26g) is much sharper than that for ethanol (Fig. 5.22). It is not clear why this should be the case since the atom pair in question is the same in each case (O-C). One possible explanation is the difference in chemical environment of the oxygen in each case. In ethanol, the oxygen is bonded to carbon and hydrogen atoms whereas ethoxy is bonded to the surface through the oxygen atom. As can be seen from Fig.5.21 the substrate-adsorbate interaction produces a sharp feature on the oxygen K-edge at 531eV. It may be that substrate-adsorbate interactions are also contributing something to the near-edge structure of ethoxy. If this is the case it would pose a serious problem for the use of NEXAFS for surface studies which are justified by the general belief that the resonances are only dependent on intra-molecular scattering. If substrate scattering were found to be very important, then it would seriously restrict the use of the simplistic NEXAFS analysis method for the extraction of structural parameters. Such problems would necessit-

ate the use of full multiple scattering data simulation methods employing a cluster which includes substrate atoms.

5.13 CONCLUSIONS FOR THE ETHOXY/Cu(110) SYSTEM

It has been shown that the adsorption of oxygen and ethanol at low temperatures followed by heating to produce the ethoxy intermediate results in the coexistence of two species: ethoxy and ethanol. No combination of heating rates, ultimate temperature and amount of oxygen predose was found which could produce ethoxy alone. This restricts the amount of quantitative structural information which can be extracted for the ethoxy species (and indeed for the co-adsorbed ethanol). Despite this problem, the angular dependence of the shape resonance intensity indicates that the C-O bond is at an angle smaller than 54.7° to the surface normal whereas the same bond in the co-adsorbed ethanol species is at an angle larger than 54.7° to the surface normal (assuming that there is no preferred azimuthal orientation for any angle of tilt).

There is a large difference in the apparent width of the shape resonance between ethoxy and ethanol. This may be an effect caused by the change of species or it may be due to adsorbate-substrate interactions. If the latter is the case, then it could have serious implications for the simple analysis procedures currently used for surface NEXAFS.

CHAPTER 5 : REFERENCES

1) See for example D.P. Woodruff in "The Chemical Physics of Solid Surfaces" ed. D.A. King and D.P. Woodruff, Vol. 1, 81-181.

2) H. Ibach and D.L. Mills, "Electron Spectroscopy and Surface Vibrations", Academic Press, (1982).

3) F.M. Hoffmann, Surf. Sci. Reports 3, 107-192 (1983).

4) D.H.S. Ying and R.J. Madix, J. Cat. 61, 48-56 (1980).

5) M. Bowker and R.J. Madix, Surf. Sci. 102, 542-565 (1985).

6) B.E. Hayden, K. Prince, D.P. Woodruff and A.M. Bradshaw, Surf. Sci. 133, 589-604 (1983).

7) J. Stöhr, J.L. Gland, W. Eberhardt, D. Outka, R.J. Madix, F. Sette, R.J. Koestner and U. Döbler, Phys. Rev. Lett. 57, 2414-2417 (1983).

8) J. Stöhr and R. Jaeger, Phys. Rev. B26, 4111-4131 (1982).

9) P. Hoffmann, S.R. Bare, N.V. Richardson and D.A. King, Surf. Sci. 133, L459-L464 (1983).

10) D.A. Shirley, Phys. Rev. B5, 4709-4714 (1972).

11) S.D. Peyerimhof, J. Chem. Phys. 47, 349-359 (1967).

12) T. Gustavsson and H.J. Levinson, Chem. Phys. Lett. 78, 28-31 (1981).

13) F. Sette, J. Stöhr and A.P. Hitchcock, Chem. Phys. Lett. 110, 517-520 (1984).

14) J. Stöhr, F. Sette and A.L. Johnson, Phys. Rev. Lett. 53, 1684-1687 (1984).

15) A.A. Bakke, H.W. Chen and W.L. Jolly, J. Elect. Spect. and Rel. Phen. 20, 333-366 (1980).

16) J. Hölzl and F.K. Schulte, in Springer Tracts in Modern Physics, Vol. 85, p.1 (1979).

17) R.W.G. Wyckoff, "Crystal Structures Vol. 5", Interscience Publishers, (1966).

18) G.A. Barclay and C.H.L. Kennard, J. Chem. Soc., 3289-3294 (1961).

19) D.M.L. Goodgame, N.J. Hill, D.F. Marsham, A.C. Skapski, M.L. Smart and P.G.H. Troughton, Chem. Commun., 629-630 (1969).

20) J. Stöhr, D.A. Outka, R.J. Madix and U. Döbler, Phys. Rev. Lett. 54, 1256-1259 (1985).

21) D.A. Outka, R.J. Madix and J. Stöhr, Surf. Sci. 164, 235-259 (1985).

22) T.H. Upton, J. Chem. Phys. 83, 5084-5091 (1985).

23) U. Döbler, K. Baberschke, J. Haase and A. Puschmann, Phys. Rev. Lett. 52, 1437 (1984).

24) E. Pantos and G.D. Firth, Daresbury Laboratory Technical Memorandum, DL/CSE/TM21, October 1982.

25) I.E. Wachs and R.J. Madix, J. Cat. 53, 208-227 (1978).

26) M. Bowker and R.J. Madix, Surf. Sci. 116, 549-572 (1982).

27) G.R. Gruzalski, D.M. Zehner and J.F. Wendelken, Surf. Sci. 159, 353-368 (1985).

28) I.E. Wachs and R.J. Madix, Appl. Surf. Sci. 1, 303-328 (1978).

29) M. Bader, A. Puschmann and J. Haase, submitted to Phys. Rev. B.

30) J. Haase, private communication.

31) R.W.G. Wyckoff, "Crystal Structures Vol. 1", Interscience Publishers, 1963.

CHAPTER 6 FINAL DISCUSSION AND CONCLUSIONS

6.1 INTRODUCTION

The application of X-ray absorption fine structure to the study of adsorbates on metal surfaces has been demonstrated for both atomic and molecular adsorption systems. The allied techniques of Surface Extended X-ray Absorption Fine Structure (SEXAFS) and Near-Edge X-ray Absorption Fine Structure (NEXAFS) have been used to provide detailed structural information of several adsorption systems and, in addition, the potential of photoelectron diffraction as a surface structural tool has been clearly demonstrated. The use of single shell and multi-shell SEXAFS analysis techniques have been compared, and some interesting results have been obtained. Whilst NEXAFS has often been used to obtain qualitative information about molecular adsorption systems, the resonance intensities have rarely been used to obtain quantitative information. The possibilities of quantification have been investigated here, and the technique has been capable of providing detailed information about molecular orientations, but not without some difficulties. The technique of photoelectron diffraction has been shown to be capable of providing very detailed structural information, with the use of single scattering simulation techniques.

6.2 SUMMARY OF THE STRUCTURAL INFORMATION OBTAINED

Analysis of SEXAFS from the atomic adsorption system studied, Cu(111)[$\sqrt{3}$x$\sqrt{3}$]R30°-Cl, using both the single shell and multiple shell simulation methods yielded the same structure. The Fourier-filtering single shell method gave a Cu-Cl bond length of 2.39±0.02Å, an expansion of 0.05±0.02Å as compared with bulk CuCl. The EXAFS amplitude variation between 35° and 60° grazing incidence angles uniquely defined the adsorption site to be the three-fold hollow. Analysis with the multi-shell simulation method also gave the nearest neighbour Cu-Cl distance to be 2.39±0.02Å. This technique was found to be sensitive to the second nearest copper neighbour which was found to lie at a distance of 3.50±0.08Å. This second nearest neighbour distance, combined with the amplitude variation between the incidence angles and the relative amplitudes of the first and second nearest neighbour contributions allowed the adsorption site to be determined: the three-fold hollow as found using the single shell method. The multi-shell analysis method, however, was not able to distinguish between the two possible three-fold hollows: the 'fcc site' (ABCA packing) and the 'hcp site' (ABA packing). Photoelectron diffraction measurements at normal incidence confirmed the three-fold hollow site found by SEXAFS but the two similar sites could not be distinguished. This distinction was made by off-normal photoelectron diffraction and the Cl atom was found to adsorb in the 'fcc' or ABCA site.

Three molecular adsorption systems were studied; HCOO-/Cu(110), HCOO-/Cu(100) and CH_3CH_2OH/Cu(110). The structure of the formate intermediate on Cu(110) was studied using NEXAFS and SEXAFS. The variation of NEXAFS resonance intensities with incidence angle allowed the molecular orientation to be determined. The molecular plane was found to be perpendicular to the surface and parallel to the $[1\bar{1}0]$ azimuth. The internal O-C-O half angle was found to be $62^{\circ}\pm10^{\circ}$ and the possible angles of tilt from the surface normal and twist from the $[1\bar{1}0]$ azimuth were found to be less than 10°. SEXAFS measurements of this system were restricted by the intrusion of the C 1s photoemission peak into the partial yield detector at a photon energy of about 700eV. Despite this, the single shell Fourier-filtering analysis method extracted a bond length of 1.98±0.07Å. The variation of the SEXAFS amplitude with incidence angle identified the adsorption site as the atop site with the oxygen atoms sitting in bridge like positions. Subsequent re-analysis of this data, using the simulation method, in light of the anomalous bond length found by Outka et al.[1] for the formate intermediate on Cu(100) confirmed this result. The EXAFS were shown to be due to two similar bondlengths of 1.94±0.10Å and 2.15±0.10Å due to the mismatch of the O-O distance and the Cu-Cu separation. Re-analysis of the data collected by Outka et al. for the HCOO-/Cu(100) system using the multiple shell simulation method revealed that the interpretation of the SEXAFS data (based on the Fourier filtering analysis method) was not self-consistant.

because it required greatly different E_0 values for normal and grazing incidence. Simulation of all possible high-symmetry sites revealed that the adsorption site favoured on Cu(100) was similar yet subtly different to that found for Cu(110). The adsorption on this surface also occurs in the atop site, but with the molecular plane aligned with the [001] azimuth, not the [1$\bar{1}$0] azimuth as found on Cu(110). The bond length found for HCOO- on Cu(100) was 1.99±0.10Å compared with 2.38±0.03Å as found by Outka et al. using the single shell method. It was found that superposition of EXAFS from two different bond lengths created structure which led to the erroneous value obtained by single shell analysis.

The adsorption of ethanol on Cu(110) and its reaction with chemisorbed oxygen to form CH_3CHO was studied using NEXAFS. At temperatures close to room temperature. two σ-resonances were observed. These were interpreted as being due to two co-adsorbed species which were identified as ethanol and the intermediate ethoxy ion. At no time was the ethoxy intermediate seen to exist alone as was implied by an XPS study of the system[2]. The variation of the resonance intensities with incidence angle revealed that the ethoxy intermediate is essentially upright on the surface whereas the co-adsorbed ethanol is essentially lying down on the surface.

6.3 DISCUSSION AND CONCLUSIONS ABOUT THE STRUCTURAL TECHNIQUES

Apart from providing detailed structural information about several adsorption systems, these studies have yielded useful information about the techniques involved. One of these is the fairly new technique of NEXAFS. Although near-edge resonances have been identified for a large number of gas phase molecules the use of these for the determination of the orientation of adsorbed species has so far been restricted to a handful of studies. The majority of the structural analyses using NEXAFS have been carried out in a rather qualitative fashion and little attention has been paid to problems of background subtraction. In the work presented here, it was found that the selection of a suitable background is a major problem in the quantitative analysis of NEXAFS. This problem is heightened by the lack of knowledge of any other near-edge features caused by adsorbate-substrate scattering which may be superimposed on the NEXAFS resonances. The uncertainty about the correct background causes problems, not only in the measurement of the resonance intensities, but also in the normalisation of these intensities. This, combined with problems introduced by the completeness of the linear polarisation, restricts the accuracy by which structural parameters can be determined to about 10%.

Another interesting possibility of NEXAFS is its use for the determination of intra-molecular bond lengths. Whilst theoretical and experimental studies of gas phase

diatomic molecules have confirmed a relationship between bond lengths and the position of the σ-resonance, this could not be used here with any reliability. Gas phase studies have used the 1s binding energy as the reference point for measuring the position of the σ-resonance, but as this binding energy usually changes upon adsorption, it is difficult to relate the large amount of gas phase data to surface studies. Surface studies are further complicated by the possibility of changes induced in V_o, the interatomic potential, by adsorption; this is another parameter which is of great importance in relating the bond length to σ-resonance energy position. These problems mean that the use of this effect to measure intramolecular bond lengths on surfaces will not be reliable until far more data have been collected for a large number of adsorption systems to allow definite trends to be found.

NEXAFS also proved useful in studying a system involving two co-adsorbed species; ethoxy and ethanol on Cu(110). The σ-resonances associated with each species both because of their different energy positions and their different angular dependence of the resonance intensities. This different angular dependence allowed semi-quantitative information about the orientations of the two species to be extracted. The difference in energy position of the σ-resonances cannot definitely be assigned to a change in bond length, however, because of other differences between the two species; in particular the O 1s binding energy. It is interesting to note that the difference in position between the two σ-reso-

nances (i.e.~ 2eV) is identical (within the accuracy of the measurement) to the difference in O 1s binding energies of ethoxy and ethanol.

The work presented here has also yielded some interesting information on the technique of Surface EXAFS. The majority of the studies to date have used the single shell analysis method[3]. The multi-shell analysis method has been used for some studies[4], but with the exception of the study of iodine on Ni(100) mentioned in Chapter 1, no comparison has been made with the standard Fourier filtering method. The Ni(100) study revealed that problems could arise with the single shell analysis in circumstances where the second nearest neighbour (in this case I) is a strong scatterer in an energy region where the nearest neighbour (Ni) is a weak scaterer. This system is one example of what may turn out to be a serious problem for SEXAFS. With this in mind, the two analysis methods were applied to the adsorption systems studied here in an attempt to reveal more information about their relative merits. The study of two contrasting types of adsorption systems (namely atomic and molecular) has allowed some useful conclusions about the applicability of the two methods to be drawn.

In the case of chlorine on Cu(111), the results of single shell analysis yielded essentially the same result; both gave the bond length to be 2.39±0.02Å with adsorption in the three-fold hollow. The multi-shell analysis method also gave the second nearest neighbour distance (3.50±0.08Å). In one of the molecular adsorption systems (HCOO/Cu(100)), however, multi-shell anal-

ysis was found to yield a result which is radically different to that found by single shell analysis. These results differed both in the adsorption site and (by a large amount) in the bond length. In the other molecular adsorption system (HCOO/Cu(110)) the two analysis methods gave consistant results.

The reason for the problems with the HCOO/Cu(100) system is that the adsorption site resulted in two bond lengths which were similar. The superposition of the EXAFS from these gave a misleading result when analysed using the single shell method. The single shell method is based on the assumption that different near neighbour distances are different enough to allow the separate shells to be resolved in the Fourier transform; this was not the case for formate on both Cu(100) and Cu(110). The single shell analysis did not go awry for the Cu(110) system; this may be because both shells were very similar in both bond length and amplitude of the contributions (see Figure 6.1). This is the classical situation for the discussion of the effect of multiple bond lengths on SEXAFS analysis. The conventional wisdom is that the apparent bond length will be the average of the two contributions (as was found for this system). In the Cu(100) formate adsorption system, however, ΔR is of the order 0.5Å and the relative contribution of the two shells varies strongly with incidence angle (see Figure 6.1). The single shell analysis of this configuration generated a result which was erroneous. Multi-shell simulations, however, allowed the adsorption site to be found. This shows the usefulness

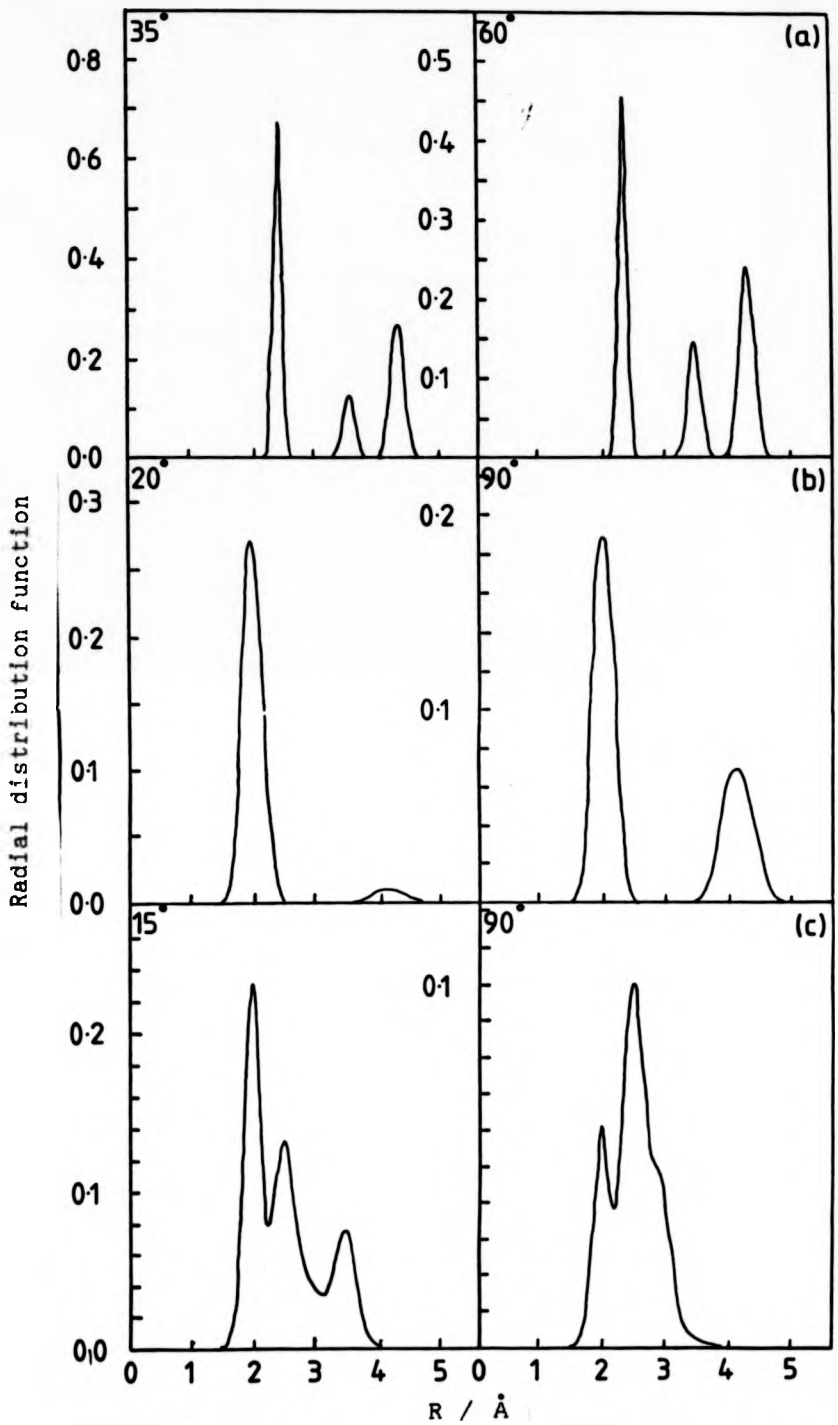

Figure 6.1 Radial distribution functions for Cu(111) [√3x√3]R30°-Cl (a), Cu(110)/HCOO (b) and Cu(100)/HCOO (c), including the Debye-Waller type factors and weighted by $1/R^2$.

of the simulation method as a means of checking the results obtained using Fourier filtering as well as illustrating the power of the method itself.

The applicability of the single shell analysis to Cu(111)[√3x√3]R30°-Cl arises from the high symmetry of the system. This symmetry results in a series of well defined shells (see Figure 6.1) which can be distinguished in the Fourier transform. The symmetry of the formate adsorption systems is drastically reduced due to the mismatch between the O-O distance and the surface lattice parameters. In this aspect, the formate intermediate is unusual; few systems have been studied in which bonding to the surface occurs through two atoms. This means that the problems encountered here may be peculiar to this system and multiple bond lengths may not, in general, cause serious problems.

Another feature of the multi-shell analysis of formate adsorption is the influence of the other oxygen atom on the EXAFS. The effects of scattering off light atoms such as oxygen have generally been ignored in SEXAFS analysis because of the low back scattering magnitude of these atoms. Analysis of the SEXAFS of formate on Cu(100) at normal incidence has shown that structure due to scattering from the oxygen is important at low electron wavenumber. This could have an influence on SEXAFS studies because low k data is often used in the analysis to increase the typically short data ranges. It is also interesting to note that scattering from the carbon atom in the formate ion is not important despite its proximity to the central atom.

In fact, this short bond length leads to EXAFS of very low frequency which is removed by the background subtraction.

The third technique used in the work presented here was photoelectron diffraction. This was used with a fixed detector geometry (both normal and off-normal) with variable photon energy. With normal take off angle, single scattering simulation analysis was capable of distinguishing the main features of the bonding geometry; the site was identified as the three fold-hollow in agreement with the SEXAFS result. The Normal Photoelectron Diffraction (NPD) data did not allow a distinction to be made between the two three-fold hollows, however. This distinction was made using Off-normal Photoelectron Diffraction (OPD) and the chlorine was found to adsorb in the 'ABCA' (fcc-like) site. An interesting feature of this photoelectron diffraction study was that, in the 100-400eV energy range, single shell simulation techniques were sufficient to analyse the data. This is in agreement with a recently published study[5]. This apparent simplicity of analysis is because many of the arguments which justify the single scattering approach to EXAFS also apply to PD because both techniques rely on a 'local source' for the probe electron. The same arguments which limit the number of shells needed for a SEXAFS analysis also apply to PD to a certain extent, but it was found to be more sensitive to distant shells than SEXAFS. This increased sensitivity to more distant shells is because, unlike SEXAFS, PD does not involve a local detector.

This lack of a local detector, which makes the analysis of PD more difficult than SEXAFS, is also the reason for an interesting advantage of the technique over SEXAFS for determining adsorbate structures. The detector geometry means that PD is very sensitive to structure in the region of space directly behind the central atom as viewed from the detector. The NPD measurements could not differentiate between the two three-fold hollows because they are fairly similar here (they do differ substantially in the second row, but this is quite a large distance from the central atom). It was possible, however, to change the angle of detection until the region behind the central atom would be very different for the two sites; in this case 35° off normal in the [110] azimuth. This retention of azimuthal sensitivity (which is not present in SEXAFS because of the lack of angular resolution of the detector - namely the central atom) allowed the distinction between the two sites to be made.

The work presented here has demonstrated the potential of three related techniques; SEXAFS, NEXAFS and PD. The advantage of using these three in combination is that they use the same experimental geometry and apparatus. Together these techniques have allowed rather complete local structural determinations of both atomic and molecular adsorbates to be made with relative simplicity of analysis.

CHAPTER 6: REFERENCES

1) D. Outka, R.J. Madix and J. Stöhr, Surf. Sci. 164, 235-259 (1985).

2) M. Bowker and R.J. Madix, Surf. Sci. 116, 549-572 (1982).

3) J. Stöhr, R. Jaeger and S. Brennan, Surf. Sci. 117, 503-524 (1982).

4) G. Lamble and D.A. King, Proc. Roy. Soc. in press.

5) D.P. Woodruff, Surf. Sci. in press.